2009-06

Investigating the electrothermal characteristics of a Gate Turn Off thyristor during turn-off using þÿ S I L V A C O A T L A S!"

Vineyard, Gerald E.

Monterey, California. Naval Postgraduate School

NAVAL POSTGRADUATE SCHOOL

MONTEREY, CALIFORNIA

THESIS

INVESTIGATING THE ELECTROTHERMAL CHARACTERISTICS OF A GATE TURN OFF THYRISTOR DURING TURN-OFF USING SILVACO ATLAS™

by

Gerald E. Vineyard

June 2009

Thesis Advisor:	Todd Weatherford
Co-Advisor:	John Ciezki

Approved for public release; distribution is unlimited.

THIS PAGE INTENTIONALLY LEFT BLANK

REPORT DOCUMENTATION PAGE		Form Approved OMB No. 0704-0188

1. AGENCY USE ONLY *(Leave blank)*	2. REPORT DATE	3. REPORT TYPE AND DATES COVERED
	June 2009	Master's Thesis

4. TITLE AND SUBTITLE	5. FUNDING NUMBERS
Investigating the Electrothermal Characteristics of a Gate Turn off Thyristor during Turn-off using SILVACO ATLAS™	
6. AUTHOR(S) Gerald E. Vineyard	
7. PERFORMING ORGANIZATION NAME(S) AND ADDRESS(ES) Naval Postgraduate School Monterey, CA 93943-5000	**8. PERFORMING ORGANIZATION REPORT NUMBER**
9. SPONSORING /MONITORING AGENCY NAME(S) AND ADDRESS(ES) Office of Naval Research. Ship Systems and Engineering Division (Code 331)	**10. SPONSORING/MONITORING AGENCY REPORT NUMBER**

11. SUPPLEMENTARY NOTES The views expressed in this thesis are those of the author and do not reflect the official policy or position of the Department of Defense or the U.S. Government.

12a. DISTRIBUTION / AVAILABILITY STATEMENT	12b. DISTRIBUTION CODE
Approved for public release; distribution is unlimited.	A

13. ABSTRACT (maximum 200 words)

This thesis presents data from a simulation study of the thermal and electrical characteristics of a Gate Turn Off (GTO) thyristor. At present, most of the research on GTO thyristors has focused on their use in power electronic systems at high switching frequencies. As a result, the behavior of GTO thyristors at very low switching frequencies is not well understood. Previous research projects have shown experimentally that GTO thyristors are capable of interrupting significantly more than their nominal turn-off current rating when used in pulsed power applications at low switching frequencies.

This work demonstrates the use of physics-based computer simulation to study the electrothermal turn-off characteristics of a GTO thyristor at low switching frequencies. The computer model used in this project simulated both the electrical and the thermal characteristics of a GTO thyristor and allowed its internal properties—such as current density, electric fields, and lattice temperature—to be investigated. The model was used to track the generation, transfer, and dissipation of energy within the structure of the device and show that the current interruption capability of a GTO thyristor may depend on its switching frequency due to the thermal energy that is generated and stored in the device during turn-off.

14. SUBJECT TERMS	15. NUMBER OF PAGES
Gate Turn Off Thyristor, GTO, Pulsed power, Current Interruption, Thermal and Electric Modeling, Inductive Turn-off, Safe Operating Area, SOA	149
	16. PRICE CODE

17. SECURITY CLASSIFICATION OF REPORT	18. SECURITY CLASSIFICATION OF THIS PAGE	19. SECURITY CLASSIFICATION OF ABSTRACT	20. LIMITATION OF ABSTRACT
Unclassified	Unclassified	Unclassified	UU

NSN 7540-01-280-5500 Standard Form 298 (Rev. 8-98) Prescribed by ANSI Std. Z39.18

THIS PAGE INTENTIONALLY LEFT BLANK

Approved for public release; distribution is unlimited.

INVESTIGATING THE ELECTROTHERMAL CHARACTERISTICS OF A GATE TURN OFF THYRISTOR DURING TURN-OFF USING SILVACO ALTAS™

Gerald E. Vineyard
Ensign, United States Navy
B.S.E.E., United States Naval Academy, 2008

Submitted in partial fulfillment of the
requirements for the degree of

MASTER OF SCIENCE IN ELECTRICAL ENGINEERING

from the

NAVAL POSTGRADUATE SCHOOL
June 2009

Author: Gerald E. Vineyard

Approved by: Todd R. Weatherford
Thesis Advisor

John G. Ciezki
Thesis Co-Advisor

Jeffrey B. Knorr
Chairman, Department of Electrical and Computer Engineering

THIS PAGE INTENTIONALLY LEFT BLANK

ABSTRACT

This thesis presents data from a simulation study of the thermal and electrical characteristics of a Gate Turn Off (GTO) thyristor. At present, most of the research on GTO thyristors has focused on their use in power electronic systems at high switching frequencies. As a result, the behavior of GTO thyristors at very low switching frequencies is not well understood. Previous research projects have shown experimentally that GTO thyristors are capable of interrupting significantly more than their nominal turn-off current rating when used in pulsed power applications at low switching frequencies.

This work demonstrates the use of physics-based computer simulation to study the electrothermal turn-off characteristics of a GTO thyristor at low switching frequencies. The computer model used in this project simulated both the electrical and the thermal characteristics of a GTO thyristor and allowed its internal properties—such as current density, electric fields, and lattice temperature—to be investigated. The model was used to track the generation, transfer, and dissipation of energy within the structure of the device and show that the current interruption capability of a GTO thyristor may depend on its switching frequency due to the thermal energy that is generated and stored in the device during turn-off.

THIS PAGE INTENTIONALLY LEFT BLANK

TABLE OF CONTENTS

LIST OF FIGURES

LIST OF TABLES

THIS PAGE INTENTIONALLY LEFT BLANK

EXECUTIVE SUMMARY

This thesis presents data from a simulation study of the thermal and electrical characteristics of a Gate Turn Off (GTO) thyristor during turn-off. At present, most of the research on GTO thyristors has focused on their use in power electronic systems at high switching frequencies. As a result, the behavior of GTO thyristors at very low switching frequencies is not well understood. Previous research projects have shown experimentally that GTO thyristors are capable of interrupting significantly more than their nominal turn-off current rating when used in pulsed power applications at low switching frequencies.

In this thesis, a physics-based computer simulation of a GTO thyristor was developed to study the electrothermal characteristics of a GTO thyristor turn-off at low switching frequencies. The computer model simulated both the electrical and the thermal characteristics of a GTO thyristor and allowed its internal properties—such as current density, electric fields, and lattice temperature—to be investigated. Additionally, the project implemented a SPICE circuit model of a simplified inductive pulsed power source. The SPICE circuit model created the electrical bias conditions required for the physics-based device simulator to study the low switching frequency operating characteristics of a GTO thyristor.

In addition to the physical device model and the SPICE circuit model, a method was developed to track the generation, transfer, and dissipation of energy within the GTO thyristor's structure and the SPICE circuit. The method was able to accurately measure the energy in the SPICE circuit components and track the amount of electrical energy input to the GTO thyristor during each current pulse. The energy tracking method was able to approximate the thermal energy stored within the structure of the GTO thyristor and track the flow of energy into and out of the device. The energy tracking method provided useful insights into the operation of the GTO thyristor; however, significant refinement will be required before the method can be employed for future device studies.

By analyzing the internal structure of the device, it was determined that the primary mechanism for thermal energy generation in a GTO thyristor is joule heating. Although joule heating occurs throughout the internal structure of the GTO thyristor, it is prominent anywhere a high current density coincides with a high electric field. During conduction, joule heating is prominent in the center of the n-Base region and along the perimeter of the anode short regions. During turn-off, the location of maximum heating shifts upwards to the gate/n-Base junction as the turn-off gate current creates an electric field across the junction between the gate and the n-Base region and pinches off the anode current. The resulting high electric field and high current density result in significant joule heating and the formation of hot spots within the GTO thyristor.

Using the energy tracking method it was determined that most of the electrical energy input to the GTO thyristor was converted into thermal energy and stored within the structure of the device. Furthermore, the majority of the thermal energy in the device was stored in the aluminum electrodes. Given the size of the anode and gate electrodes (and thus their total heat capacity) and the thermal resistance of the thermal contact, it would take a fairly long time for the GTO thyristor to reach thermal equilibrium under the operating conditions used in the multiple pulse simulations.

The findings of this project suggest an explanation for the discrepancy between the rated current interruption capability of GTO thyristors and their actual current interruption capability in a pulsed power circuit. During each current pulse and especially at turn-off, the GTO thyristor receives electrical energy from the external circuit; this energy is converted into thermal energy and stored inside the device until it can be output through the thermal contact. The device requires significantly more time to output the thermal energy to the thermal contact than it does to absorb the electrical energy from the external circuit. Consequently, at high switching frequencies the turn-off current (usually the peak of the current pulse) has to be reduced to ensure that the device can dissipate all of the electrical energy through the thermal contact.

GLOSSARY OF TERMS

Anode Current: The electric current flowing from the anode terminal to the cathode terminal of a Gate Turn Off (GTO) thyristor.

Anode Voltage: The difference in voltage potential between the anode terminal and the cathode terminal of a GTO thyristor.

Current Crowding: As a GTO thyristor turns off, the current through each unit cell is forced towards the center of each cell, which causes the current density to increase; this increase in current density is commonly called current crowding.

Current Filament: Isolated sections of high current density that occur due to slight differences in the turn-off times of the unit cells. During turn-off, the anode current is forced into a decreasing number of unit cells, which can lead to high current densities in isolated sections of the device.

Energy Density: Ratio of the energy capacity (storage or supply) to the volume of a power source or system. Energy density values are primarily used to compare different energy storage technologies.

Gate Current: Electric current flowing from the gate terminal to the cathode terminal of the GTO thyristor; used to turn the GTO thyristor on and off.

Gate Driver: Circuit components connected between the gate and cathode terminals of a GTO thyristor to supply the positive and negative current pulses required to turn a GTO thyristors on and off.

Gate Turn Off (GTO) Thyristor: A current controlled semiconductor switch designed for high power applications; commonly used as an “opening switch” to interrupt (turn off) current. Gate Turn Off Thyristors are sometimes referred to simply as GTOs.

Gate Voltage: The difference in voltage potential between the gate terminal and the cathode terminal of the GTO thyristor.

Holding Current: The minimum anode current required to maintain a GTO thyristor in its conducting state. When the anode current drops below the holding current, the GTO thyristor will turn off.

Latching Current: The minimum anode current required for the device to turn on. If the anode current does not rise above the latching current during turn-on, then the device will not remain in the on-state following the removal of the turn-on gate current pulse.

Maximum Interruptible Current: The maximum amount of anode current that a GTO thyristor can successfully turn off. If the anode current exceeds the maximum interruptible current during turn-off, then the GTO thyristor will not turn off and will likely suffer device failure.

Maximum Surge Current: The maximum amount of anode current that a GTO thyristor is rated to conduct. If the anode current exceeds the maximum surge current at any point, then the GTO thyristor is likely to fail.

Pulsed power source: An electrical system designed to store energy over a long charge time and rapidly discharge the energy in a high current pulse. Pulsed power sources allow power supplies with low average power capability to drive applications requiring high instantaneous power levels

Safe Operating Area (SOA): The range of anode current and gate current values over which the GTO thyristor can operate without failing. The Safe Operating Area is related to energy dissipation within the GTO thyristor structure.

Snubber: A collection of components designed to protect the GTO thyristor during turn-on and turn-off. Turn-on snubbers typically consist of an inductor, resistor, and a diode, while turn-off snubbers typically consist of a capacitor, resistor, and a diode. Turn-on snubbers limit the rate at which the anode current rises during turn-on and turn-off snubbers control the rate at which the anode voltage can rise during turn-off.

Stray Inductance: Extra inductance found in any complete path (loop) in a circuit due to the surface area enclosed by the loop. Stray inductance becomes an issue in circuit paths where the current changes abruptly because it causes large voltage spikes.

ACKNOWLEDGMENTS

First, I would like to thank my thesis advisors, Dr. Todd Weatherford and Dr. John Ciezki, for providing expertise and guidance that was essential to the completion of this project.

Second, I would like to thank Mr. Joe Borraccini and the Office of Naval Research Ship Systems and Engineering Division, Advanced Naval Power Systems (ONR 331) program for providing the financial support for this project.

Third, I would like to thank Eric Adint for his invaluable instruction and assistance with the use of the high performance computing resources at the Naval Postgraduate School. Without his patience and effort, I would not have been able to complete this project.

Fourth, I would like to thank my parents for supporting and encouraging my interest in electronics and for teaching me the perseverance and dedication that I needed to complete this thesis.

THIS PAGE INTENTIONALLY LEFT BLANK

I. INTRODUCTION

Recent research efforts focused on increasing the energy storage and power output capacity of pulsed power sources have demonstrated that certain semiconductor switches can be used to interrupt (turn off) significantly more current than they are normally designed to turn off. Researchers at the Institute for Advanced Technology (IAT) at the University of Texas in Austin have found that Gate Turn Off (GTO) thyristors can be used in some railgun pulsed power sources to interrupt more than twice the amount of current that they are normally designed to interrupt. It may be possible to construct more energy dense pulsed power sources, particularly for railgun systems, if the factors responsible for increasing the current interruption capacity of the GTO thyristors can be identified and exploited.

The goal of this project was to develop a computer model of a GTO thyristor to investigate the electrical and the thermal characteristics of the devices when they are operated in a pulsed power circuit. The computer model was used to study the transfer, generation, conversion, and storage of electrical and thermal energy within the structure of the GTO thyristor during turn off. The simulation results were then used to predict the locations where device degradation and failure is likely to occur. This project demonstrates the use of physics-based computer modeling for the study of semiconductor power devices within the context of the external circuitry in which they operate.

A. RESEARCH APPROACH

This research project utilized a semiconductor simulation program suite to construct a physical model of a GTO thyristor and simulate its operation in a pulsed power circuit. The suite of programs, called SILVACO, was developed to perform physics-based simulation studies of semiconductor devices. The primary programs used for this research project were the device simulator, ATLAS^{TM}, and the plotting program, TonyPlot^{TM}.

The first phase of this project consisted of developing the physical model of the GTO thyristor and the SPICE circuit model of the inductive pulsed power circuit. ATLAS^{TM} comes with a variety of built in example files that demonstrate the various capabilities of the software suite. One of these example files simulated the basic electrical characteristics of a GTO thyristor turn-off [1]. The GTO thyristor example provided the basic framework for the physical model that was developed for this research project.

The second phase of the project involved validating the physical model of the GTO thyristor and the SPICE circuit model. The physical model and SPICE circuit were validated using a set of voltage and current waveforms that were collected during a previous experimental study of GTO thyristor turn-off [2]. In the circuit validation phase, the physical model was adjusted to match the IV characteristics of the simulated GTO thyristor to the experimentally measured IV characteristics. The validation phase was also used to account for the stray inductance of the experimental circuit in the SPICE simulation of the pulsed power circuit.

In the third phase of the project, the physical model and the SPICE circuit were used to investigate the turn-off characteristics of a multiunit GTO thyristor. This step further verified the physical model of the GTO thyristor by correctly simulating the current crowding, current filamentation, and local heating effects that have been shown in previous GTO thyristor modeling efforts [3] and [4]. For this part of the research project, the simulations were set up such that a structure file for the physical device was saved at each transient time point. Each structure file stored the solutions to the semiconductor physics equations at each point within the structure of the GTO thyristor for a specific transient time point. This data (electrical potential, current density, lattice temperature, carrier concentration, joule heating, carrier temperature, etc.) was used to investigate the transient electrical and thermal characteristics of the GTO thyristor during its operation in the pulsed power circuit.

In the fourth and final phase of the project, the simulations were used to investigate energy transfer within the GTO thyristor and the external pulsed power circuit. For each simulation, ATLAS^{TM} generated a log file that contained the nodal voltages and device currents for the SPICE based circuit. This data was used to calculate the amount of energy that was transferred to the GTO thyristor from the external pulsed power circuit. Additionally, the simulation was set up to probe the electrical and thermal properties (temperature, quasi-Fermi level, electron and hole concentration, etc.) at various points within the physical structure of the GTO thyristor. The resultant data was used to investigate the internal conversion, storage, and dissipation of electrical and thermal energy in the GTO thyristor.

B. RESEARCH OBJECTIVE

The goal of this project was to develop a computer model of a GTO thyristor to investigate the electrical and the thermal characteristics of the device when used in a pulsed power circuit. At present, most of the research into GTO thyristors and their limitations has focused on high switching frequency applications such as motor drives and switching mode power converters. However, the results of several research projects suggest that the limitations and electrical characteristics of GTO thyristors are very different for low switching frequency applications like pulsed power sources.

This project also sought to demonstrate a method for tracking the flow of energy through a semiconductor device. The simulations were set up to measure and record data that was used to calculate the amount of electrical and thermal energy that was input to or output from the GTO thyristor during its operation in a pulsed power circuit. Additionally, the data was used to track the conversion and storage of energy within the structure of the GTO thyristor. By tracking the flow of energy through the GTO thyristor, it is possible to predict the likely location(s) of device degradation and the potential mechanism(s) of device failure.

C. RELEVANCE TO THE DEPARTMENT OF DEFENSE

In a recent conference, the Interagency Advance Power Group (IAPG) identified the need for a physics-based simulation tool to evaluate the operation of semiconductor devices in their intended circuit application [5]. The IAPG is a collection of various DoD and civilian research agencies that collaborate on the research and development of advanced power electronics for military and civilian applications. Much of their research effort is aimed at developing new semiconductor technologies (Silicon Carbide and Gallium Nitride for example) and improving existing semiconductor technologies to improve the energy density and reliability of power sources and electronic devices.

At present, much of the research being performed with these new switching technologies is strictly experimental—the semiconductor devices are fabricated, placed into test circuits, and operated until either the tests are completed successfully or the devices fail. Unfortunately, these experiments can take a significant amount of time and money to set up and they usually do not lend themselves to directly examining what happens within the internal structure of the devices. Thus, it can be difficult to determine exactly how a device operates (or fails to operate) through experimentation.

A physics-based simulation tool would allow researchers to evaluate semiconductor devices, both new and existing technologies, with less physical experimentation. The researchers would be able to “prescreen” new semiconductor devices and see which devices merit further study and which devices require additional design effort. The simulations would also show what happens inside the semiconductor devices, which would allow the researchers to understand exactly how the devices operate and how they are likely to fail.

D. THESIS ORGANIZATION

The remaining chapters of this thesis are organized as follows: Chapter II provides background information on GTO thyristors and discusses the past research that provided the foundation for this thesis. Chapter III describes the

development and validation of the physical device model and SPICE circuit model that were used to simulate the operation of the GTO thyristor. Chapter IV outlines the method used to track the storage and transfer of thermal and electric energy within the structure of the GTO thyristor. Chapter V discusses the results obtained using the energy analysis method for single pulse and multiple pulse simulations of the GTO thyristor. Chapter VI compares the thermal and electric operating characteristics of uniform and non-uniform GTO thyristor devices. Chapter VII discusses the conclusions that can be made from the simulation results and Chapter VIII outlines the future work than can be done to extend this thesis.

THIS PAGE INTENTIONALLY LEFT BLANK

II. BACKGROUND

A. GATE TURN OFF THYRISTORS

Gate Turn Off thyristors (commonly referred to simply as GTOs) are solid-state semiconductor switches that are designed for high power switching applications. They have excellent voltage blocking capacity and very low forward conduction drop. They were developed in the 1980s to be one of the first fully controllable semiconductor power switches employing both turn-on and turn-off capability.

1. Physical Structure

Physically, a GTO thyristor is a four-layer semiconductor device that consists of multiple unit cells connected together in parallel. Each unit cell is comprised of alternating layers of n-type and p-type semiconductor material. In many GTO thyristors, the anode electrode is shorted directly to the wide n-base region as shown below in Figure 1; the anode shorts are typically added to improve the turn-off capability of a GTO thyristor [6].

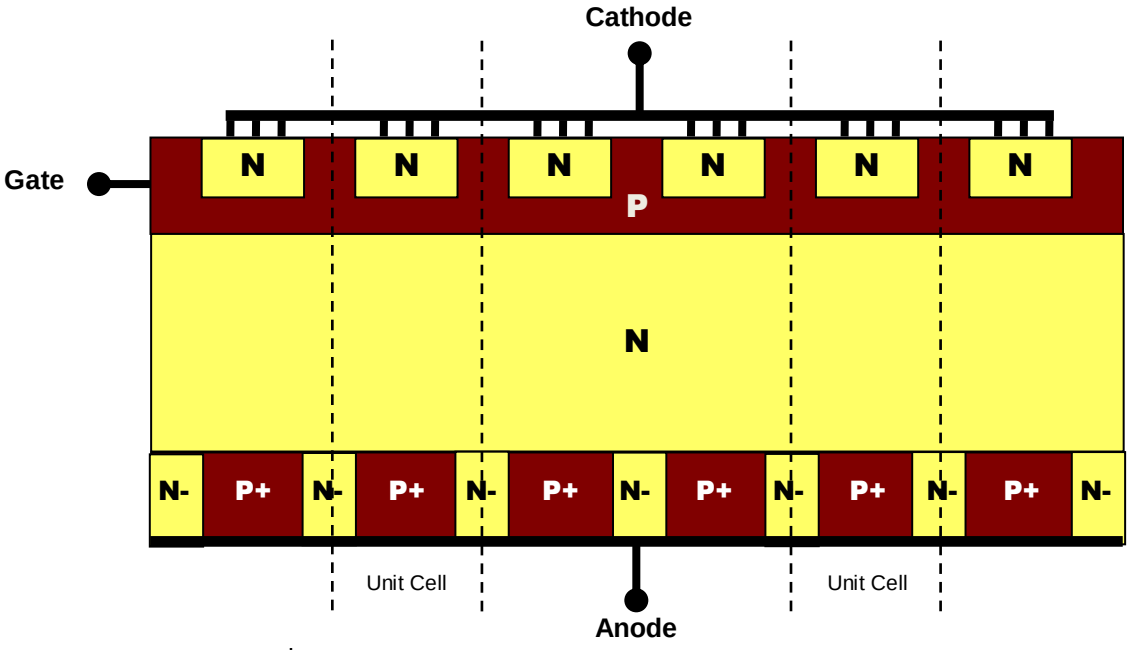

Figure 1. Physical Structure of a GTO Thyristor.

The four-layer structure of a GTO thyristor allows each unit cell to operate like a pair of coupled bipolar junction transistors as shown in Figure 2. In the off state, the wide n-base region is able to support a large depletion region, which allows the GTO thyristor to block a significant amount of voltage. In the on-state, the anode current keeps the transistor regions highly saturated which gives the GTO thyristor a low on-state voltage. Furthermore, since the anode current continually regenerates the n-base and p-base currents required to keep the two transistor regions saturated, the GTO thyristor continues to conduct even with no current flowing into its gate terminal [7].

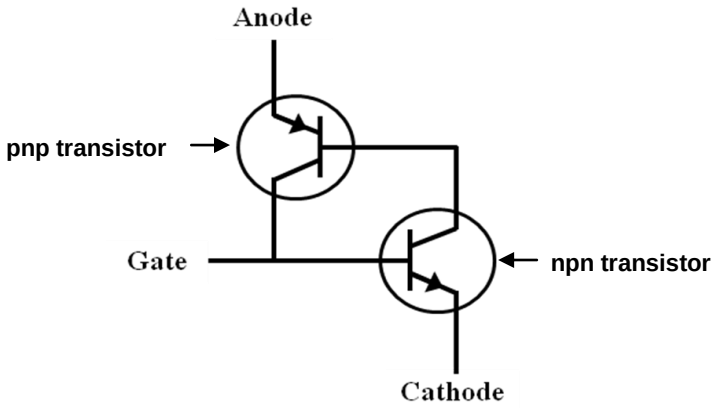

Figure 2. Two-Transistor Representation of a GTO Thyristor Unit Cell.

GTO thyristors are current-controlled devices that have two stable operating states, conducting and blocking. Like Silicon Controlled Rectifiers (SCRs), GTO thyristors have excellent voltage blocking and current conducting capabilities and, as described above, do not require a continuous gate current to remain in the conducting state. In the blocking state, the base currents for the transistor regions in each unit cell of the GTO thyristor are effectively zero and the transistor regions remain in the cutoff mode. In the conducting state, the anode current drives the two transistor regions in each unit cell into saturation and keeps the GTO thyristor in the current conducting state, so long as there is sufficient anode current to keep the two transistor regions saturated. The minimum amount of current needed to maintain current conduction is a physical device property commonly referred to as the “holding current” [7].

2. Operating Characteristics

GTO thyristors are turned on by applying a positive current pulse to the gate terminal. The gate pulse supplies the initial current necessary to drive the transistor regions of each unit cell into saturation, thereby allowing current flow from the anode to the cathode of the device. The turn-on current pulse has to last long enough to drive both transistor regions into saturation and allow the anode current to rise to a level sufficient to self-generate the base current needed to keep the transistor regions saturated. This minimum current level is another physical device property typically referred to as the “latching current.” A GTO thyristor will remain in the conduction state until either the anode current drops below the holding current or a turn-off current pulse is applied to the gate.

GTO thyristors are turned off by applying a negative current pulse to the gate terminal. The turn-off current pulse removes excess carriers from the p-base region of the thyristor, which interrupts the anode to cathode current flow and forces the transistor regions to enter their cutoff mode. The turn-off current pulse has to remove enough charge to force the p-base transistor into cutoff and it has to last long enough for the anode current to drop to zero and allow the n-base transistor to drop out of saturation and enter the cutoff mode [8].

In the blocking and conducting states, GTO thyristors are very robust devices; the wide n-base region allows GTO thyristors to safely block significant anode voltages and the low on-state voltage allows GTO thyristors to conduct large anode currents. However, GTO thyristors are susceptible to damage when transitioning between the blocking and conducting states. If the anode current rises too fast during turn-on or the anode voltage rise too fast during turn-off, a GTO thyristor will experience additional switching power losses and can suffer thermal degradation and/or failure as a result [9]. Because of this weakness, GTO thyristors are typically equipped with snubber circuits that limit the rate of anode current rise during turn on and anode voltage rise during turn off.

GTO thyristors have another interesting turn-off characteristic that can lead to device failure. In the conducting state, the anode current is split between the unit cells and evenly distributed across each individual unit cell. (Slight differences in on-state voltage cause the unit cells to have slightly different current densities.) During turn-off, the anode current is forced to the center of each unit cell until it is finally extinguished; this process, known as “pinch off,” creates local heating at the p-base/n-base junction in the center of each unit cell. Due to differences in on-state voltage and p-base resistance, the unit cells have slightly different turn-off times; consequently, as each successive unit cell turns off, the anode current is forced into the unit cells that are still conducting (a process known as current filamentation), which further increases the current density in those unit cells and causes increased local heating [10]. If one or more of the unit cells takes too long to pinch off, the GTO thyristor can fail because of excessive local heating.

The plot in Figure 3 shows the turn-off voltage and current waveforms for a typical GTO thyristor, [6]. The top plot shows the anode voltage (solid line) and the anode current (dotted line) during turn off. The bottom plot shows the gate voltage (solid line) and the gate current (dotted line) during switch turn off. A GTO thyristor typically turns off in three distinct stages – the storage phase, the fall phase, and the tail phase. In the storage phase, the gate current removes holes from the p-base and n-base regions, which establishes a potential barrier that starts pinching off the anode current. In the fall phase, the anode current falls quickly and the anode voltage starts to rise as the transistor regions drop out of saturation. In the tail phase, the anode voltage rises to its final value and the transistor regions enter cutoff as the remaining excess carriers in the n-base region are eliminated through recombination [9].

The two spikes in the anode voltage are caused by the stray inductances that are introduced by the external circuit components connected to the GTO thyristor. Stray inductance in the turn-off snubber is largely responsible for the initial voltage spike (V_{DSP}). The stray inductance delays the snubber action and

allows the anode voltage to rise uncontrolled until the snubber capacitor starts to charge (the snubber capacitor limits the rate of anode voltage rise – dv/dt). Stray inductances in the circuit load and the gate driver cause the anode voltage to overshoot its off-state value, which produces a voltage spike (V_{DM}) at the end of the turn-off transient. It is important to minimize stray inductance in the external circuitry in order to ensure safe operation of a GTO thyristor.

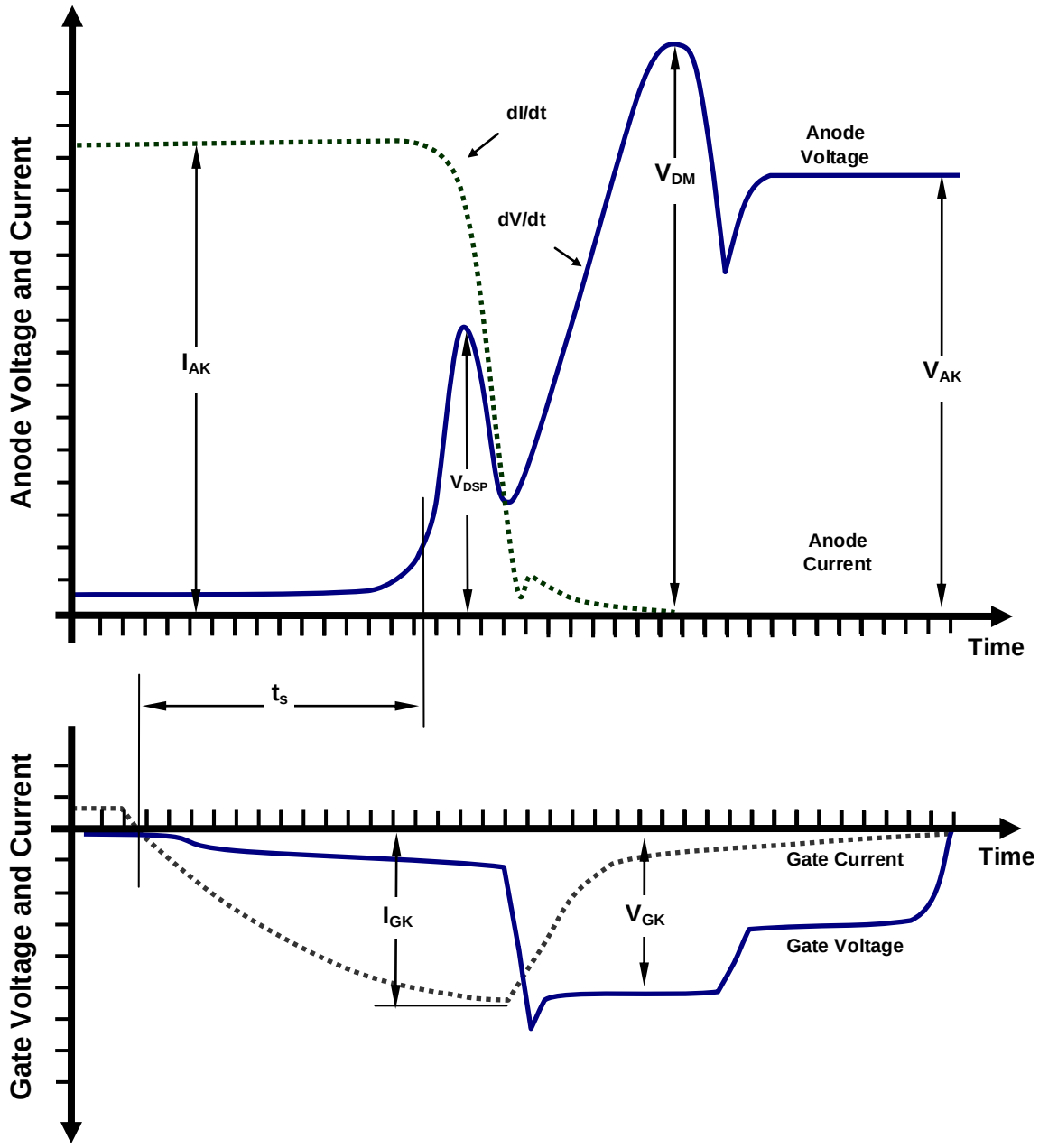

Figure 3. Nominal GTO Thyristor Turn-off Waveforms (From [6]).

The gate control circuit, typically referred to as the gate driver, has a significant impact on the turn-off characteristics of a GTO thyristor. The amount of turn-off current, I_{GK}, generated by the gate driver, directly affects the storage time required to remove enough carriers from the n-base and p-base regions to initiate the fall phase of the turn-off process. If the gate current is too small, the GTO thyristor can take too long to enter the fall phase, which can result in excessive local heating and device failure. Additionally, research has shown that the magnitude of the turn-off current affects the amount of anode current that the GTO thyristor can successfully turn off [2].The maximum turn-off current is often referred to on device datasheets as the "maximum interruptible current."

Safe operation of a GTO thyristor depends in large part on successfully maintaining proper voltage bias across the gate-cathode junction. The gate-cathode junction has to be forward biased (higher voltage at the gate relative to the cathode) in order to inject carriers into the p-based region and drive the GTO thyristor into its conduction state. Likewise, the gate-cathode junction needs to be reverse biased in order to remove carriers from the device and drive the device into its blocking state. If the gate-cathode junction is allowed to become forward biased during turn-off, one or more of the unit cells may "retrigger" and start conducting; the resultant anode current, combined with a high electric field at the n-base/p-base junction (due to the rising anode voltage), can cause excessive local heating and lead to device failure as shown in [6].

B. PAST RESEARCH INTO GTO THYRISTORS

The past research into modeling GTO thyristors can be divided into two broad categories, lumped element modeling and physics-based analytic modeling. Lumped element models, such as those seen in [11], [12], and [13], are circuit simulations (usually SPICE based) that use resistors, inductors, capacitors, transistors, and diodes, to mimic the electrical characteristics of GTO thyristors. Depending upon their complexity, lumped element models provide a computationally efficient method for approximating the electrical characteristics of

GTO thyristors. Physics-based analytic models use a structural representation of a semiconductor device, the thermal and electric properties of the device materials, and the external bias conditions as inputs to a simulation engine. The simulation engine takes the inputs and uses numerical methods to solve semiconductor physics equations at various points throughout the device (this approach is essentially a form of Finite Element Modeling). Physics-based models can more accurately simulate the electrical and thermal characteristics of a device; however, they generally require a significant level of computational effort to solve.

The underlying framework for the physical device model and the basic circuit simulation method were taken from several previous GTO thyristor modeling efforts. The physical device model was also validated using experimental data from a previous experimental investigation into the turn-off characteristics of GTO thyristors. The following subsections briefly outline the aspects of the projects that were relevant to the current research effort and discuss how the current research effort extends the past work done in those projects.

1. Experimental Analysis

The experimental data that was used to validate the physical model of the GTO thyristor device and the SPICE simulation of the external inductive pulsed power circuit came from an experimental study into the turn-off characteristics of GTO thyristors that was performed during a Trident Research Project at the United States Naval Academy in 2008. The study used a simplified inductive pulsed power circuit to study relationship between turn-off gate current and the maximum interruptible current of a GTO thyristor at low switching frequencies [2]. In the course of the project, a series of voltage and current waveforms were recorded for the GTO thyristor; these waveforms show the low frequency (single pulse) characteristics of a GTO thyristor operation.

The experimental data was useful for model validation because the current research project used a SPICE simulation of the same simplified inductive pulsed power circuit to provide the bias conditions for the physical device model. In addition to validating the physical model of the GTO thyristor, the experimental data allowed the SPICE simulation to be adjusted in order to model the stray inductances that were present in the experimental test circuit. This was important because stray inductance in certain circuit paths (the gate driver or turn-off snubber for example) can have a major impact on the turn-off characteristics of the GTO thyristor.

2. Electrical Modeling – Single Unit Cell

In [9], researchers used an analytical simulator (BAMBI) to examine current crowding, avalanche breakdown, and punch-through in a GTO thyristor. The model showed how current crowding occurs in a GTO thyristor and was used to determine the anode voltage at which punch-through and avalanche breakdown can occur during turn-off. The report identified the basic turn-off characteristics of a GTO thyristor and provided a qualitative validation of the physical model that was developed for the current research project.

The current research project sought to extend this past research project by developing a more complete physical model of the GTO thyristor. The original model did not consider the impact of temperature on the operating characteristics of the thyristor. Since the model only simulated the electrical characteristics of the GTO thyristor, the researcher only modeled one-half of a single unit cell to reduce the computational overhead of the simulations. Such a simplification is valid if the simulation only considers a single, symmetric unit cell. In the current research project, the physical model was expanded to represent the full unit cell in order to allow for the study of GTO thyristors with multiple and/or asymmetric unit cells.

3. Electrical Modeling – Multiple Unit Cells

In [3], researchers developed a physics-based model of a full GTO thyristor using the numerical simulator TACTICS. The physical model incorporated multiple unit cells and accounted for the electric and the thermal characteristics of the GTO thyristors. The researchers used a model consisting of three unit cells to investigate the maximum interruptible current of a GTO thyristor at high switching frequencies. As part of their investigation, the researchers showed how current filamentation occurs in a GTO thyristor. This information was used to further validate the multi-unit model developed in the current research project.

While the model used in [3] did account for temperature when solving the semiconductor equations, the researchers were not concerned with thermal energy generation and storage within the device structure. The current research project extends their multi-unit modeling effort by showing where thermal energy is generated and stored within the device structure. This knowledge is important to heat sink design, management of thermal stresses, and improving device reliability.

4. Electrothermal Modeling – Single Unit Cell

The simulation approach used to evaluate the operation of the GTO thyristor within the context of its external circuit were taken from the research project discussed in [14]. In this project, researchers used SILVACO to study the electrical and thermal turn-off characteristics of a GTO thyristor. The simulation used MixedMode, a function built into the device simulator ATLAS^{TM}, to incorporate a SPICE simulation of the external circuit into the simulation of the GTO thyristor. The researchers used the model to study the operation of a low frequency switching mode power converter (0 - 400 Hz switching frequency). The researchers were able to show local heating and the formation of hot spots during turn off; however, they only modeled one-half of a unit cell in order to limit the computational overhead and achieve reasonable simulation times.

The current research project utilized the same MixedMode approach to study the impact of the external circuit on the operation of the GTO thyristor. However, the physical device model was expanded to include the full unit cell in order to allow study of structural asymmetry and its effect on the turn-off process. Due to the availability of high performance computing resources, the full unit cell model was also expanded to study the turn-off characteristics of a multi-unit GTO thyristor device. The following chapter outlines the development and validation of the physical model of the GTO thyristor device and the SPICE circuit model of the inductive pulsed power circuit.

The current research project sought to expand on the work performed in [14] by developing a method for monitoring the flow of energy through a GTO thyristor during its operation. The device simulations were set up to probe the internal structure of the device and record how the lattice temperature, electron and hole concentration, electron and hole quasi-Fermi level, electron and hole temperature, and potential changed over time. The data was then used to track the conversion, transfer, storage, and dissipation of electrical and thermal energy within the semiconductor structure of the GTO thyristor. (Chapter IV discussion the energy tracking methodology that was developed for this project.)

The current chapter provided background information on the structure and operation of GTO thyristors and outlined the past research that provided the foundation for this project. The results of those projects were used to develop and validate the physics-based simulation that was used to investigate the operation of a GTO thyristor in an inductive pulsed power circuit. The following chapter describes the development and validation of the primary components of the physics-based simulation—the physical model of the GTO thyristor and the SPICE circuit model of the inductive pulsed power circuit.

III. SIMULATION DEVELOPMENT

A PHYSICAL DEVICE MODEL

The physical device model was created in ATLAS™ using a series of commands (listed in Appendix B) to generate a structural representation of the device and select material models to describe the electrical and thermal properties of the device. The structural representation specified the size and material composition of various sections of the device. The selected material models determined which electrical and thermal processes were considered during the simulations and the particular equations that were used to model those processes. Some of the material processes that could be incorporated into the physical device model included field dependent mobility, impact ionization, auger and Shockley-Read-Hall recombination, heat transfer and storage, band gap narrowing, and carrier energy balance (electron and hole temperature).

In SILVACO, the structural representation of a device is stored as a structure file that can be used as an input to later simulation efforts. In addition to describing the geometry and composition of a device, a structure files contains a mesh grid that specifies the locations within the device where ATLAS™ attempts to solve the semiconductor physics equations. Proper selection of the mesh grid is critically important to the success of a device simulation; if the mesh grid is not defined properly, the simulations will either not run (due to numerical convergence problems) or require excessive time to solve.

The structural representation used in this project was developed from an example file built into the SILVACO program. The example file simulated the electrical turn-off characteristics of a GTO thyristor using a structural representation of one-half of a unit cell [1]. The structure from the example file was expanded to include its mirror image in order to create the structural representation of a full GTO thyristor unit cell as shown in Figure 4. In the figure, the light-gray lines show the mesh grid that was used by the numerical simulator,

the blue diagonal lines identify the four electrodes of the GTO thyristor (anode, cathode, left gate, and right gate), and the violet lines show the junctions between the p-doped and the n-doped semiconductor regions.

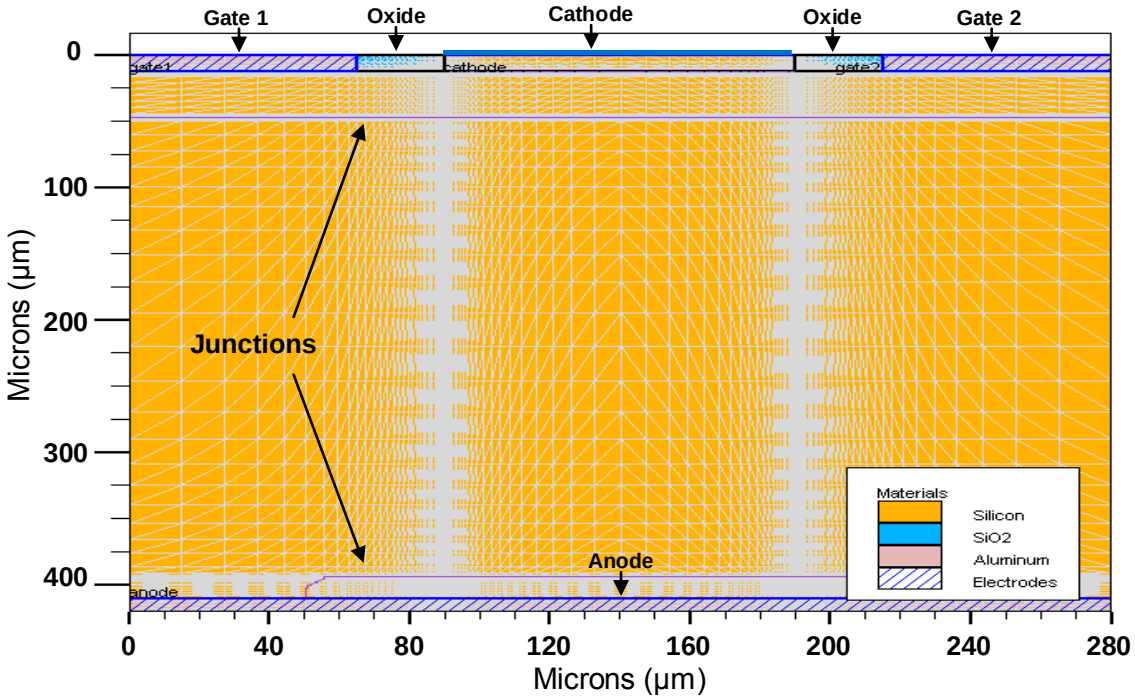

Figure 4. Thyristor Structure – Materials, Electrodes, and Mesh Grid.

During a simulation, ATLAS™ uses numerical methods to solve a series of differential equations at each point in the mesh grid. In order for the numerical solutions to converge properly, the mesh grid spacing had to be small anywhere there was high current density, high electric field, or large temperature gradients in the device. However, the grid spacing could not be kept small over the entire device because the required computational overhead and resultant simulation times would have been prohibitively large. Consequently, the grid spacing was varied across the device to provide a fine mesh grid at the junctions and interfaces while minimizing the overall number of points in the mesh grid. In Figure 4, it can be seen that the horizontal grid spacing varied from 15μm at the edges of the device to 250nm at the cathode-oxide interfaces, while the vertical grid spacing varied from 25μm at the center of the device to 200nm at the gate-cathode junction.

After creating the mesh grid and setting the geometry and composition of the device, ATLAS^{TM} applied a doping profile to the semiconductor materials to create the four-layer thyristor structure. Since SILVACO is designed to function as a “virtual” fabrication line, the doping profile was applied to the GTO structure in a series of sequential steps, just as if the device was physically being fabricated. The log plot of net doping concentration shown in Figure 5 indicates that the device has the characteristic p+npn- doping structure of a thyristor type device.

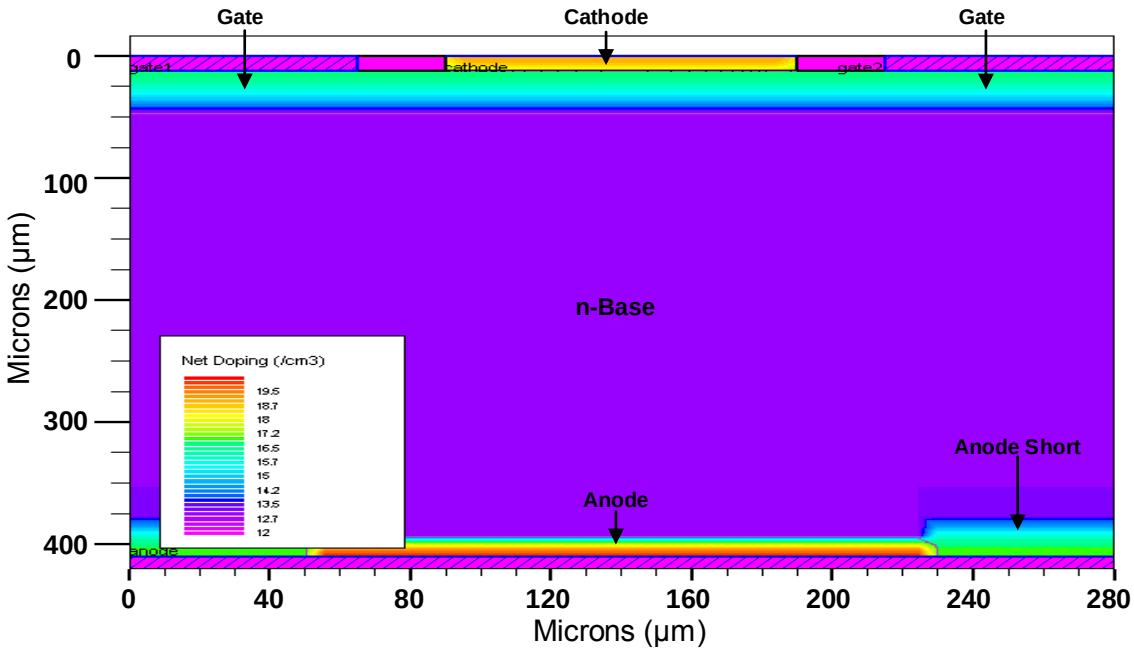

Figure 5. Net Doping of GTO Thyristor.

The following tables list the physical dimensions and composition of the GTO thyristor device, Table 1 lists the dimensions and doping concentrations for the semiconductor regions labeled in Figure 5, while Table 2 shows the dimensions and material composition of the four electrodes labeled in Figure 4. The values are similar to the actual dimensions and doping concentrations of the semiconductor regions in the small GTO thyristors studied in [2] and [14]. As in [14], the cathode was modeled as an infinitely thin sheet contact to reduce the number of grid points in the device structure and simplify the simulations.

Region	Width (μm)	Thickness (μm)	Doping (cm^{-3})
Cathode	100	13	n-type: 10^{19}
Gate	280	34	p-type: 10^{17}
n-Base	280	346	n-type: 10^{13}
Anode	170	17	p-type: 10^{20}
Anode Short	55	55	n-type: 10^{17}

Table 1. Dimensions and Doping Concentration of Thyristor Regions.

Electrode	Width (μm)	Thickness (μm)	Material
Cathode	100	--	Aluminum
Gate 1	65	13	Aluminum
Gate 2	65	13	Aluminum
Anode	280	10	Aluminum

Table 2. Dimensions and Composition of Thyristor Electrodes.

Most of the simulations performed for this project were run using the single unit cell structure shown in Figure 4. However, due to the availability of high performance computing resources, several simulations were run using an expanded structure file that modeled three unit cells. The expanded structure shown in Figure 6, was generated using the commands listed in Appendix C and was used to investigate the thermal and electric characteristics of current crowding and current filamentation.The multiple unit cell structure was used to evaluate the impact of non-uniform gate doping on the operation of GTO thyristors.

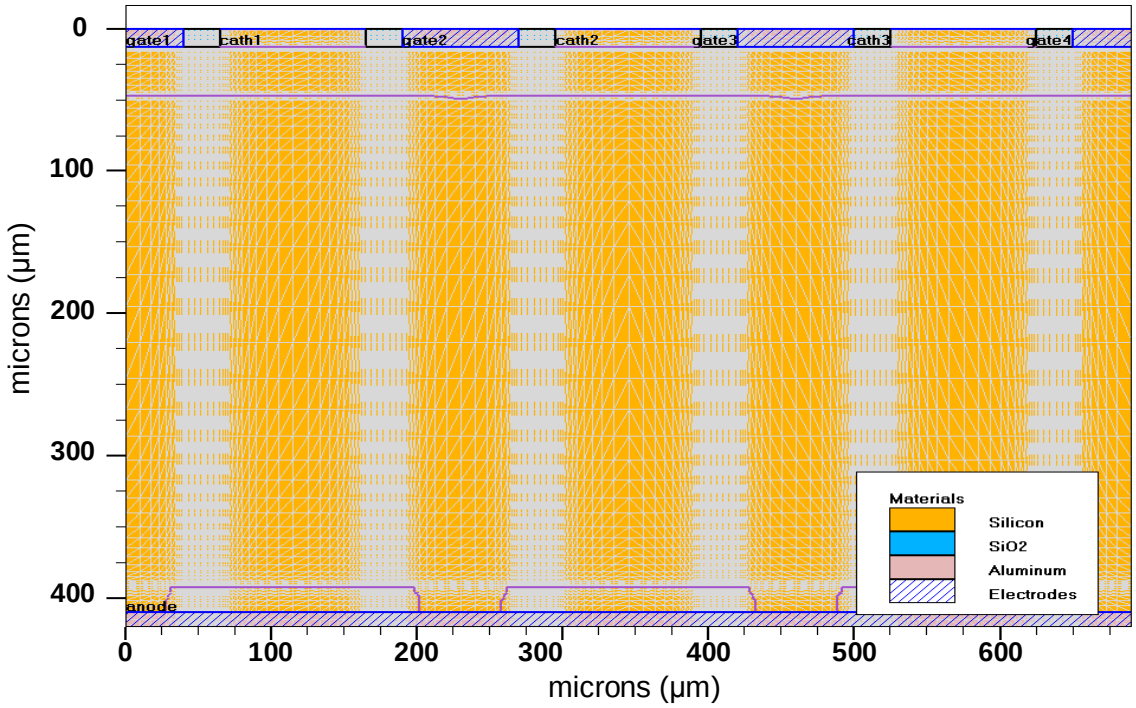

Figure 6. Expanded Thyristor Structure (Three Unit Cells).

SILVACO uses a collection of material models to simulate the various physical processes that take place within a semiconductor device during operation. Incorporating the correct material models into the physical device model allows the device simulator to accurately simulate the operation of a semiconductor device. For this project, material models were incorporated into the physical device model to account for the following physical process: concentration dependent mobility, electric field dependent mobility model, band gap narrowing, Auger and Shockley-Read-Hall recombination, impact ionization, temperature dependent thermal conductivity and heat capacity, joule heating, heating due to carrier recombination-generation, and Peltier-Thompson heating. These material models, which are discussed in [15], were selected based on the GTO thyristor operating characteristics identified in [4], [13], [16], [17], and [18].

In order to simulate the thermal characteristics of the GTO thyristor device, a thermal contact was added to the bottom surface of the anode electrode. The thermal contact had a specified external temperature of 300K and a thermal resistance of 1 K-cm^2/W. The thermal resistance was selected based

on the junction-case thermal resistance for the experimental GTO thyristor device that was used to validate the device model. (Appendix F contains the data sheet for the GTO thyristor device).

B. SPICE MODEL OF THE PULSED POWER CIRCUIT

The stated objective of this research project was to study the operating characteristics of a GTO thyristor within an inductive pulsed power circuit. SILVACO incorporated a SPICE-type circuit simulator into its semiconductor device simulator. As shown in [14], these MixedMode simulations can be used to study the operation of semiconductor devices under realistic circuit conditions.

For this project, the SPICE circuit model was constructed based on the simplified inductive pulsed power source used in [2]; Figure 7 shows the notional design for this simplified inductive pulsed power circuit. The circuit is essentially a simplified inductive pulse forming network. When the GTO thyristor turns on, energy is transferred from the capacitor bank to the pulse forming inductor; then, when the GTO thyristor turns off, that energy is forced from the inductor into the attached diode as a high power current pulse. The essential elements of this circuit are the capacitor bank/voltage source, the pulse forming inductor, and the GTO thyristor with its attached circuitry.

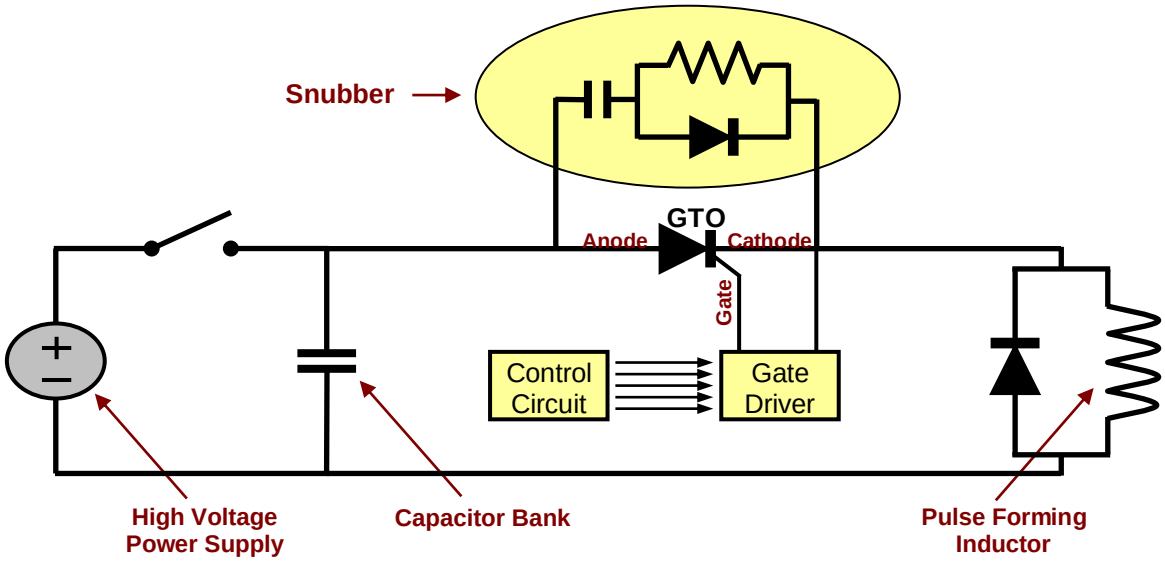

Figure 7. Notional Inductive Pulsed Power Circuit (From [2]).

Figure 8 shows the circuit diagram for the SPICE model that was ultimately developed for the GTO thyristor simulations; the parameters for the various circuit components are listed in Table 3. From the circuit diagram, it can be seen that the SPICE model incorporates many components that are not part of the notional inductive pulse power circuit shown in Figure 7. These components were added during validation of the circuit model in order to fit the simulation waveforms to the experimental data. The inductors Lgto, Lstray, Lsnubber, and Lgate were added to model the stray inductance in the experimental circuit; the resistors Rsource, Resr, Rpulse, and Rgate-src were used to model the series resistance of the power supply, capacitor bank, pulse forming inductor, and gate supply respectively. To ensure that the SPICE simulator operated properly, four resistors were added to the circuit to ensure that every node in the circuit model had a DC path to ground; these resistors, labeled Rgnd, had very large resistance values to minimize their impact on the operation of the circuit.

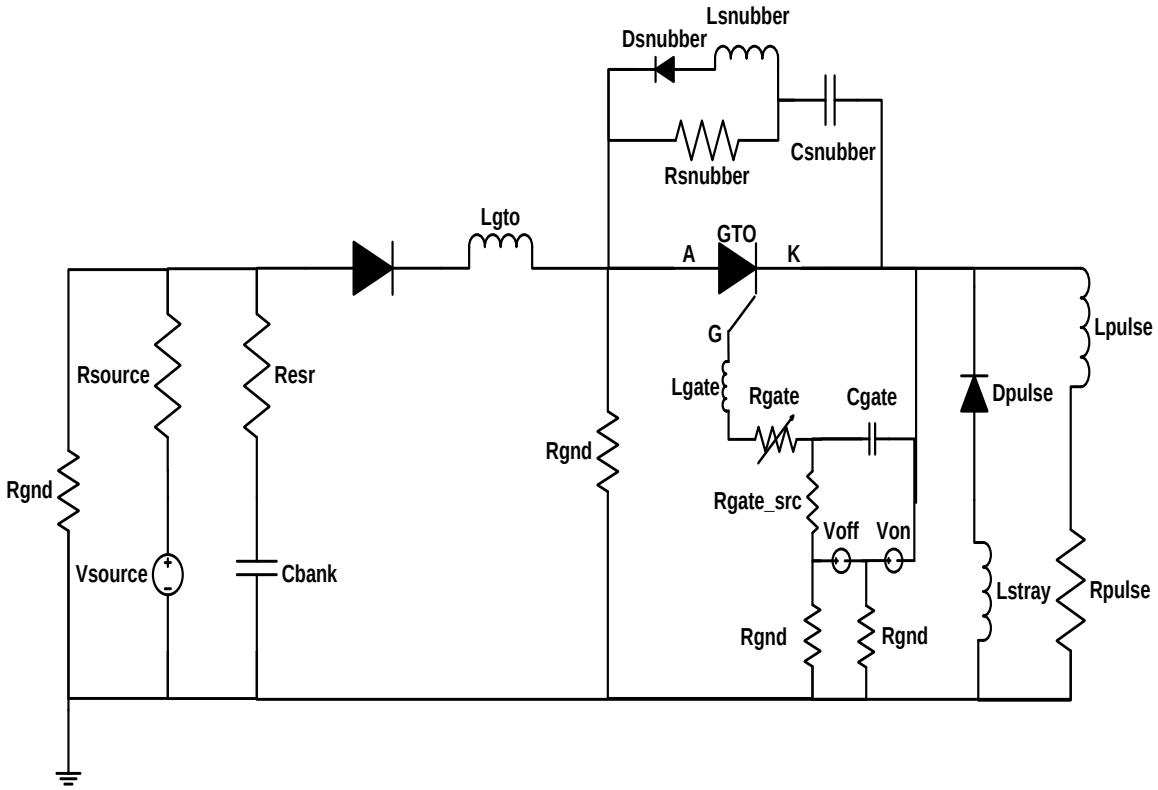

Figure 8. SPICE Model of the Inductive Pulsed Power Circuit.

Component	Value		Component	Value
Vsource	0-100V		Rsource	1Ω
Cbank	9.6mF		Resr	54.3mΩ
Ldgto	10nH		Rsnubber	100Ω
Lsnubber	10nH		Csnubber	470nF or 940nF
Lgate	10nH		Rgate	5mΩ – 1kΩ
Voff+Von	0-±25V		Cgate	2mF
Lpulse	4.62mH		Rpulse	1.03Ω
Lstray	10nH		Rgnd	100kΩ

Table 3. Component Values for SPICE Circuit Model.

The gate driver for the experimental test circuit used in [2] had two separate capacitors that were connected to the GTO thyristor through four MOSFETs arranged in an H-bridge; one of the capacitors supplied the turn-on pulse and the other capacitor supplied the turn-off pulse. In order to meet the time constraints of the thesis, the gate driver circuit was simplified by replacing the MOSFETs with a time varying resistor (Rgate) and using two variable DC voltage sources (Von and Voff) to provide the appropriate polarity to the gate capacitor (Cgate) in order to generate the turn-on and turn-off gate current pulses.

C. MODEL VALIDATION

The SPICE circuit model and the physical device model were validated by comparing the results of several simulations to the experimental IV waveforms (anode voltage, anode current, gate voltage, and gate current) collected in [2]. Initially, the simulated device waveforms were compared with several full-pulse experimental waveforms to verify that the simulations ran properly. The models were further validated by comparing the simulated turn-off transients to the experimental turn-off transients. During this phase of the validation process, the stray inductance values (lgate, lgto, lsnubber, and lstray) were adjusted to approximately fit the simulation waveforms to the experimental data.

The following figures show how the simulated device waveforms compare to the full pulse experimental waveforms. Figure 9 shows how the simulated anode voltage (blue) and current (red) compare to the experimental anode voltage (black) and current (green) for a 5ms pulse where the initial voltage on the capacitor bank was 80V. Figure 10 shows how the experimental and simulated anode currents and voltages compare for a 8ms pulse with an initial capacitor bank voltage of 100V (both plots use the same color scheme).

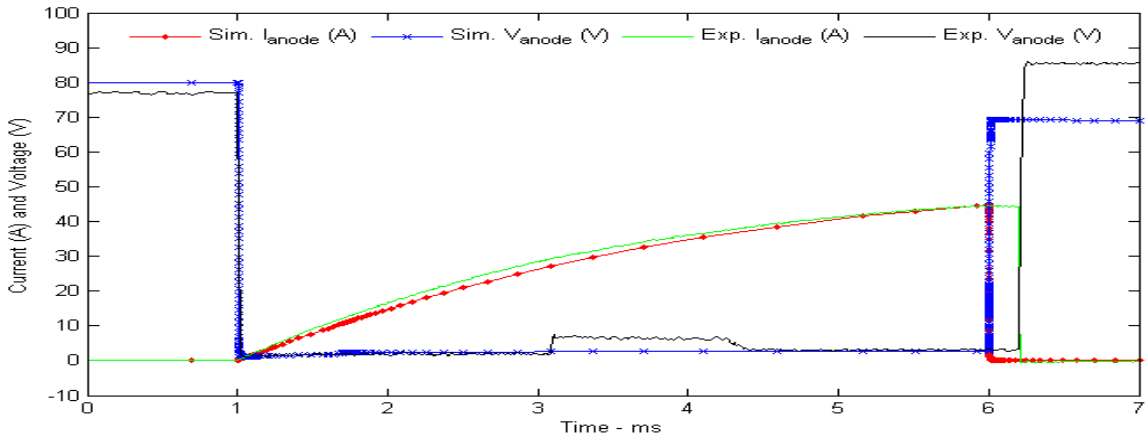

Figure 9. Full Pulse Comparison – 5ms Pulse with 80V Cbank.

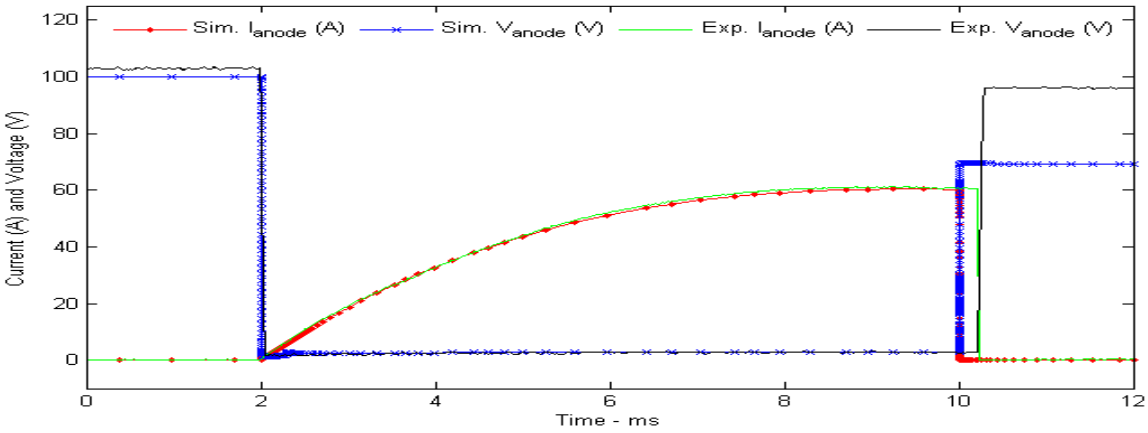

Figure 10. Full Pulse Comparison – 8ms Pulse with 100V Cbank.

From the plots shown in the preceding figures, it can be seen that the physical device model accurately simulates the on-state characteristics of the GTO thyristor that was studied in [2]. From the plot, it appears that the off-state characteristics of the physical device are different from the experimental device;

the simulated device turns off sooner and has a lower final voltage than the experimental device. These differences are actually due to the SPICE circuit model, not the physical device model. The simulated device turned off sooner because the SPICE circuit model does not account for the propagation delays in the experimental gate control circuitry (the experimental test circuit used an FPGA device to control the gate driver). The final anode voltage of the simulated device was smaller than the measured anode voltage because the SPICE circuit model uses a simple voltage source with series resistance instead of the more complex switching mode power supply used in the experimental test circuit.

Final validation of the physical model of the GTO thyristor device was achieved by running turn-off simulations using two different snubber capacitance values. One simulation was performed using a 470nF snubber capacitor, while a second simulation was performed using a 940nF snubber capacitor. In both simulations, the capacitor bank had an initial voltage of 100V and the GTO thyristor was turned off after conducting for 5ms. The resulting turn-off waveforms were compared with the experimental data and used to adjust the stray inductances in order to match the simulated anode voltage spikes (initial and final) to the experimental waveforms. Unfortunately, it was not possible to perfectly match the simulation waveforms to the experimental data[1] due to the time constraints of the thesis process.

Figure 11 shows the simulated GTO thyristor turn-off waveforms that were generated using a 470nF snubber capacitor, while Figure 12 shows the corresponding experimentally measured turn-off waveforms. Figure 13 shows the simulated turn-off waveforms that were generated using a 940nF snubber capacitor, while Figure 14 shows the corresponding experimental turn-off waveforms. The figures show that the physical device model and SPICE circuit model correctly simulate the transient turn-off characteristics of a GTO thyristor device.

---

[1] The high frequency oscillations in the experimental waveforms were caused by electromagnetic interference in the differential voltage probes used to measure the anode and gate voltages [2].

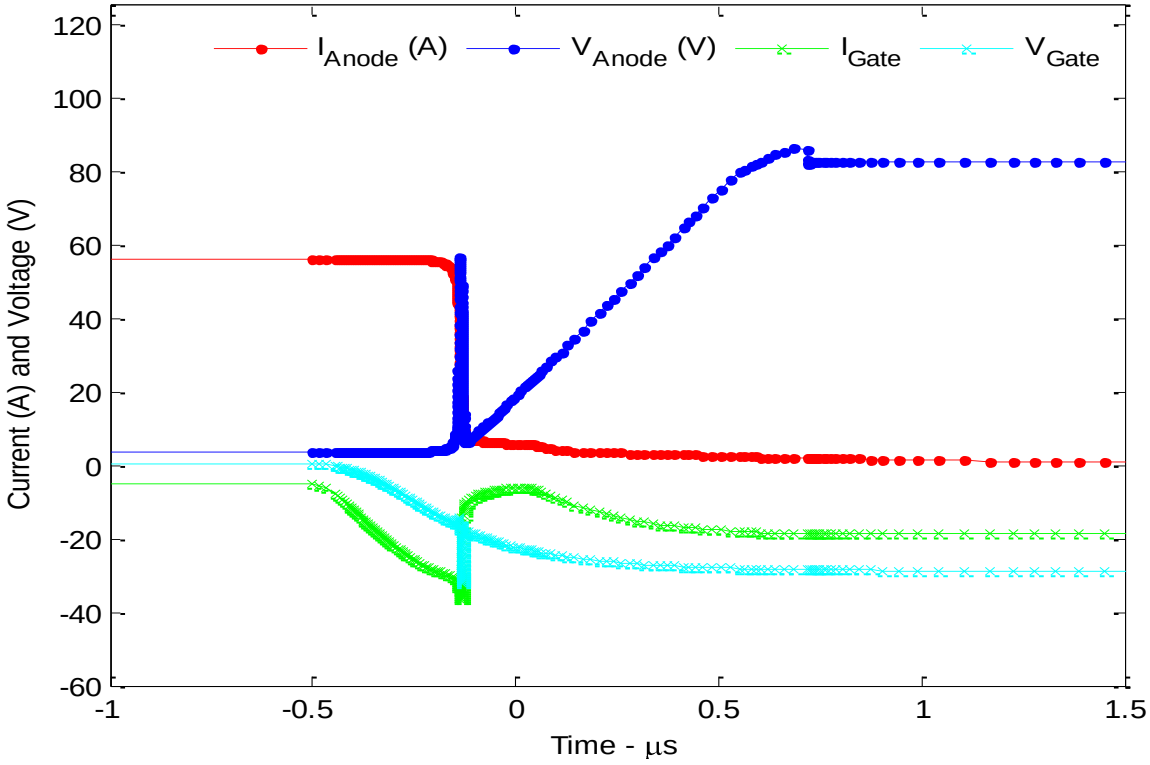

Figure 11. Simulated Turn-off Transient (470nF Snubber Capacitor).

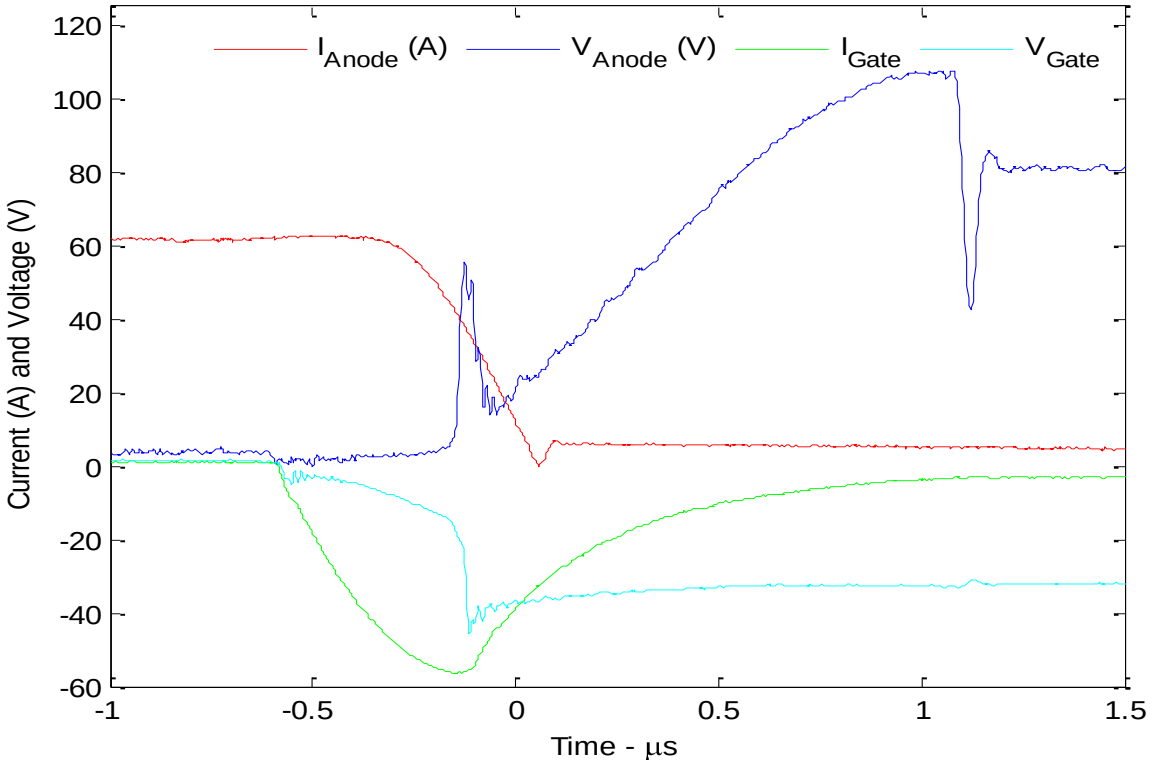

Figure 12. Experimental Turn-off Transient (470nF Snubber Capacitor).

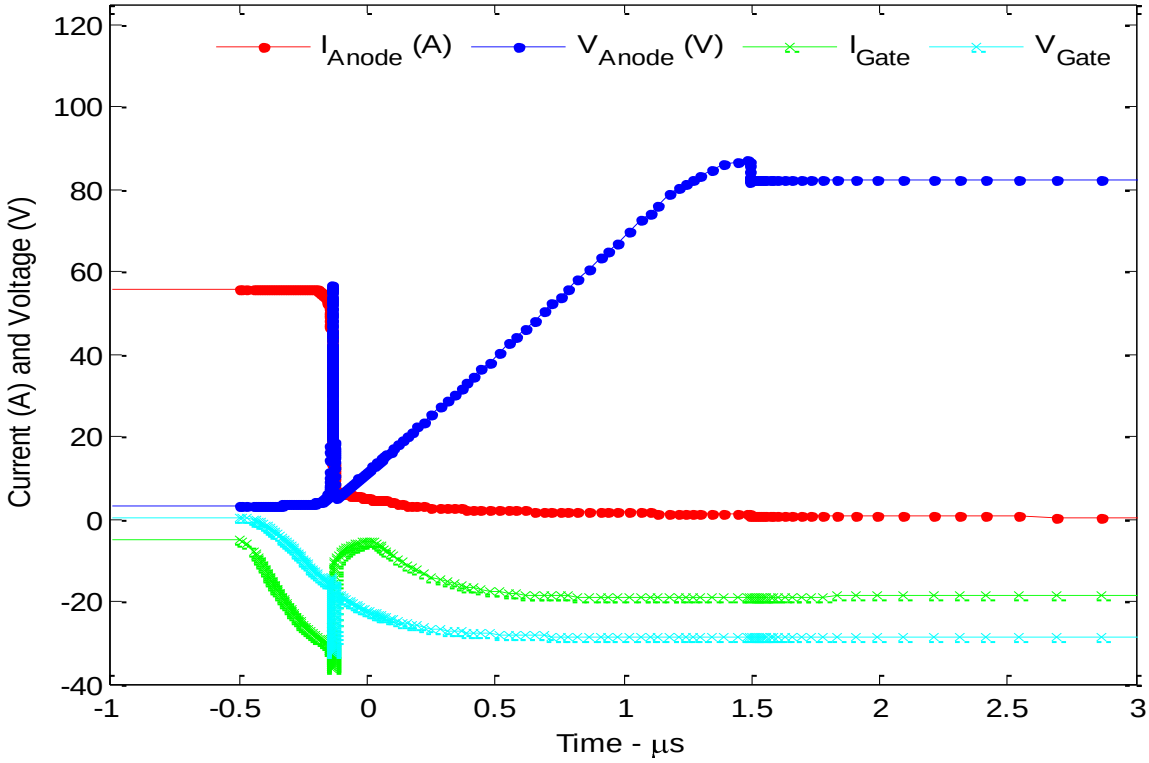

Figure 13. Simulated Turn-off Transient (940nF Snubber Capacitor).

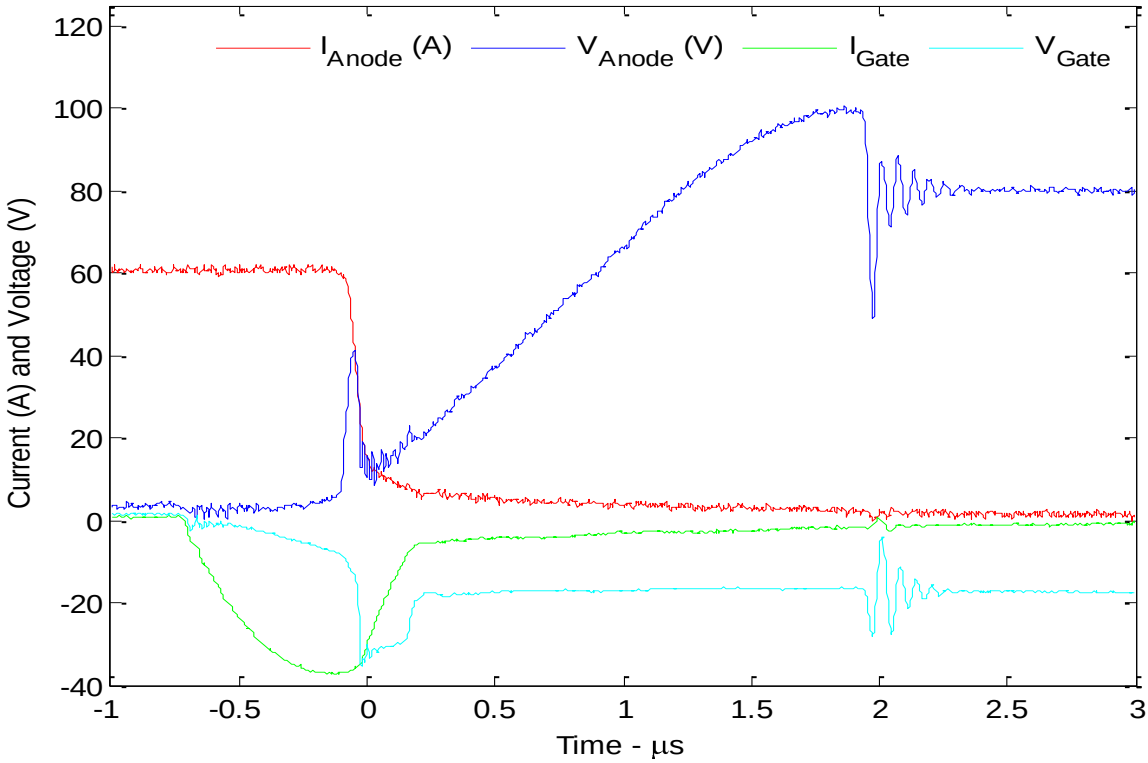

Figure 14. Experimental Turn-off Transient (940nF Snubber Capacitor).

This chapter describes the physical device model and the SPICE circuit model that were uses to simulate the operation of a GTO thyristor in an inductive pulsed power circuit. The chapter also outlines the validation of the models using experimental voltage and current waveforms. The next chapter discusses the energy tracking method that was developed in this project to investigate the transfer and storage of thermal and electric energy inside the GTO thyristor.

THIS PAGE INTENTIONALLY LEFT BLANK

IV. ENERGY TRACKING METHODOLOGY

The primary objective of this project was to develop a method for tracking the flow of energy within a semiconductor device using a physics-based device simulator. The most accurate way to track the storage, generation, and transfer of energy in a semiconductor device would be to compute the electrical and thermal energy stored in the device for each simulation time point using the data from every point in the mesh grid. This method would require ATLAS™ to save a solution file for the device at each transient time point and then use the solutions to compute the energy stored in the device – one solution file at a time. Unfortunately, this particular method was not practical for the current project because each GTO thyristor simulation had a significant number of transient time points (usually in excess of 700 time points).

Ultimately, it was decided to approximate the stored energy values using a much smaller set of points within the device. During each simulation, ATLAS™ measured the lattice temperature, electric potential, and carrier concentration at 181 probe points in the device (for comparison, the device mesh grid had 8854 points). These measurements were stored in a single log file and used with a MATLAB® script (shown in Appendix E) to compute the electrical and thermal energy stored in the device. The following sections show the location of the probe points, describe how the measurements were converted into energy values, and discuss how electrical energy was tracked in the simulated inductive pulsed power circuit.

A. PROBE LOCATIONS AND DEVICE SECTIONS

Instead of saving a structure file for each transient time point of a simulation, ATLAS™ stored the data generated by each simulation in a text-based log file. The log file contained the nodal voltages and component current for the SPICE circuit model of the inductive pulsed power circuit; additionally, the log file contained measured data from 181 different locations in the GTO thyristor

device. Figure 15 shows the locations in the device structure where ATLAS™ probed the device and measured the lattice temperature, electron and hole quasi-Fermi level (related to electric potential), and electron and hole concentration. From the figure, it can be seen that the spatial density of probe locations was higher in gate and cathode regions than in the n-Base region or device electrodes. The higher density was necessary to ensure that the device simulator properly tracked the steep temperature, current, and potential gradients that occur in the gate and cathode regions during turn off.

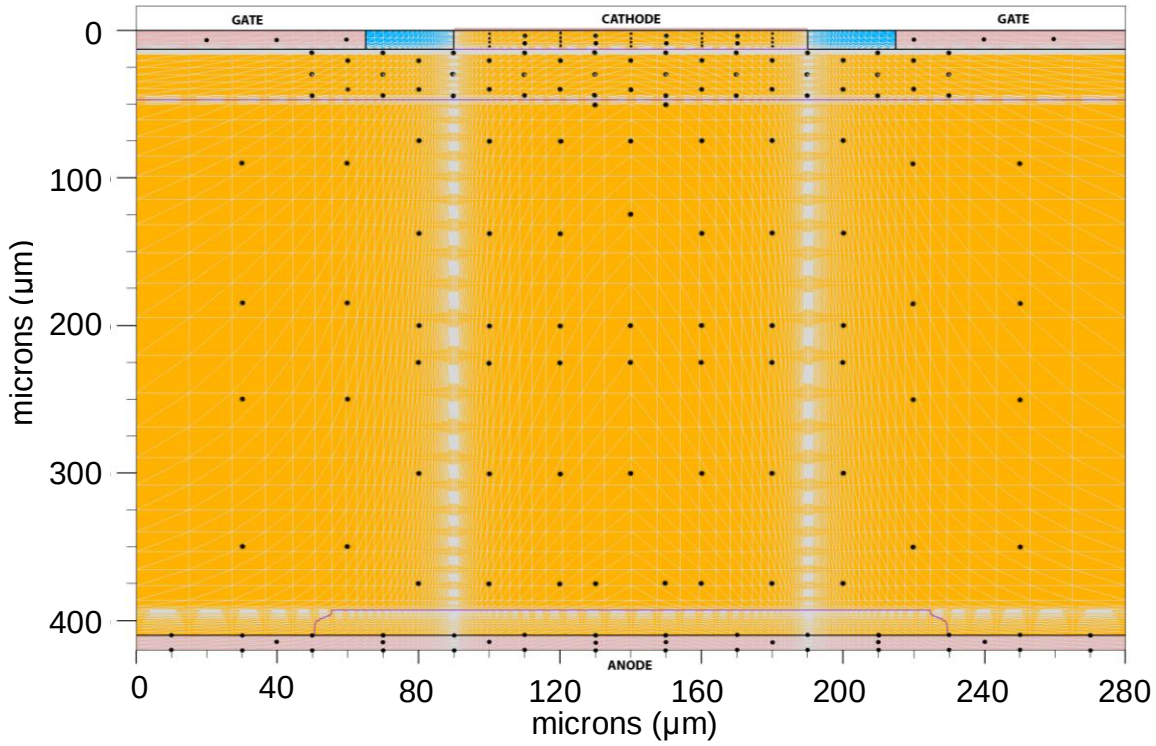

Figure 15. Probe Locations Used for Energy Storage Calculations.

The device structure was divided into the ten different sections shown in Figure 16 in order to calculate the amount of energy stored in the GTO thyristor. The data measured from the different probe points was used to compute the average lattice temperature, quasi-Fermi levels, and mean carrier concentration in each section; from these values, it was possible to determine the amount of energy stored in the device. Additionally, it was possible to calculate the amount of energy that was transferred out of the device through the thermal contact.

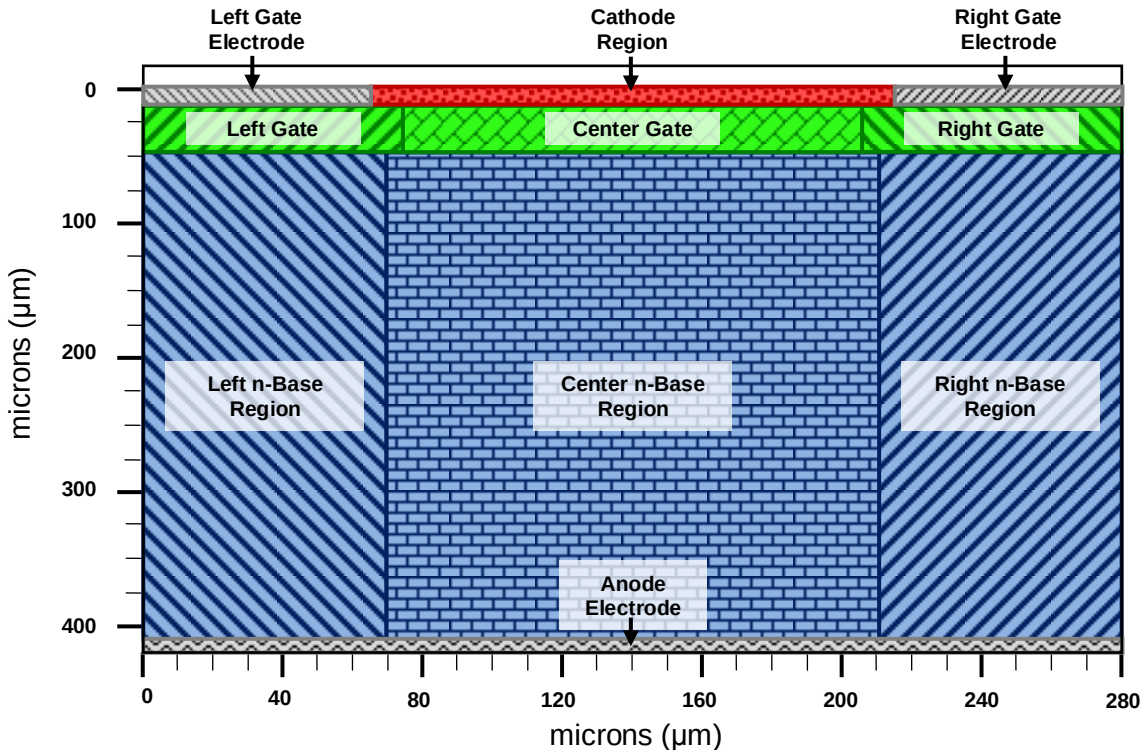

Figure 16. Device Sections Used for Energy Storage Calculations.

In addition to the average lattice temperature, quasi-Fermi levels, and carrier concentrations, the volume of each section was required to compute the energy stored in the device. Table 4 lists the width and thickness (height) of the device sections (all of the sections have a length of 10^4µm). The type of material for each section, also shown in the table, determined which heat capacity and thermal conductivity values were used in the energy calculations.

Section	Dimensions	Section	Dimensions
Cathode Region	150µm x 13µm (Silicon)	Left n-Base Region	70µm x 376µm (Silicon)
Left Gate Region	75µm x 34µm (Silicon)	Center n-Base Region	140µm x 376µm (Silicon)
Center Gate Region	130µm x 34µm (Silicon)	Right n-Base Region	70µm x 376µm (Silicon)
Right Gate Region	75µm x 34µm (Silicon)	Left Gate Electrode	65µm x 13µm (Aluminium)
Anode Electrode	280µm x 10µm (Aluminium)	Right Gate Electrode	65µm x 13µm (Aluminium)

Table 4. Material Composition and Dimensions of Device Sections.

B. TRACKING ENERGY FLOW IN THE GTO THYRISTOR DEVICE

The previous section showed how the GTO thyristor structure was divided into sections and discussed how the measured data was used to compute the average lattice temperature, quasi-Fermi levels, and carrier concentration for each section. The current section shows how the temperature, Fermi level, and concentration value were converted into energy values. In particular, this section discusses the equations that were used to evaluate thermal energy output, thermal energy storage, and electrical energy storage (both static and dynamic) in the GTO thyristor.

1. Thermal Energy Output

For this project, the thermal contact was placed along the bottom of the anode electrode and given a specified thermal resistance R_{th} = 1 K-cm^2/W. During the simulations, the temperature of the thermal contact would rise above the external ambient temperature (T_{base} = 300K) as thermal energy was generated inside the device. By measuring the temperature of the thermal contact, i.e., the bottom of the anode electrode, it was possible to determine the thermal output power and heat flow through the thermal contact.

The heat flow (Q_{out}) through the thermal contact of the GTO thyristor was computed by numerically integrating the thermal output power with respect to the simulation time. The thermal output power of the thermal contact was determined using the expression shown in (1).

$$P_{thermal} = \frac{w \cdot l}{R_{th}} \left(T_{contact} - T_{ext} \right) \qquad (1)$$

where *l* and *w* are the length and width of the thermal contact (cm), R_{th} is the thermal resistance of the contact (K-cm^2/W), $T_{contact}$ is the average temperature of the thermal contact (K), and T_{ext} is the external ambient temperature (K).

2. Stored Thermal Energy

When a GTO thyristor conducts current, thermal energy is generated inside the device by joule heating and recombination-generation heating. The thermal energy spreads out into the device and causes the lattice temperature of the device to increase. Using the appropriate specific heat capacity, the thermal energy stored in any given section of the GTO thyristors can be calculated from the average lattice temperature of the section.

SILVACO provides a number of material models to describe specific heat capacity [15]. For this project, the physical device model was implemented using the temperature dependent model shown in (2).

$$C_h\ \ T_{lat}\ \ = hc.a + hc.b \cdot T_{lat} + hc.c \cdot T_{lat}{}^2 + \frac{hc.d}{T_{lat}{}^2} \qquad \textbf{(2)}$$

where T_{lat} is the lattice temperature (K) and C_h is the specific heat capacity of the material (J/K-cm^3). The four coefficients *hc.a* (J/K-cm^3), *hc.b* (J/K^2-cm^3), *hc.c* (J/K^3-cm^3), and *hc.d* (JK/cm^3) were used to fit the temperature dependent heat capacity model to the properties of the material being studied (aluminum or silicon in the case of this project). The equation was used with the average lattice temperature to compute the approximate heat capacity of each semiconductor region.

The total thermal energy stored in the GTO thyristor was determined by adding up the thermal energy stored in each section of the device. The thermal energy in each section of the GTO thyristor was computed using the expression shown in (3).

$$E_{thermal} = C_{\mathrm{h}} V_{\mathrm{section}}\ \ T_{lat} - T_{ext} \qquad \textbf{(3)}$$

where C_h was the specific heat capacity of the material, $V_{section}$ was the volume of the section, T_{lat} was the average lattice temperature in the section, and T_{ext} was the external temperature.

3. Electric Potential Energy

Electrical energy is stored in a semiconductor device by establishing a potential difference between two or more quasi-stationary charges. Thus, the electric potential energy in a semiconductor device is directly proportional to the number of charges and the positions of the quasi-Fermi levels. The expression used to compute the electrostatic potential energy density in the GTO thyristor sections is shown in (4)

$$E_{\text{electrostatic}} = n \ \ QFN - FL_{ref} \ \ + p \ \ QFP - FL_{ref} \quad \textbf{(4)}$$

where n and p are the average electron and hole concentrations (cm^{-3}), QFN and QFP are the average electron and hole quasi-Fermi levels (eV), and FL_{ref} is the reference Fermi level for the device (eV). The electric potential energy in each section of the device was computed by multiplying the potential energy density from (4) by the fundamental charge of an electron (to convert the energy value from electron volts to joules) and the volume of the section. The total electric potential energy was determined by adding up the potential energy in the individual sections of the device.

4. Net Change in Energy of GTO Thyristor

By calculating the energy output through the thermal contact and computing the total energy stored in the GTO thyristor, it was possible to create an energy balance expression for the GTO thyristor. This expression, shown below in (5), represents the net change in the energy of the GTO thyristor device.

$$\Delta E_{gto} = E_{in\_electric} - E_{out\_thermal} - E_{electrostatic} - E_{thermal} = 0 \quad \textbf{(5)}$$

where $E_{in\_electric}$ is the electrical energy that is input to the device from the SPICE circuit, $E_{out\_thermal}$ is the thermal energy that is output from the device through the thermal contact, and $E_{thermal}$ and $E_{electrostatic}$ arethe stored thermal energy and electric in the device . In order for the GTO thyristor to satisfy the first law of thermodynamics, the net change in energy of the GTO thyristor must be zero.

C. TRACKING ENERGY FLOW IN THE SPICE CIRCUIT

In order to determine the amount of electrical energy that was input to the GTO thyristor, it was necessary to track the flow of energy through the SPICE circuit model. ATLAS™ saved the nodal voltages and device currents for the SPICE circuit at each time point in the simulations; so it was easy to calculate the energy supplied, stored, or dissipated in the various circuit components. The computed energy values were then used to verify that the net change in energy was zero for the inductive pulsed power circuit and the GTO thyristor.

Several different methods were used to determine the energy stored, dissipated, or supplied by the different components in the inductive pulsed power circuit: For the capacitors and inductors in the circuit, the stored energy was calculated directly from the device voltage (capacitor) or current (inductor). For the resistors, the dissipated energy was computed by numerically integrating the instantaneous power dissipation with respect to simulation time; the power dissipation for each resistor was computed using the device current and resistance value. For the voltage sources, the supplied energy was computed by integrating the instantaneous supply power (the product of current and voltage) over the simulation time.

The electrical energy input (dissipated in) the GTO thyristor was computed by integrating the anode power and gate power with respect to the simulation time. In order to determine the anode power and gate power, the MATLAB® script multiplied the anode and gate current by the corresponding voltage values. The gate and anode voltages were computing using the SPICE nodal voltage for the anode, cathode, and gate terminals of the GTO thyristor device.

Determining the amount of energy stored, dissipated, or supplied by each component in the SPICE circuit allowed the total change in energy of the inductive pulsed power circuit to be evaluated. Given that the SPICE circuit model represents a closed system, the net change in energy of the circuit should

be zero for the entire simulation. Equation (6) represents the net change in energy for the SPICE circuit model of the inductive pulsed power circuit.

$$\Delta E_{SPICE} = E_{input} + E_{resistors} + E_{GTO} + E_{store\_LC} = 0 \quad \textbf{(6)}$$

where E_{input} is the total energy provided by the voltage sources, $E_{resistors}$ is the energy dissipated in all the circuit resistance, E_{gto} is the electrical energy input to the GTO thyristor, and E_{store_LC} is the energy stored in the inductors and capacitors of the circuit.

This chapter has outlined a methodology for tracking the flow of energy in a semiconductor device using physics-based device simulation. The next chapter shows the use of this method to analyze several different simulations of the GTO thyristor.

V. ENERGY ANALYSIS RESULTS

For this project, data from four different simulations of the GTO thyristor was used to demonstrate the energy tracking methodology. In two of the simulations, the GTO thyristor was operated for a single pulse using a different size snubber capacitor for each simulation. In the remaining simulations, the GTO thyristor was operated for multiple pulses using different thermal contact resistances. The following sections of this chapter show the results of the energy analysis of the simulations and discuss how the snubber capacitance and thermal contact resistance influence the operating characteristics of the GTO thyristor.

A. SINGLE PULSE ENERGY TRANSFER AND STORAGE

In both single pulse simulations of the GTO thyristor, the capacitor bank (labeled *Cbank* in Figure 8) was given an initial voltage of 100V and the GTO thyristor was turned off after conducting for 5ms. The single pulse simulations were run using different capacitors in the turn-off snubber; one used a 470nF capacitor, while the other used a 940nF capacitor. The voltage and current waveforms for the GTO thyristor are shown in Figure 17; for the time scale used in the plot, the waveforms were identical for both simulations.

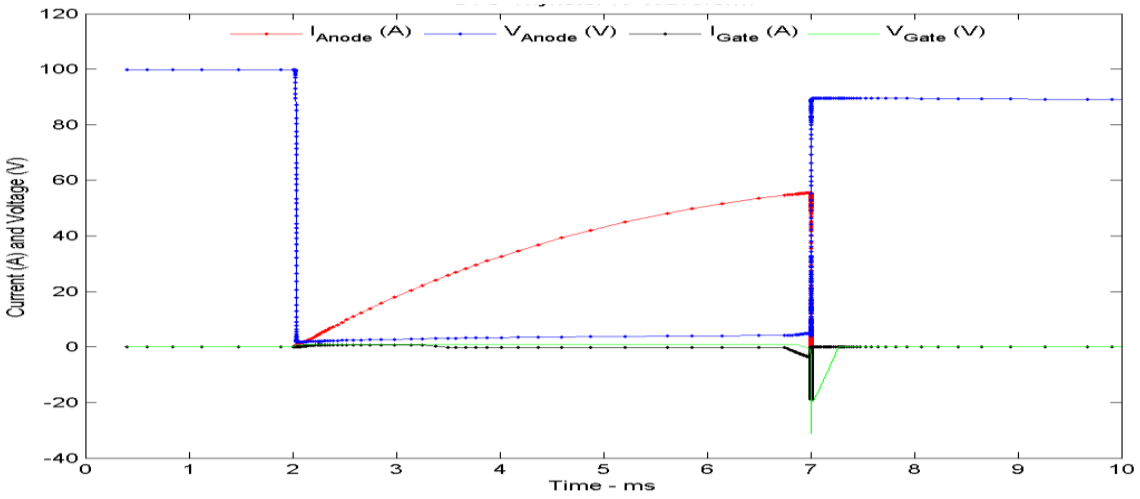

Figure 17. Single Pulse Waveform with a 100V Capacitor Bank Voltage.

The simulated voltages and currents of the GTO thyristor during turn-off are shown below in Figure 18; the plot on the left shows the turn-off waveforms for the GTO thyristor using the 470nF snubber capacitor, while the plot on the right shows the turn-off waveforms for the GTO thyristor using the 940nF snubber capacitor. From the plots, it can be seen that both simulations correctly modeled both anode voltage spikes (the one at the end of the current fall phase and the other at the end of the voltage rise phase). It can also be seen that the rise time for the anode voltage of the GTO thyristor with the 940nF snubber capacitor is almost double the voltage rise time for the GTO thyristor with the 470nF snubber capacitor; this particular observation is consistent with the experimental observations outlined in [2]. From the figure, it can be seen that the gate drive circuit generated a 20A peak turn-off current pulse in both simulations; thus, the simulated GTO thyristor had a turn-off gain of approximately three. (Turn off gain is the ratio of the anode current being interrupted to the gate current used to initiate turn-off of the device.)

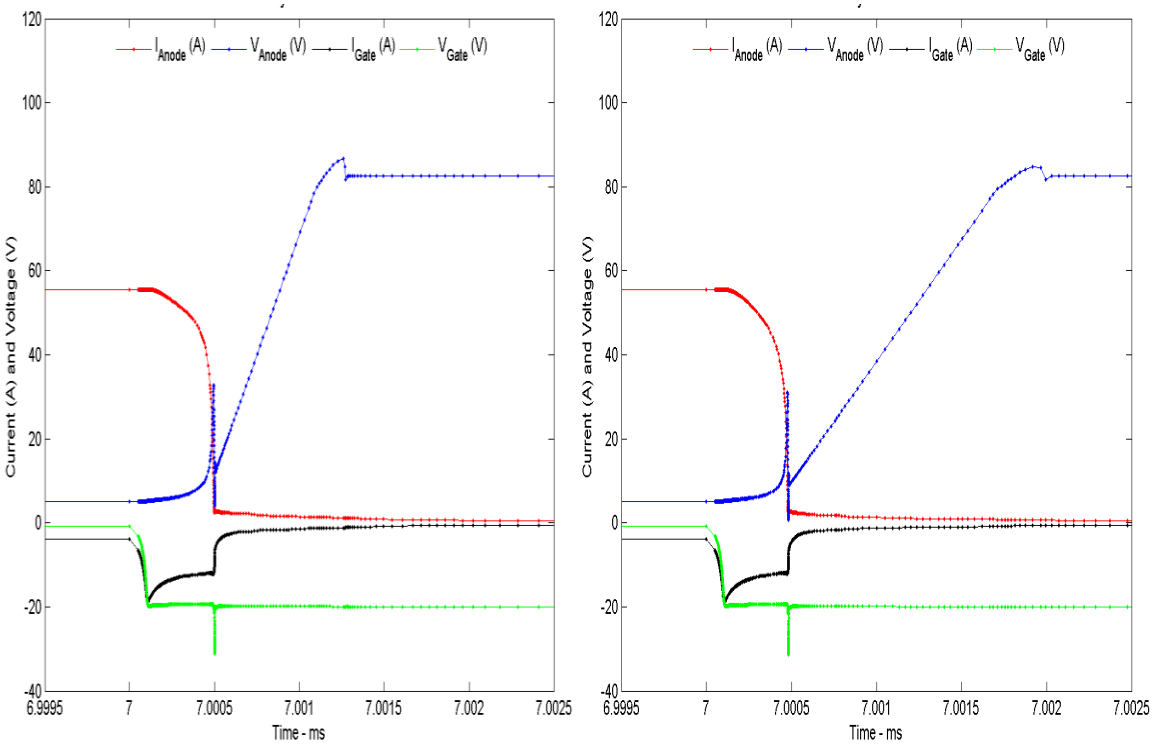

Figure 18. Single Pulse Waveforms Showing GTO Thyristor Turn-off.

The plots in Figure 19 show the thermal energy stored in each section of the GTO thyristor for the two single pulse simulations. The plots on the left show the stored thermal energy for the GTO thyristor with the 470nF snubber capacitor and the two plots on the right show the stored thermal energy for the GTO thyristor with the 940nF snubber capacitor.

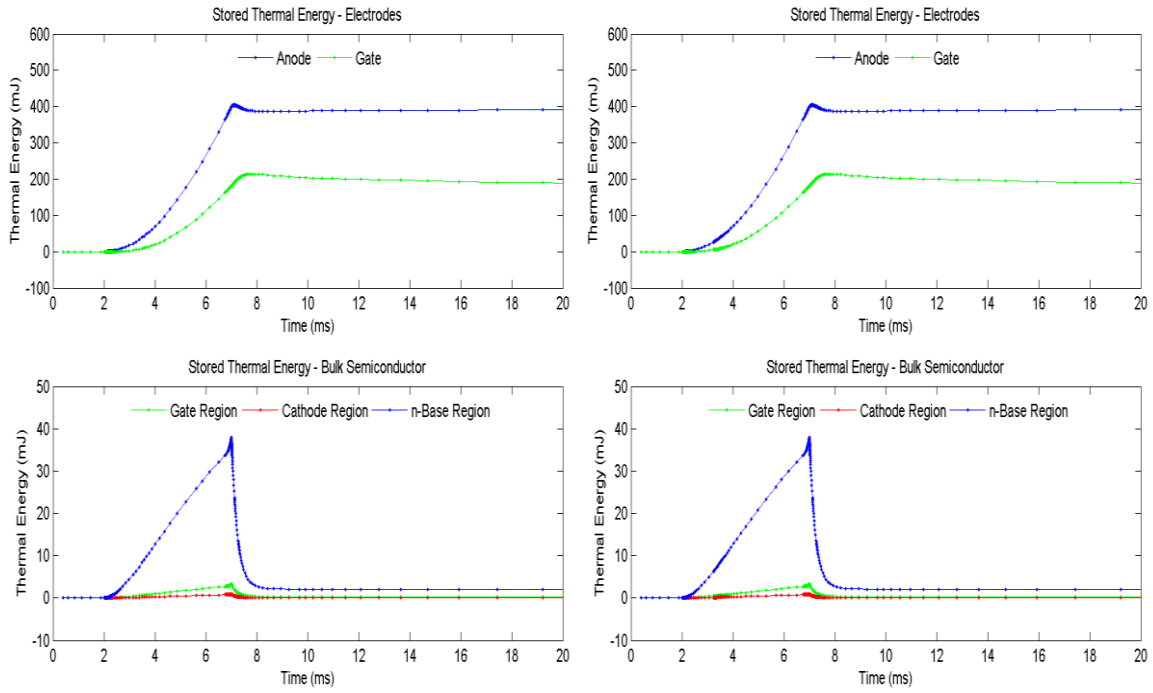

Figure 19. Thermal Energy Stored in Device Sections.

Several important conclusions regarding the nature of thermal energy storage in a GTO thyristor can be made from the plots in Figure 19. First, most of the thermal energy is stored in the aluminum electrodes; this is consistent with the fact that the specific heat content of aluminum is significantly higher than that of silicon. Second, most of the thermal energy that is stored in the silicon of the GTO thyristor is stored in the n-Base region of the device; this is partly because the n-Base region is larger than the gate and cathode regions. However, the primary reason that more thermal energy is stored in the n-Base region, especially during conduction, is that most of the thermal energy in the device comes from joule heating in the n-Base region (shown in Chapter VI).

The plots in Figure 20 show the electrostatic potential energy in each section of the GTO thyristor. The plots on the left show the stored electrostatic potential energy in the GTO thyristor with the 470nF snubber capacitor and the two plots on the right show the stored electrostatic potential energy in the GTO thyristor with the 940nF snubber capacitor.

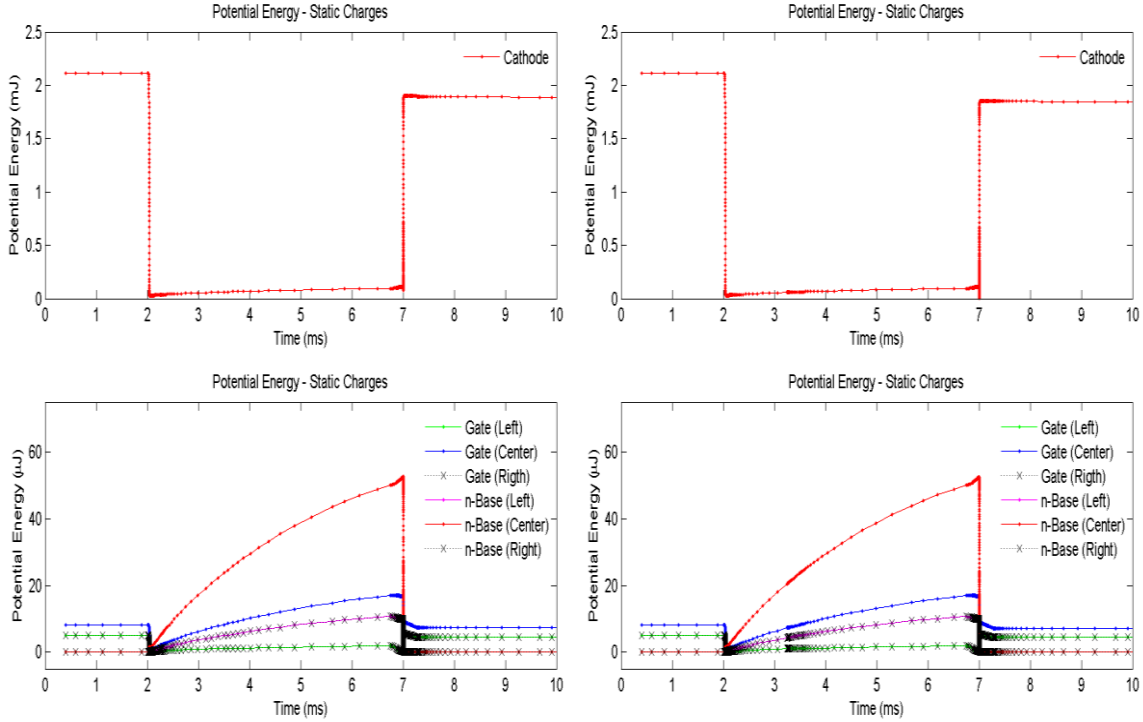

Figure 20. Electrostatic Potential Energy in the Device Sections.

From these plots, it can be seen that the snubber capacitor appears to have little effect on the stored electrostatic potential energy. This observation makes sense considering the fact that the snubber capacitor has very little influence on the quantities that determine the electrostatic potential energy in the device (charge density and quasi-Fermi level). In the off-state, most of the electrostatic potential energy is stored in the cathode region, because the n-Base and gate regions typically support a large depletion region when the device is off. The depletion regions reduce the carrier concentrations in the gate and n-Base regions of the device. In the on-state, electrostatic potential energy is stored in the center sections of the device due to the increased carrier concentration resulting from the current through the device.

In order to determine the accuracy of the energy balance method, the total change in the energy of the GTO thyristor was evaluated for both single pulse simulations. Figure 21 contains two plots that show the input electrical energy (blue trace), the stored thermal energy (black trace), the total stored electric potential energy (green trace), and thermal energy output (cyan trace) for the single pulse simulations; the plots also show the net change in energy of the GTO thyristor (red trace). The plot on the left represents the energy in the GTO thyristor with the 470nF snubber capacitor, while the plot on the right represents the energy in the GTO thyristor with the 940nF snubber capacitor.

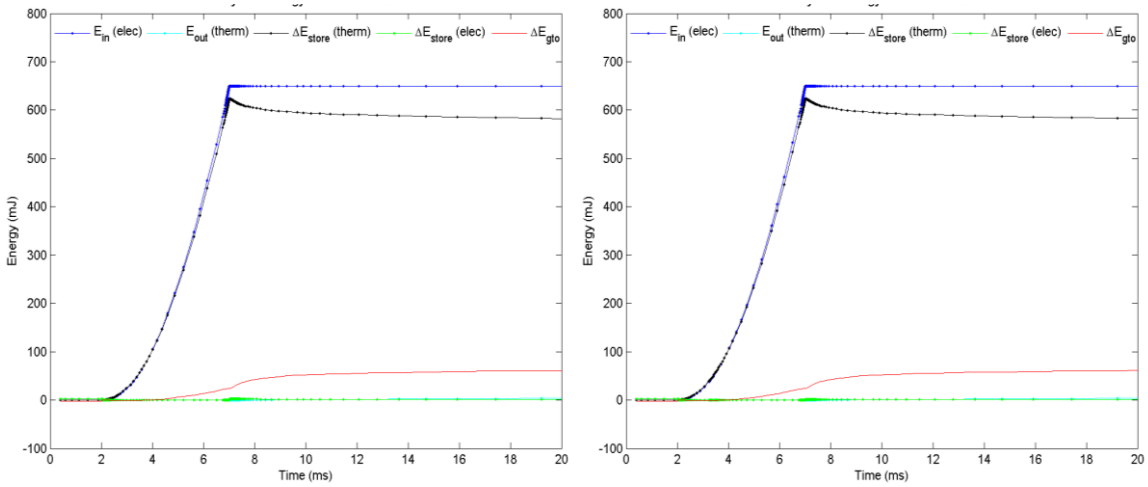

Figure 21. Energy Balance for the GTO Thyristor.

The obvious conclusion from the plots in Figure 21 is that the energy tracking method does not account for all the energy in the GTO thyristor—the energy tracking method accounts for 595mJ of the approximately 649mJ of electrical energy that was input to the device during the single pulse simulations. The discrepancy in energy values was most likely due to the manner in which the stored thermal energy was calculated. The stored thermal energy was calculated using average temperature values that were based on the measured lattice temperature at 181 points in the device. It is highly possible that the selected locations, while providing a good first-order approximation of the stored thermal energy, did not allow the total thermal energy to be accurately calculated.

Another conclusion that can be drawn from the plots in Figure 21 is that most of the energy that was input to the GTO thyristors was converted into thermal energy and stored inside the device. Very little energy was transferred out of the device through the thermal contact because the temperature of the thermal contact (bottom of the anode electrode) did not increase significantly during the simulations. Figure 22 shows the temperature of the top (blue), middle (red), and bottom (green) of the anode electrode; the left plot is for the GTO thyristor with the 470nF snubber and the right plot is for the GTO thyristor with the 940nF snubber.

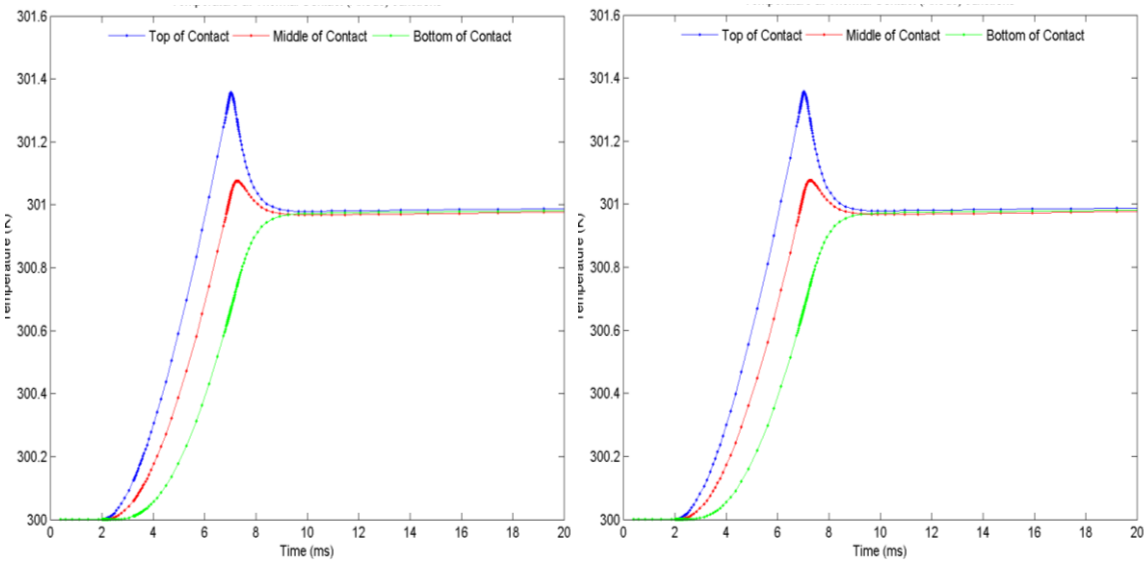

Figure 22. Temperature of the Anode Electrode.

Figure 22 shows that while the GTO thyristor was on, the temperature at the top of the electrode was higher than the temperature at the bottom of the electrode, which was consistent with the flow of thermal energy into the electrode. Due to its size and the large heat capacity of aluminum, the temperature at the bottom of the anode electrode only increased by one degree during the simulations. Consequently, the maximum thermal output power was only 280mW (for a thermal resistance R_{th} = 0.10 K-cm^2/W), which means that the GTO thyristor would have required over 2.3 seconds to dissipate the 650mJ of input energy and return to thermal equilibrium.

Final verification of the energy analysis was accomplished by calculating the net change in the energy of the SPICE circuit model. Since the circuit model represented a closed system, the total change in the energy of the circuit should be zero throughout the simulation. Figure 23 shows the energy balance results for the SPICE circuit model; E_{input} represents the total energy supplied by the voltage sources and capacitor bank, $E_{dissipated}$ is the total energy dissipated in the resistive elements of the circuit (*Rpulse, Rsrc, Rgate, etc.*), *Estore* is the total energy stored in the inductors and capacitors of the circuit (with the exception of the primary capacitor bank), E_{gto} is the total electrical energy input (dissipated) in the GTO thyristor, and ΔE_{total} is the net change in the energy of the circuit. From the plot, it can be seen that the energy tracking method developed for this project accurately tracks the flow of energy through the SPICE circuit.

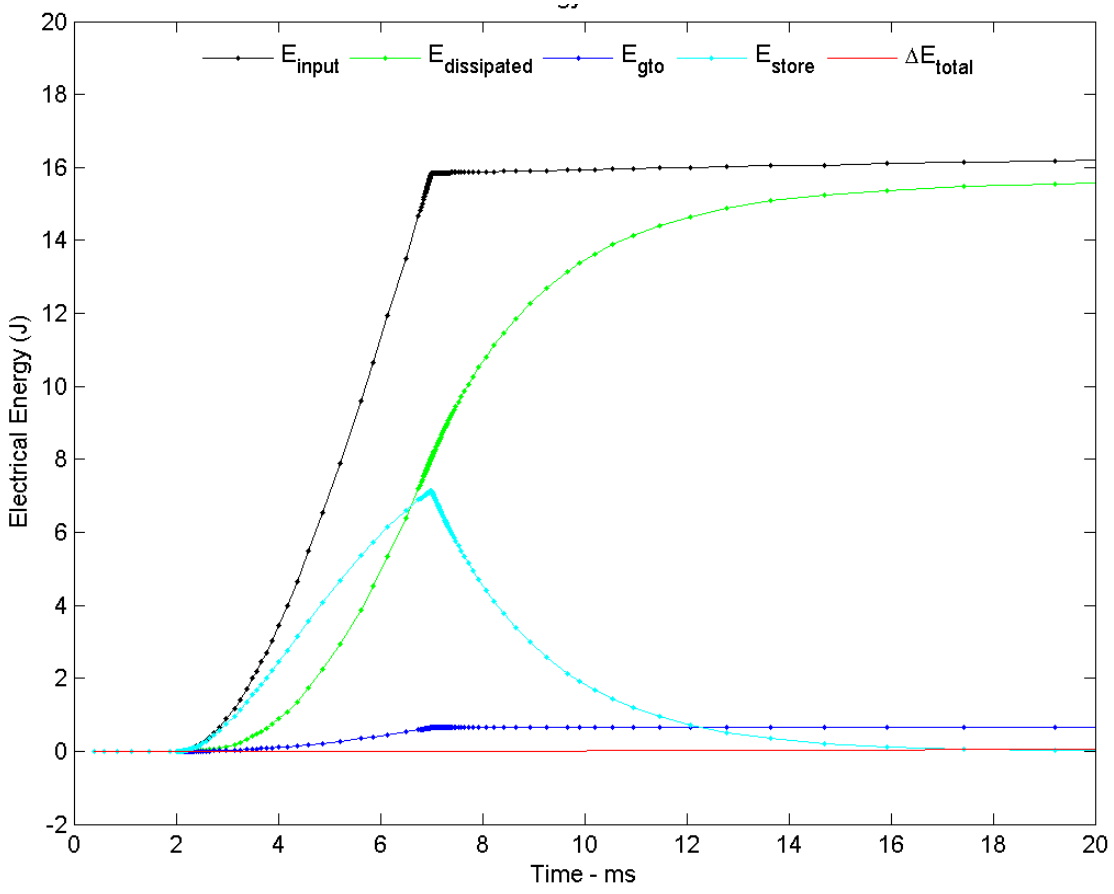

Figure 23. Energy Balance for the SPICE Circuit Model.

B. MULTIPLE PULSE ENERGY TRANSFER AND STORAGE

For the multiple pulse simulations of the GTO thyristor, the SPICE circuit used a larger capacitor bank (25mF vice 9.6mF) to ensure that the capacitor bank voltage was the same at the beginning of each pulse. The circuit also used a smaller pulse inductor (3mH instead of 4.62mH) to ensure that the current in the pulse inductor was able to full decay before the start of the next pulse. The multiple pulse simulations were run using two different thermal contact resistances; one simulation was run using a thermal resistance R_{th} = 1 K-cm^2/W, and the other simulation was run using a thermal resistance R_{th} = 0.1 K-cm^2/W.

The voltage and current waveforms for the multiple pulse simulations of the GTO thyristor are shown in Figure 24. In both multiple pulse simulations, the GTO thyristor was used to generate 5ms current pulses at a switching frequency of 50Hz; the simulations were run using a 50V capacitor bank voltage and a 470nF snubber capacitance. From the figure, it can be seen that the starting anode voltage decreases during the first few current pulses; however, the starting anode voltage settles to a steady value after five pulses.

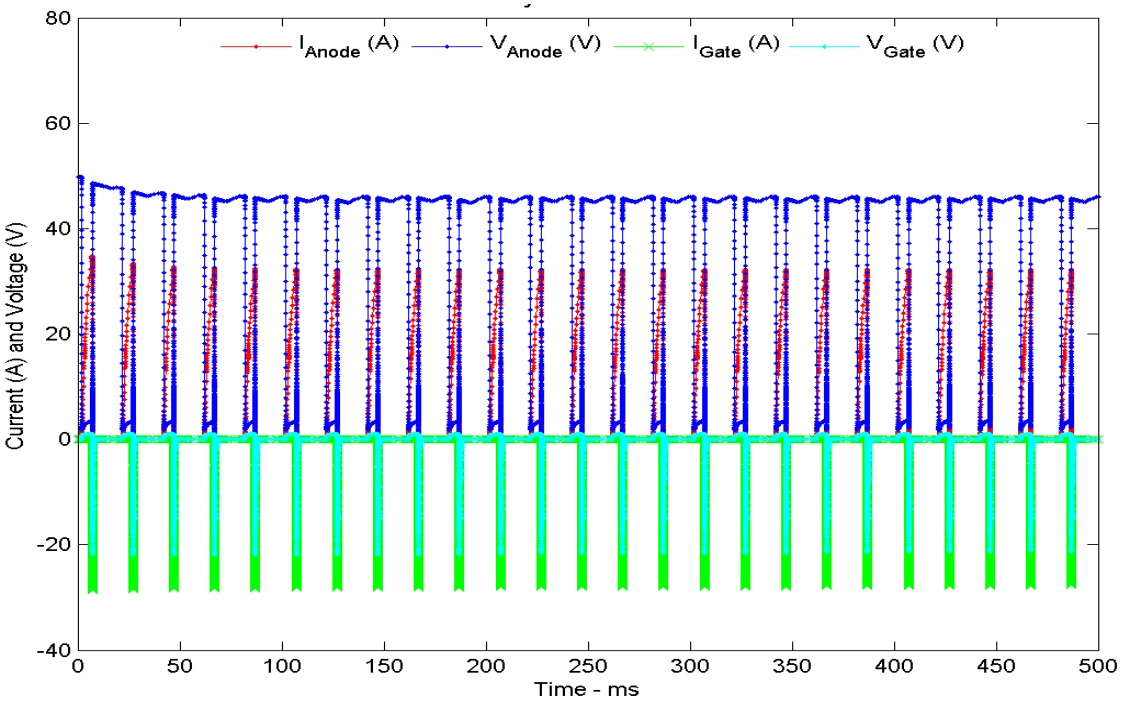

Figure 24. Multiple Pulse Waveforms with a 50V Capacitor Bank Voltage.

Figure 25 shows the simulated turn-off voltage and current waveforms for the GTO thyristor. The plot shows the waveforms for one of the final turn-off events of the multiple pulse simulations. From the plot, it can be seen that the turn-off characteristics of the device remain constant throughout the simulations. It can also be seen that the SPICE circuit did not generate an anode voltage spike at the end of the voltage rise phase. For the multiple pulse simulations, the SPICE circuit was simplified by removing the stray inductances responsible for the final anode voltage spike (Lgto and Lstray); the simplification was necessary in order to reduce the time required to compete the multiple pulse simulations. The plot shows that the anode current at turn-off was approximately 33A and the peak turn-off gate current was approximately 28A, which means that the gate drive circuit almost achieved unity gain turn off.

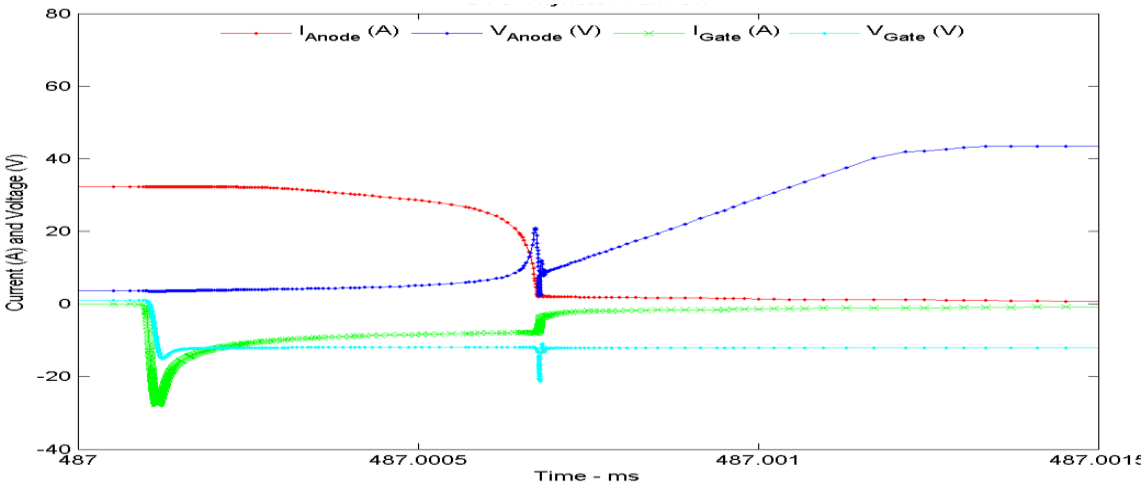

Figure 25. Multiple Pulse GTO Thyristor Turn-off Waveforms.

The energy tracking method described in Chapter IV was used to analyze the multiple pulse simulations of the GTO thyristor, with one minor modification. The analysis of the single pulse simulations showed that total electric potential energy in the GTO thyristor was several orders of magnitude smaller than the thermal energy stored in the device (less than 2.5mJ of electric potential energy compared to approximately 600mJ of thermal energy). Consequently, the stored electric potential energy was ignored during the energy analysis of the multiple pulse simulations.

The plots in Figure 26 show the thermal energy stored in each section of the GTO thyristor for the multiple pulse simulations. The plots on the left show the stored thermal energy for the GTO thyristor with a thermal resistance R_{th} = 1 K-cm^2/W, while the plots on the right show the stored thermal energy for the GTO thyristor with a thermal resistance R_{th} = 0.1 K-cm^2/W. From the plots, it can be seen that the GTO thyristor heats up over the course of both simulations; but it does not heat up as much for the simulation with the lower thermal contact resistance.

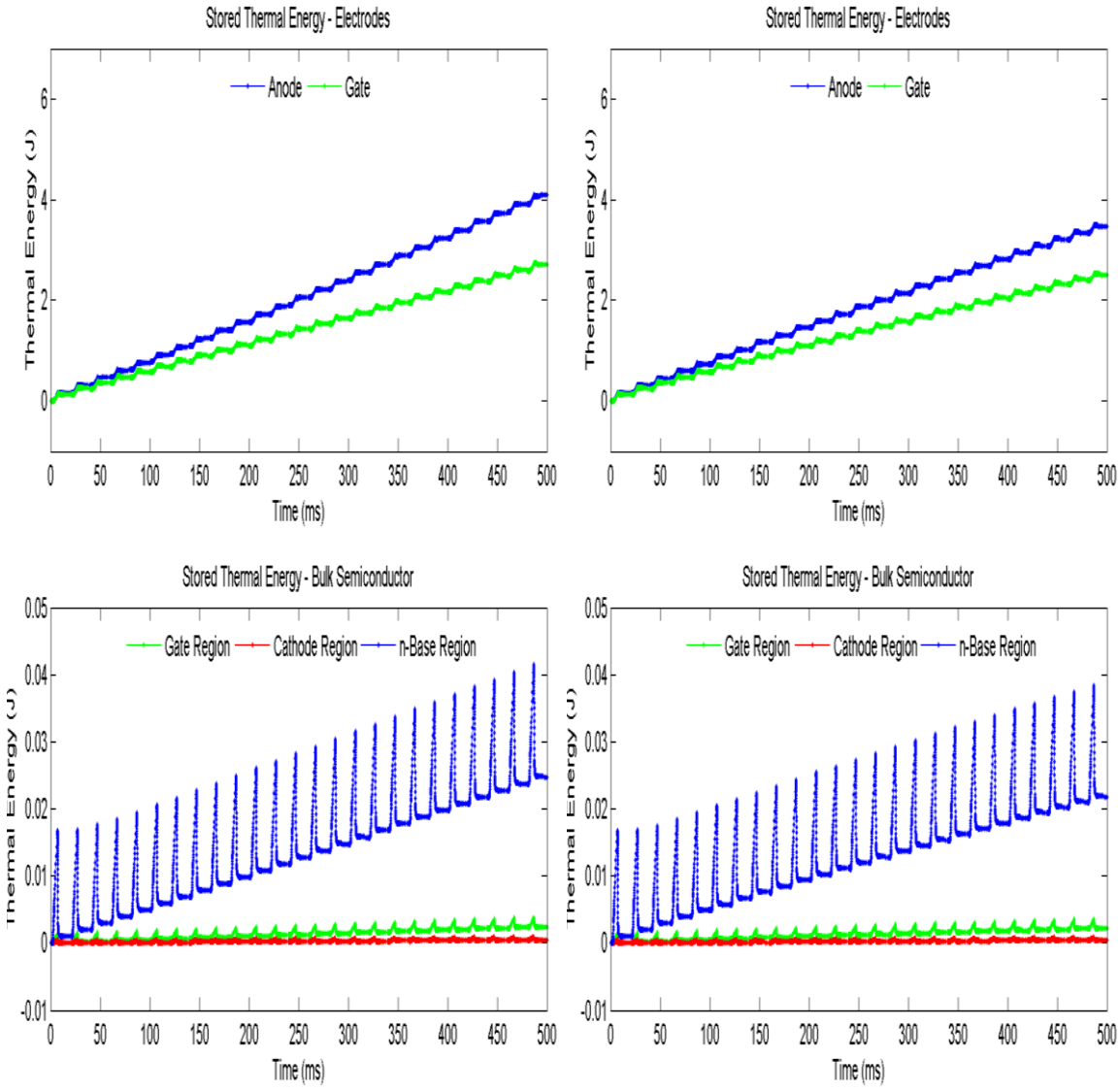

Figure 26. Thermal Energy Stored in Device Sections.

By computing the stored thermal energy, it was possible to determine the total change in the energy of the GTO thyristor for each multiple pulse simulation. Figure 27 shows the input electrical energy (blue trace), the stored thermal energy (black trace), the total thermal energy output (green trace), and the net change in energy of the GTO thyristor (red trace) for the multiple pulse simulations. The plot on the left represents the energy in the GTO thyristor with the thermal resistance R_{th} = 1 K-cm^2/W, while the plot on the right shows the energy in the GTO thyristor with the thermal resistance R_{th} = 0.1 K-cm^2/W. From the figure, it can be seen that the thermal energy output is higher for the GTO thyristor with the lower thermal contact resistance.

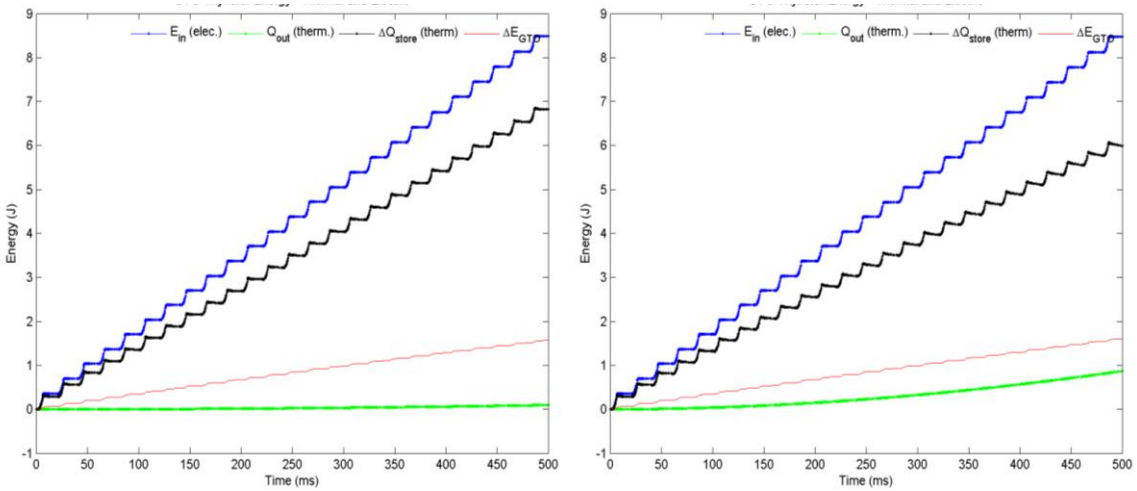

Figure 27. Multiple Pulse Energy Balance for the GTO Thyristor.

Just like the energy analysis for the single pulse simulations, the energy tracking method does not fully account for all the energy that is input to the GTO thyristor in the multiple pulse simulations. For each current pulse, the energy tracking method was only able to account for approximately 85% of the input electric energy (400mJ). Consequently, the total error in the energy tracking method (plotted as the net change in energy of the GTO thyristor) increased by 60mJ per current pulse. Most likely, the error represents thermal energy that was stored in the device but not properly accounted for by the energy tracking method.

The energy analysis of the multiple pulse simulations was verified calculating the net change in the energy of the SPICE circuit model; as in the single pulse simulations, the total change in the energy of the circuit should be zero throughout the simulations. The plot in Figure 28 shows the energy balance results for the multiple pulse simulations; E_{input} represents the total energy supplied by the voltage sources and capacitor bank, $E_{dissipated}$ is the total energy dissipated in the resistive elements of the circuit (*Rpulse, Rsrc, Rgate, etc.*), *Estore* is the total energy stored in the inductors and capacitors of the circuit (with the exception of the primary capacitor bank), E_{gto} is the total electrical energy input (dissipated) in the GTO thyristor, and ΔE_{total} is the net change in the energy of the circuit. The plot shows that the energy tracking method correctly tracks the flow of energy in the SPICE circuit over multiple pulses of the GTO thyristor device.

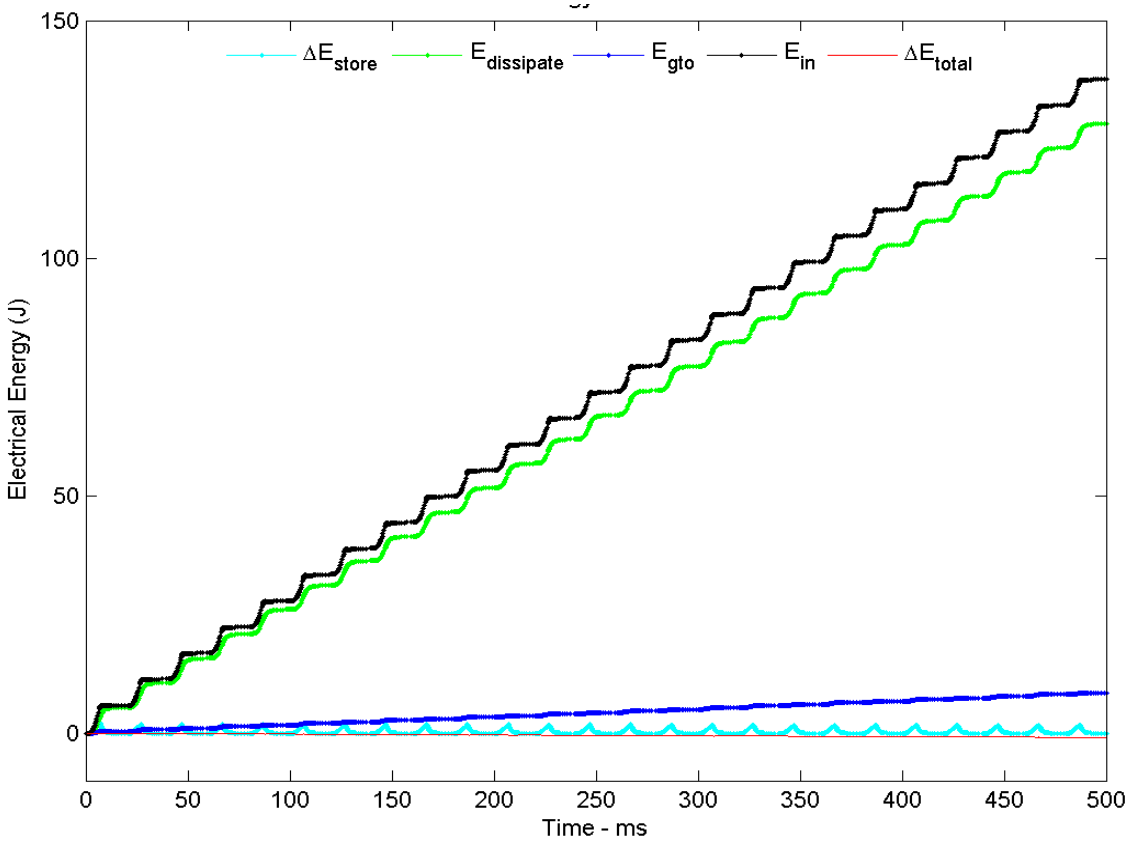

Figure 28. Energy Balance for the SPICE Circuit Model.

The following chapter outlines the results of the single pulse simulations that were performed using the three-unit-cell GTO thyristor structure shown in Figure 6. The simulations were performed to investigate current crowding and current filamentation in the GTO thyristor devices. The simulations were also used to study thermal generation in the device during conduction (on-state) and turn off.

THIS PAGE INTENTIONALLY LEFT BLANK

VI. MULTI-UNIT TURN-OFF CHARACTERISTICS

Four different simulations were performed using the multi-unit GTO thyristor structure. Two of the simulations used a GTO thyristor structure that had a uniform doping profile in the gate region; the other two used a structure that had a non-uniform doping profile in the gate region. The simulations were used to investigate current crowding, current filamentation, and joule heating in GTO thyristors and to compare the turn-off characteristics of an ideal thyristor device (uniform doping) to a realistic thyristor device (non-uniform doping).

The multiple unit simulations were conducted using two different capacitor bank voltages in order to investigate the turn off characteristics for two different anode current levels. In all four simulations, the GTO thyristor had a 470nF snubber capacitor and was operated for a 8ms pulse. Figure 29 shows the full pulse waveforms for the multiple unit GTO thyristor simulations with Cbank=50V (left plot) and Cbank=70V (right plot); the anode voltage is labeled as “Function 1” and the gate voltage is labeled as “Function 2.” The full pulse waveforms were essentially the same for the uniform and non-uniform device structures.

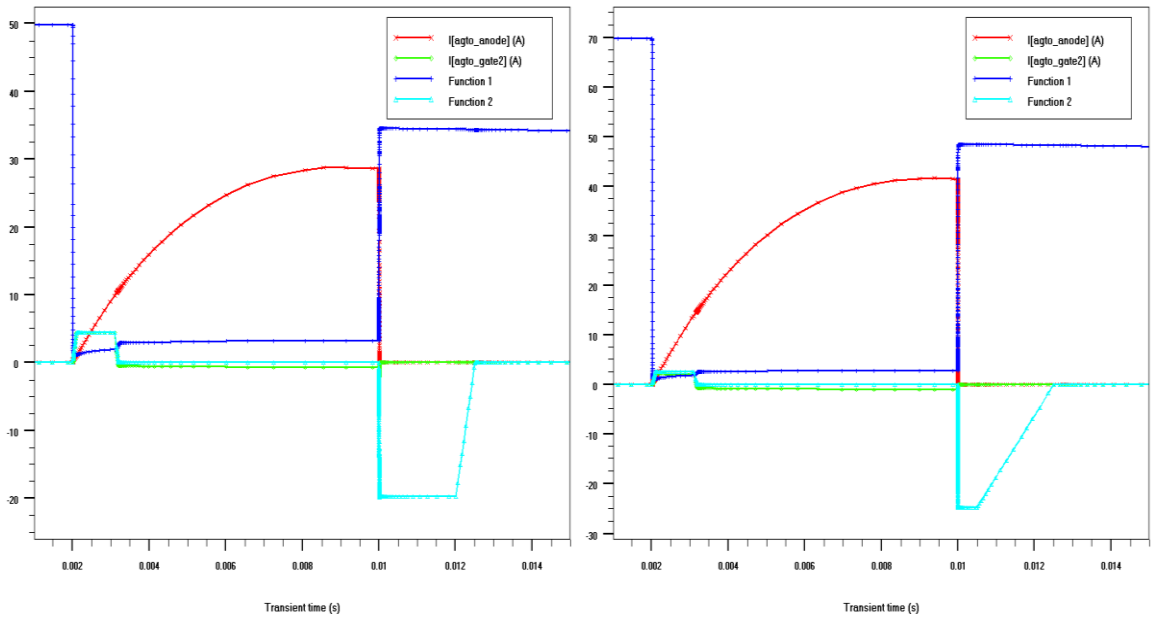

Figure 29. Full Pulse Waveforms for a Multiple Unit GTO Thyristor.

A. CURRENT FILAMENTATION

The impact of a non-uniform doping profile on the operation of a GTO thyristor can be seen by comparing the turn-off voltage and current transients of the uniform and non-uniform GTO thyristor structures. Figure 30 shows the turn-off transients for the multiple unit simulations that were performed using the 50V capacitor bank; the anode voltage is labeled as “Function 1” and the gate voltage is labeled as “Function 2.” The top plot shows the turn-off waveforms for the uniform GTO thyristor and the bottom plot shows the turn off waveforms for the non-uniform GTO thyristor. The plots show that the uniform and non-uniform structures have different turn-off characteristics. The GTO thyristor with the non-uniform doping profile has a longer storage time than the GTO thyristor with uniform doping profile. Additionally, the anode voltage during the storage phase is higher for the non-uniform GTO thyristor.

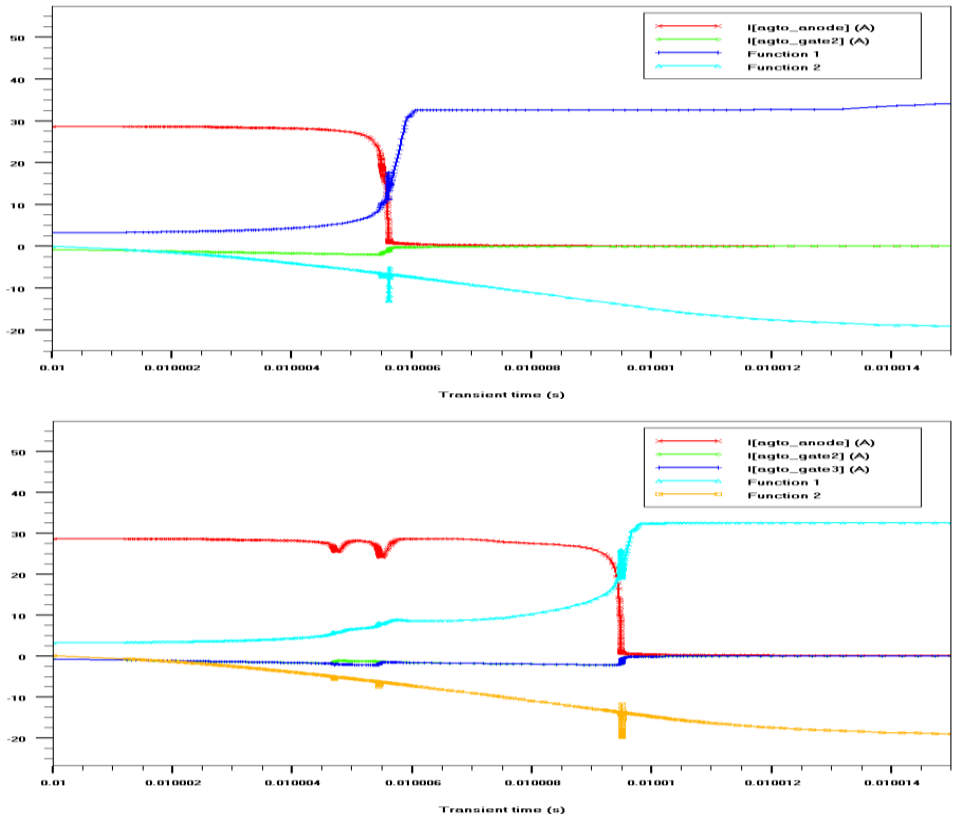

Figure 30. Turn-off Transient for a Multiple Unit GTO Thyristor.

The turn-off characteristics of the uniform and non-uniform GTO thyristor structures can be further differentiated by examining all the device currents (anode, gate, and cathode) during turn off. Figure 31 shows the turn-off currents for the multiple unit GTO thyristor simulations conducted with the 50V capacitor bank. The plots show the anode current (red), the cathode current for each unit cell (green, cyan, and blue), and current through the individual gate electrodes (yellow, brown, purple, and violet). The top plot shows the turn-off waveforms for the uniform GTO thyristor and the bottom plot shows the turn off waveforms for the non-uniform GTO thyristor. Since each unit cell has an independent cathode electrode, the cathode currents can be used to determine when each unit cell turns off. The plots show that the unit cells turn off at nearly the same time for the GTO thyristor with the uniform structure, but they turn off at different times but for the GTO thyristor with the non-uniform structure. As each unit cell turns off, the anode current shifts to the unit cells that are still conducting and increases the current density in those cells. Given a sufficient difference in turn-off times, the entire anode current can end up flowing in a single unit cell (as in the bottom plot); this process is typically referred to as current filamentation.

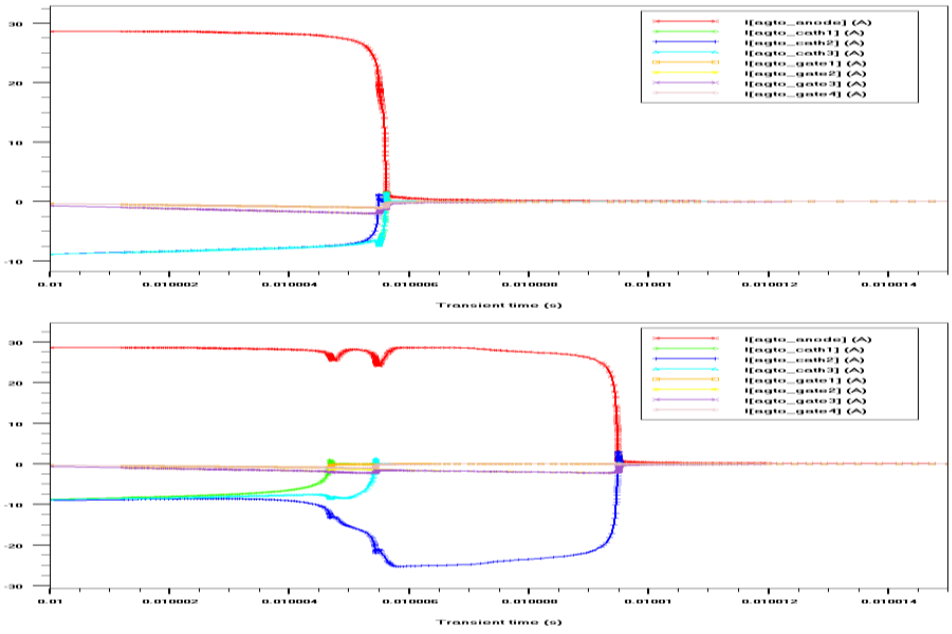

Figure 31. Turn-off Currents for a Multiple Unit GTO Thyristor.

The difference in the turn-off times of the GTO thyristor unit cells is directly related to the amount of non-uniformity in the device structure. Figure 32 shows the turn off currents for the multiple unit simulations that were performed using the non-uniform GTO thyristor structure. The device structure used in the simulation represented by the left plot had a 10% difference in the doping concentration of the three gate regions. The device structure used to generate the right plot had a 5% difference in the doping concentration of the gate regions. The plots show that the difference in turn-off times is larger for the device structure with the 10% difference in doping concentration; thus, the degree of non-uniformity in the device structure directly affects the amount of current filamentation that occurs during turn-off.

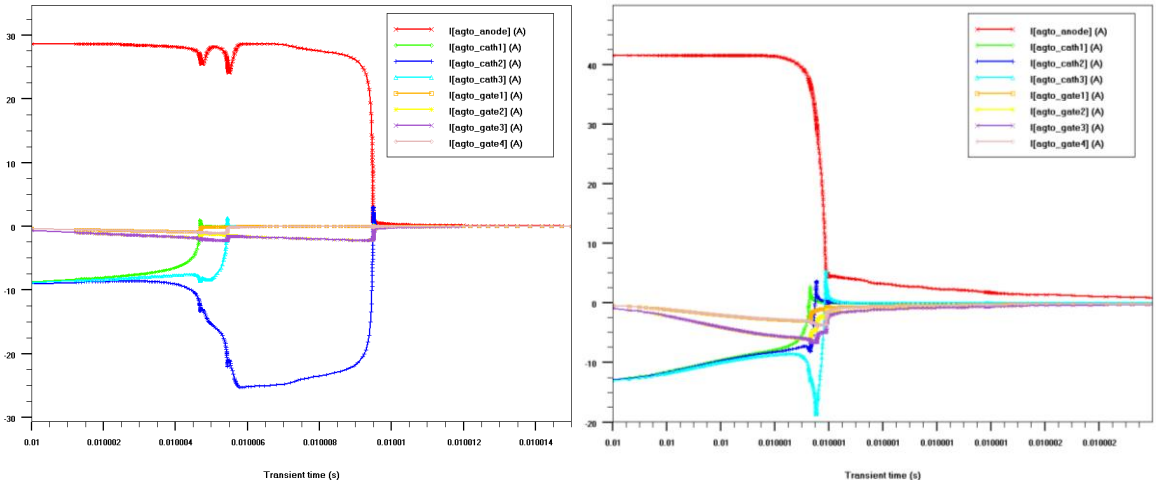

Figure 32. Current Filamentation in a Multiple Unit GTO Thyristor.

The doping differences were selected to provide a sufficient difference in turn-off times to easily illustrate how device non-uniformity affects current filamentation and the formation of hot spots during turn-off. For the simulation with a 5% difference in doping, the primary hot spot had a peak temperature of 316K during turn off. For the simulation with a 10% difference in doping, the hot spot had a peak temperature of 327K during turn off. For comparison, the peak temperature in the uniform GTO thyristor device only increased to 310K during turn-off.

B. ELECTROTHERMAL OPERATING CHARACTERISTICS

In order to better understand the electrothermal turn off characteristics of the GTO thyristor, the internal structure of the multiple unit device was examined at various time points in the simulations. In order to do this, ATLAS™ saved a solution file for each transient time point in the simulations; these files contained data representing the electrical and thermal condition at each mesh point in the device. The solution files were used to investigate current density, electric field, and local heating in the device during conduction (on-state) and turn-off. The analysis showed that with the exception of turn-off, the uniform and non-uniform structures essentially had the same operating characteristics.

1. On-State Characteristics

Figure 33 shows a log plot of the current density in the multiple unit GTO thyristor just prior to device turn-off (approximately 6.75ms into the simulation). The plot was generated from the solution file for the uniform GTO thyristor structure simulated using the 70V capacitor bank. From the figure, it can be seen that the device structure causes the anode current to distribute evenly between the unit cells and to spread out uniformly (or nearly so) across each unit cells. Additionally, it can be seen that much of the anode current passes through the anode shorts (highly doped n- regions between the anode electrode and the n-Base region) instead of the anode regions.

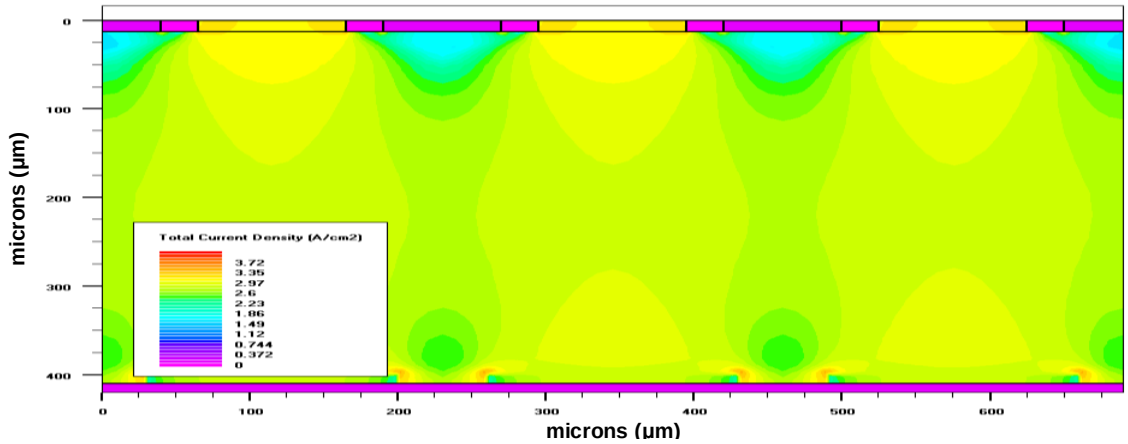

Figure 33. On-State Current Density in a Multiple Unit GTO Thyristor.

Figure 34 shows a log plot of the electric field in the multiple unit GTO thyristor just prior to device turn-off (approximately 6.75ms into the simulation). The plot was generated from the solution file for the uniform GTO thyristor structure simulated using the 70V capacitor bank. From the figure, it can be seen that the structure of the GTO Thyristor minimized the number and size of high electric field regions. With the exception of the anode shorts, the device creates a smooth change in potential (low electric field) anywhere the current density is large.

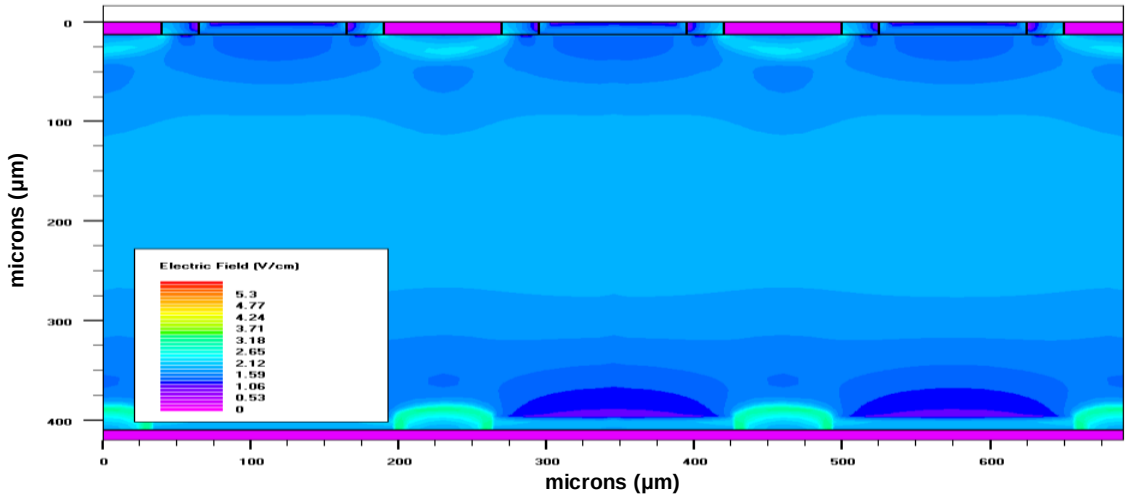

Figure 34. On-State Electric Field in a Multiple Unit GTO Thyristor.

The on-state electric field and current density characteristics of a GTO thyristor minimize the overall thermal energy generation during conduction. Figure 35 shows the on-state heat power for the primary heating mechanisms in a GTO thyristor. From the plots, it can be seen that recombination/generation heating, shown in the bottom plot, occurs predominantly in the anode and cathode regions due to the high doping concentration in those regions (the high doping concentration increases the number of possible recombination/generation sites within those regions). Joule heating, shown in the top plot, occurs predominantly where the current density and electric field in the device are both large (along the perimeter of the anode short regions and the center of the n-Base regions). It can also be seen that the recombination/generation heat power is two orders of magnitude smaller than the joule heat power.

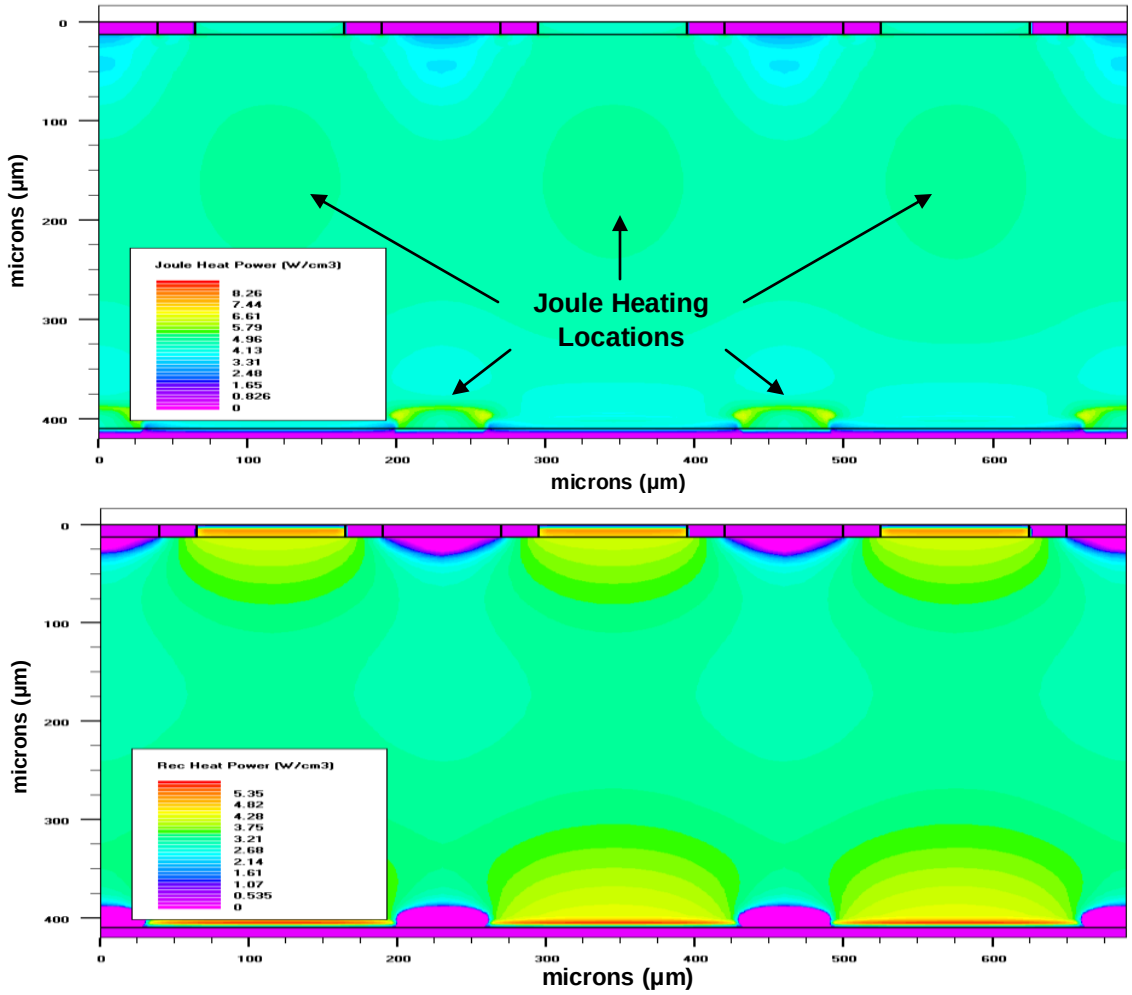

Figure 35. On-State Heat Power in a Multiple Unit GTO Thyristor.

Figure 36 shows the lattice temperature of the multiple unit device for the same solution represented by the preceding four figures. From the figures, it can be seen that most of the thermal energy in the semiconductor material was stored at the center of the device. Even though the heat power density in the n-Base region was smaller than the heat power density at the perimeter of the anode shorts, more thermal energy was generated in the center of the n-Base region. This is most likely due to the fact that the joule heating in the n-Base region occurred over a larger area than the heating at the anode shorts; however, there may have been other thermal energy generation mechanisms in the device (such as Peltier-Thompson heating) that were accounted for by the device simulator but not examined during the analysis of the device.

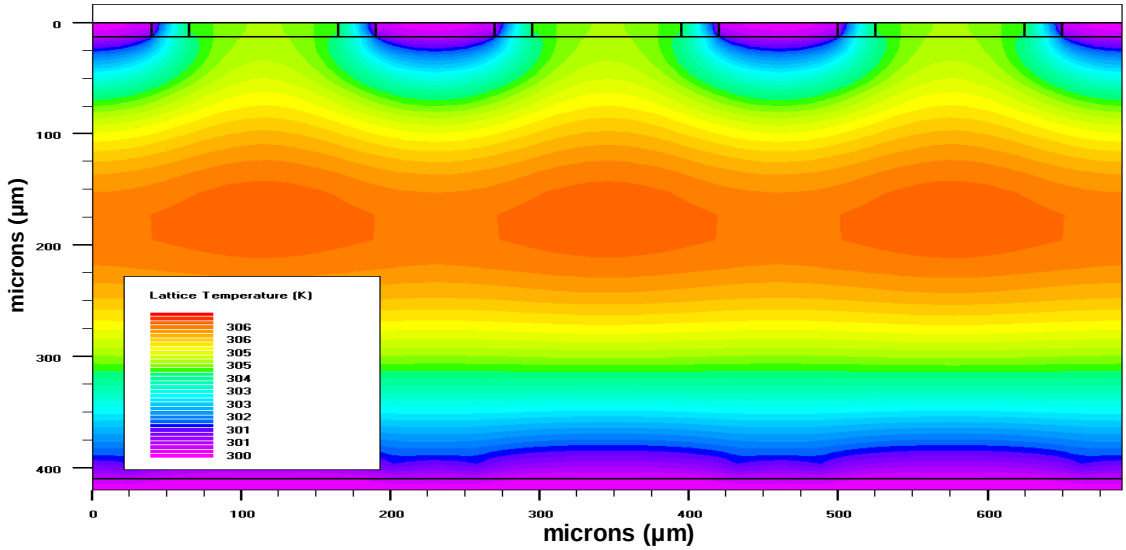

Figure 36. On-State Lattice Temperature in a Multiple Unit GTO Thyristor.

The thermal and electric characteristics outlined in this subsection provided a comparison baseline for the examination of the turn-off characteristics of a GTO thyristor. The solution files were used to determine how non-uniform doping affects the turn-off characteristics of a GTO thyristor. For this project, particular attention was made to examining current density and joule heating in the device during turn-off.

2. Turn-off Characteristics

Figure 37 shows the current density in the uniform and non-uniform devices during turn-off for the simulations using the 70V capacitor bank. The plots on the left were generated using the uniform GTO thyristor structure and the plots on the right were generated using the non-uniform GTO thyristor structure. From the figure, it can be seen the current in each unit cell is pinched towards the center of the cell during turn off, which causes the current density to increase through a process commonly referred to as current crowding. Additionally, it can be seen that the unit cells in the non-uniform device turn off at different times, which increases the current densities in the conducting unit cells still further. By comparison, the current in the uniform GTO thyristor remains evenly distributed between the unit cells throughout the entire turn-off process.

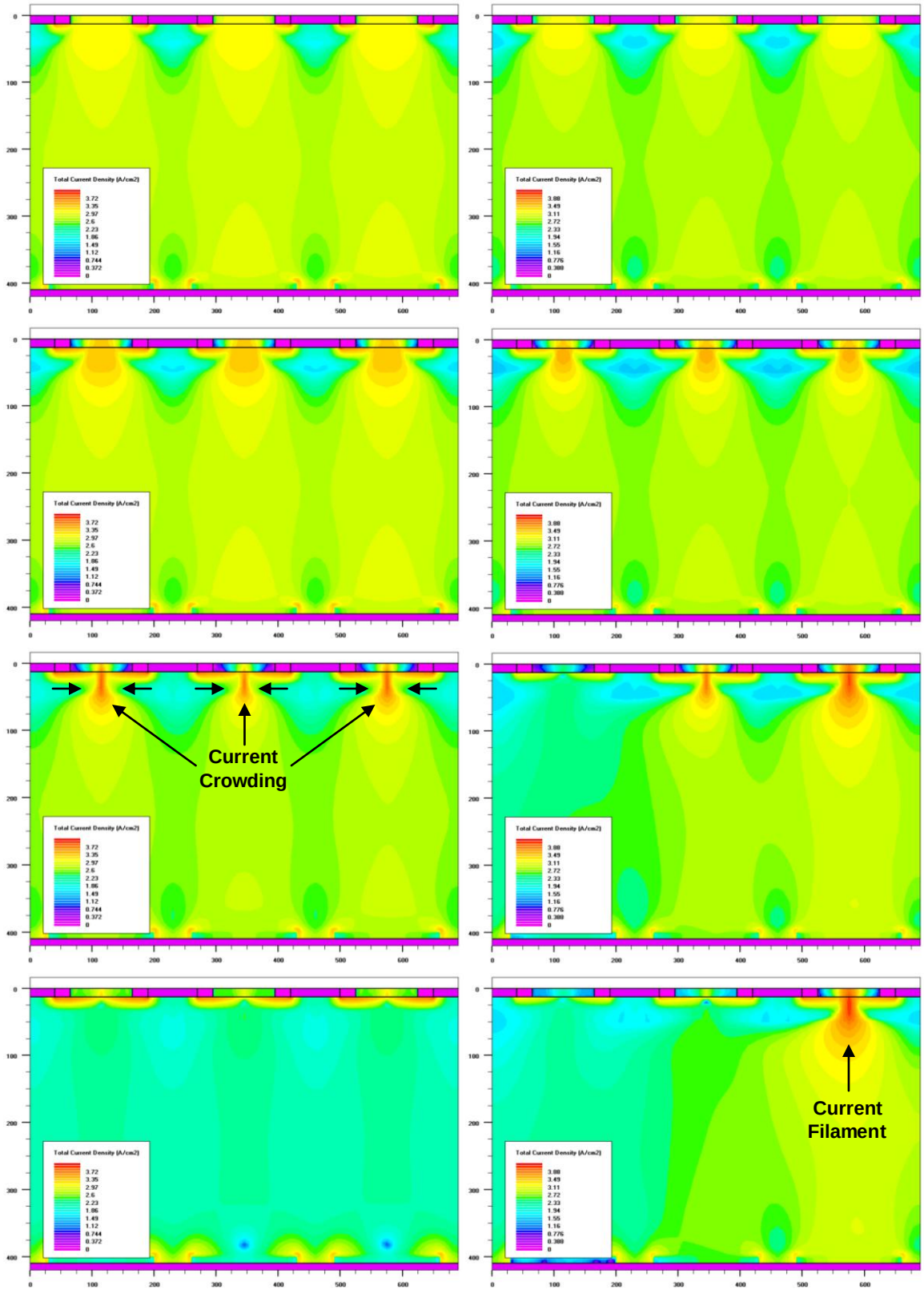

Figure 37. Turn-off Current Density in Multiple Unit GTO Thyristors.

Figure 38 shows a log plot of the electric field in the multiple unit GTO thyristor during turn off. The plots on the left represent the uniform GTO thyristor, while the plots on the right represent the non-uniform GTO thyristor. From the figure, it can be seen that an electric field is established at the junction between the n-Base and gate regions of the device during turn off; this electric field pinches off the anode current and ultimately causes the device to turn off. In the non-uniform structure, the electric fields in the unit cells are established at different rates, which causes the unit cells to turn off at different times.

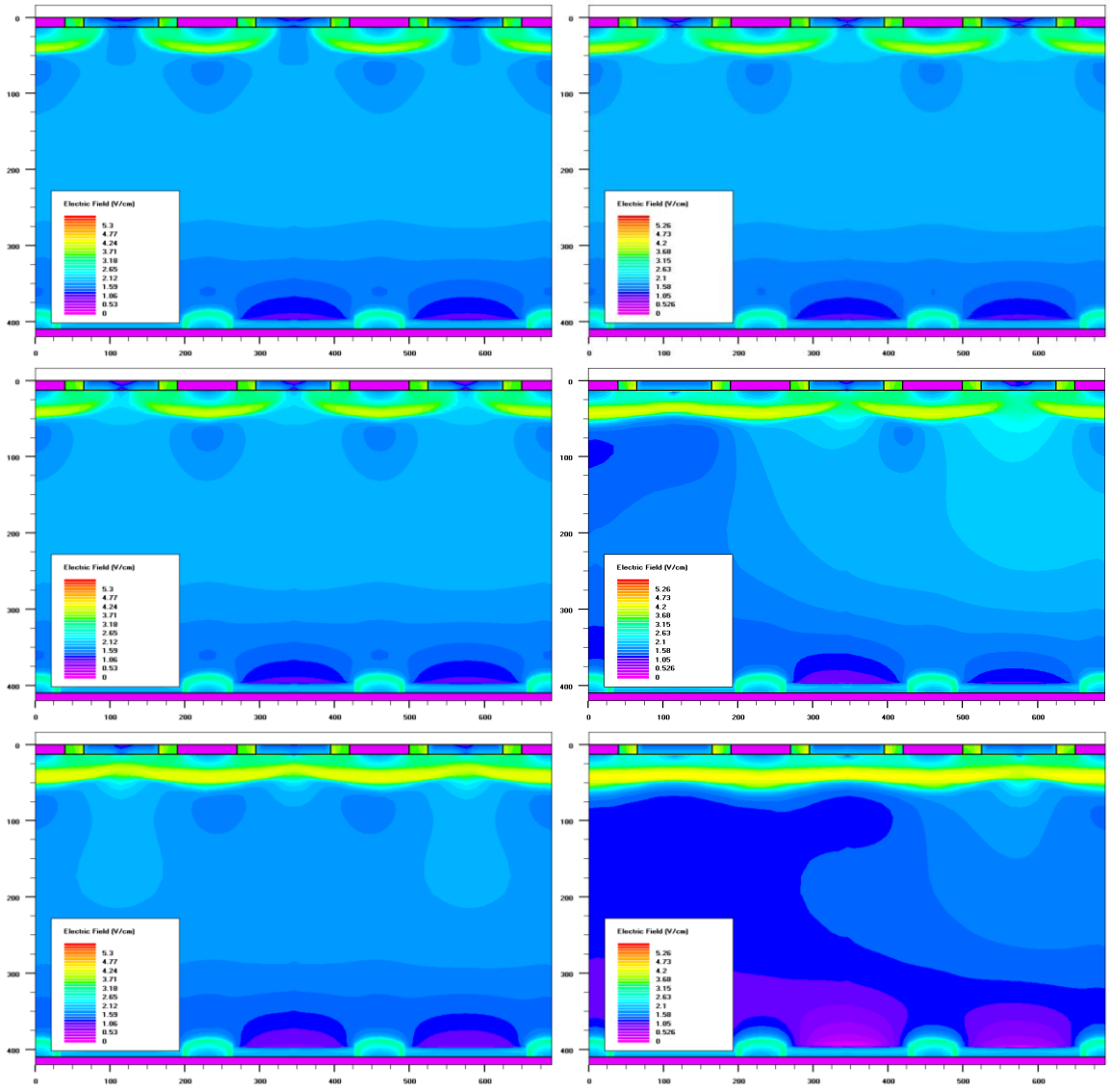

Figure 38. Electric Fields in Multiple Unit GTO Thyristors During Turn-off.

In the preceding subsection, it was shown that the most of the thermal energy in the GTO thyristor was generated by joule heating; in the on-state, most of the joule heating took place along the perimeter of the anode short regions and in the center of the n-Base region. During turn-off, the location of maximum joule heating shifts upwards from the center of the n-Base region to the junction between the gate region and the n-Base region. Figure 39 shows the joule heating in the uniform (right plots) and non-uniform (left plots) GTO thyristors during turn-off. It can be seen from the plots that the location of maximum joule heating corresponds to the locations of highest current density and electric field shown in the preceding figures. As in the on-state, the heat power due to recombination and generation is two orders of magnitude smaller than the joule heat power.

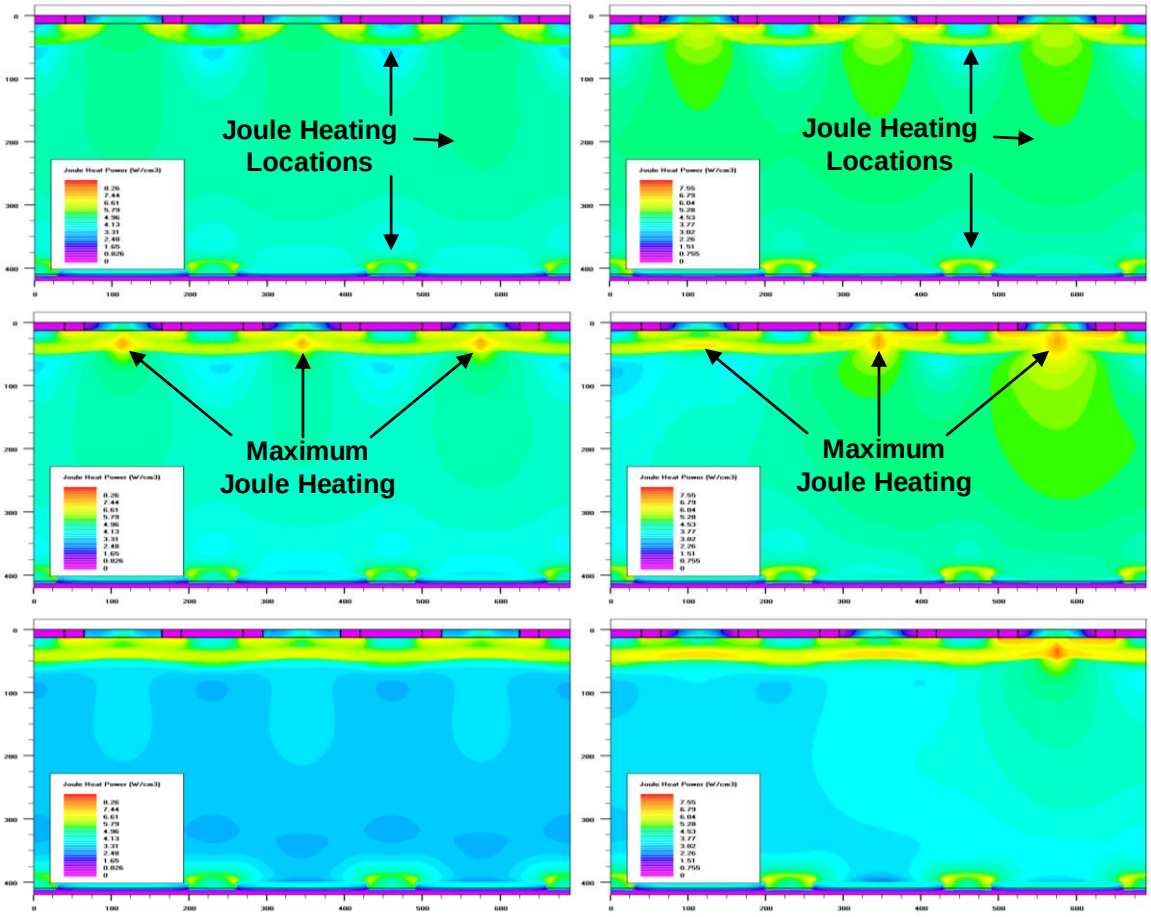

Figure 39. Turn-off Joule Heat Power in a Multiple Unit GTO Thyristor.

Figure 40 shows the lattice temperature for the uniform and non-uniform GTO thyristors during turn-off. From the figures, it can be seen that the extra joule heating during turn-off does not heat the device up significantly. However, it is evident that the current filamentation in the non-uniform GTO thyristor causes hot spots to form. The unit cell that turns off last gets hotter, both at the junction between the gate and n-Base regions and in the center of the n-Base region.

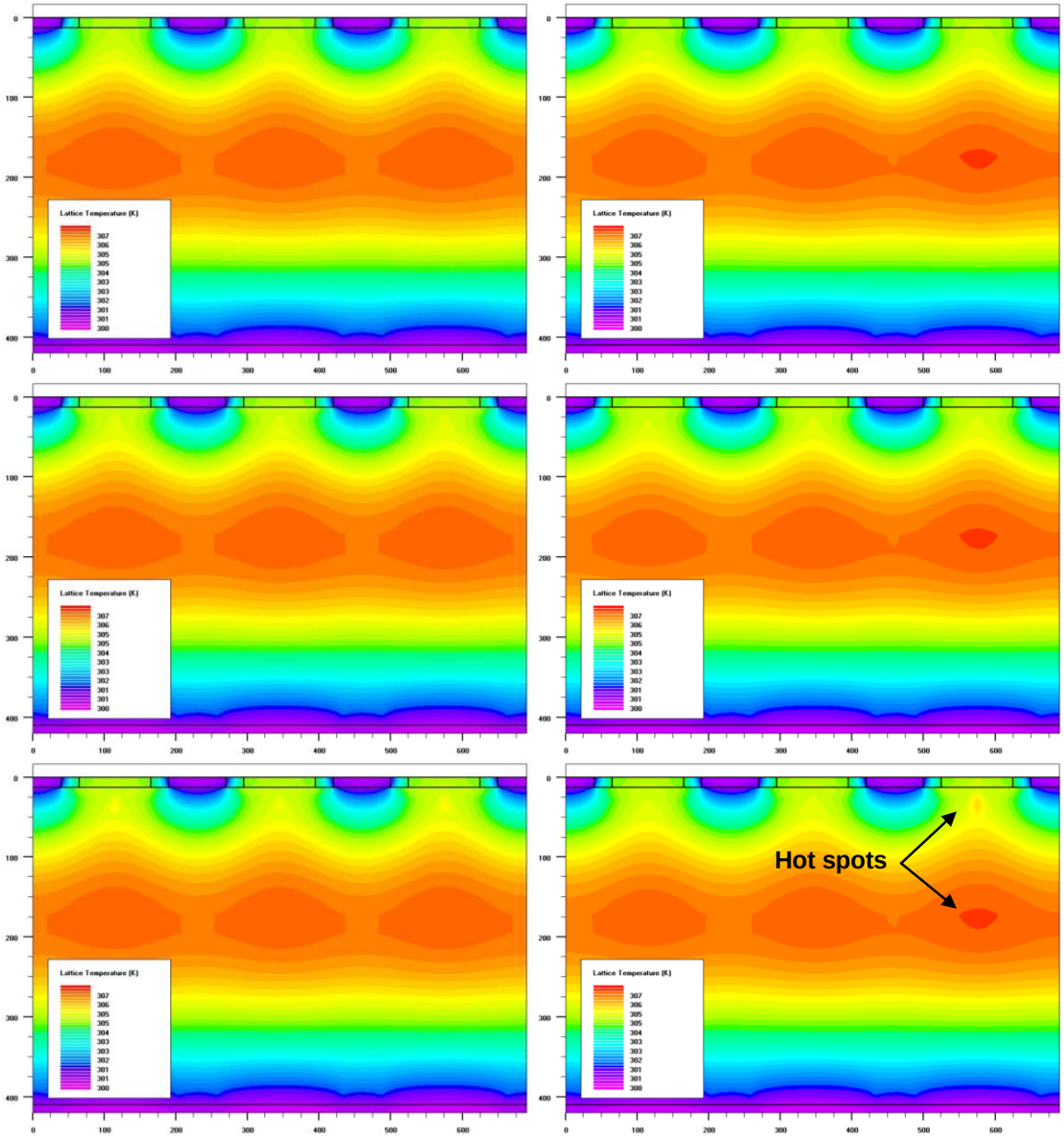

Figure 40. Temperature in a Multiple Unit GTO Thyristor During Turn-Off.

C. JOULE HEATING IN A GTO THYRISTOR

In the previous section, it was shown that the primary heating mechanism in a GTO thyristor is joule heating due to the combination of current density and electric field. One way to improve the performance and reliability of a semiconductor device is to reduce the amount of localized joule heating that occurs in the device; this can sometimes be accomplished by modifying the device structure to reduce the current density in regions of high electric field or to reduce the electric field in regions of high current density. Since modifications to the device structure affect the electric field and current density differently, it is not sufficient just to know the locations where high joule heating occurs, the dominant cause of the high joule heating must also be known before the structure can be modified.

In most semiconductor devices, the electric charges scatter of the atoms in the crystal lattice as they move through the device. Joule heating describes the energy that is transferred to the lattice structure as the electric charges move through the device. The joule heat power in a given region of the device is proportional to the number of charges moving through the region and to the size of the electric field that causes those charges to move. Consequently, the expression shown in (7) can be used to determine the joule heat power density at any given location in a semiconductor device.

$$P_{\text{joule}} \propto J \cdot E \tag{7}$$

where P_{joule} is the joule heat power density (W/cm^3), J is the current density (A/cm^2), and E is the electric field (V/cm).

Figure 39 shows the joule heat power for the uniform and non-uniform GTO thyristors at three different points in the multiple unit simulations. From the plots, it can be seen that there are three locations of high joule heating in each unit cell: in the center of the n-Base region, along the perimeter of the anode shorts, and at the junction between the gate and n-Base region. In order to

determine the dominant cause of joule heating at those locations, the multiple unit simulation solutions were replotted using the expression in (8).

$$x = \frac{J}{\max\ J} - \frac{E}{\max\ E} \tag{8}$$

where J is the current density (A/cm^2), E is the electric field (V/cm), and x is a unitless number between -1 and 1. The expression normalizes the current density and electric field and compares the two values; the expression outputs a value greater than zero if the current density is the dominant cause of joule heating and outputs a value less than zero if the electric field is the dominant cause of joule heating.

Figure 41 shows a plot of the expression in (8) for one of the multiple pulse simulation solution that represents the GTO thyristor in the on-state. The green, yellow, and red areas represent locations where current density is the primary cause of joule heating. The dark blue areas represent locations where electric field is the dominant cause of joule heating. The cyan areas represent locations where the electric field and current density have a similar impact on joule heating. From the figure, it can be seen that current density is the dominant cause of joule heating for most of the device during conduction.

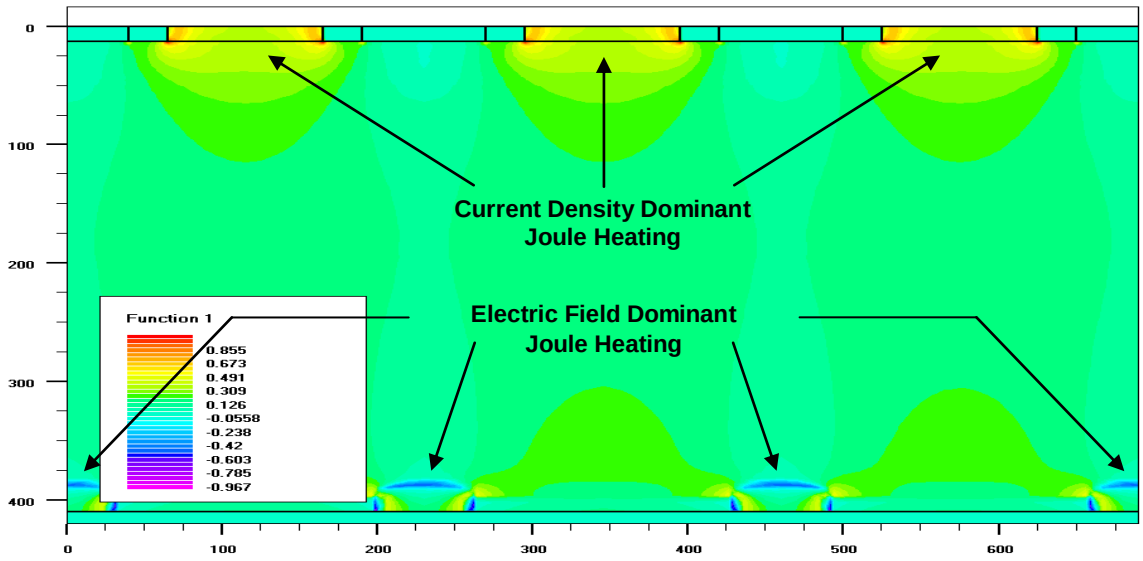

Figure 41. Dominant Cause of Joule Heating in a GTO in the On-State.

Figure 42 shows a plot of the expression in (8) for one of the multiple pulse simulation solution representing the GTO thyristor during turn-off. The green, yellow, and red areas represent locations where current density is the primary cause of joule heating. The dark blue areas represent locations where electric field is the dominant cause of joule heating. The cyan areas represent locations where the electric field and current density have a similar impact on joule heating. From the figure, it can be seen that current density is slightly more prominent in the gate region of the device where the anode current is pinched off and electric field is more prominent in the junction between the gate and n-Base regions. However, due to the increase in current density and electric field during turn-off, they both have similar effects on the joule heating for most of the device.

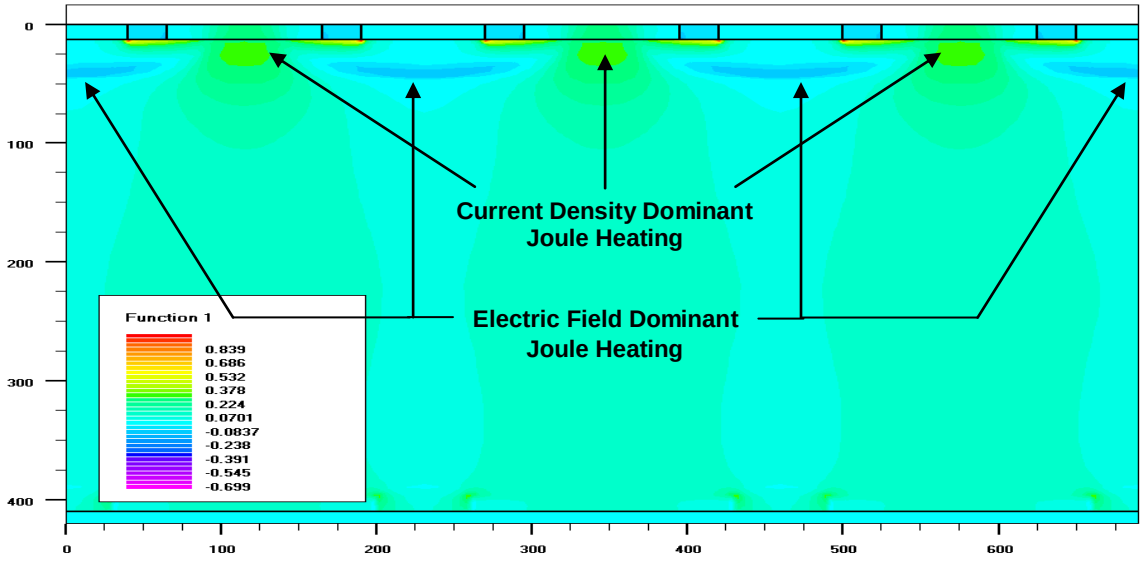

Figure 42. Dominant Cause of Joule Heating in a GTO During Turn-Off.

The final two chapters of this thesis discuss the conclusions that can be made from the research performed in this project and the future work that can be done to extend this project. In addition to discussing the operating characteristics of a GTO thyristor, Chapter VII comments on the energy tracking methodology that was developed in this project. The future work section includes some recommended changes to the SILVACO simulation suite that would extend its usefulness as a physics-based device simulation tool.

THIS PAGE INTENTIONALLY LEFT BLANK

VII. CONCLUSIONS

The physical device model that was implemented for this project correctly simulated the general electrical characteristics of a GTO thyristor. The model made it possible to examine the internal electrical and thermal operating characteristics of the GTO thyristor device. The SPICE circuit model that was constructed for this thesis correctly simulated the electrical characteristics of the simplified inductive pulsed power circuit that was used in the Trident Research Project [2]. The following sections discuss some of the conclusions that can be drawn from the simulation results.

A. DOMINANT HEATING MECHANISM IN A GTO THYRISTOR.

By analyzing the internal structure of the device, it was determined that the primary mechanism for thermal energy generation in a GTO thyristor is joule heating. Although joule heating occurs throughout the internal structure of the GTO thyristor, it is prominent anywhere a high current density coincides with a high electric field. During conduction, joule heating is prominent in the center of the n-Base region and along the perimeter of the anode short regions. During turn-off, the location of maximum heating shifts upwards to the junction between the gate and n-Base regions as the turn-off gate current creates an electric field along the junction and pinches of the anode current. The resulting high electric field and high current density cause significant joule heating and the formation of hot spots within the GTO thyristor.

The simulation solution files were used to examine the current density and electric fields in the GTO thyristor in order to determine the dominant cause of joule heating in the device. The structures show that current density is the dominant cause of joule heating for most of the device during conduction, especially in the n-Base region at the center of each unit cell. During turn-off, the electric field and current densities increase such that they both have a similar impact on the joule heating in the device.

The simulation solution files showed that the peak temperatures in the GTO thyristor were located in the n-Base region at the center of each unit cell (except during turn-off when the locations of peak temperature shifted up towards the gate/n-Base junction). Since thermal energy flows from high temperature to low temperature, a significant amount of stored thermal energy must have been generated at the center of the n-Base region. Joule heating alone might not account for all the thermal energy generated at the center of the n-Base region (the joule heat power density was greater along the perimeter of the anode shorts than it was in the center of the n-Base region). It is possible that another heating mechanism, such as Peltier-Thompson heating, was responsible for a significant amount of the thermal energy generated in the device.

In semiconductor devices, temperature gradients can cause electric charges in the conduction and valance bands to move. As the electrons and holes move, they scatter off the atoms in the semiconductor material and transfer energy to the crystal lattice. Peltier-Thompson heating describes the thermal energy that is generated in a semiconductor device due to thermally induced currents in the device. The simulations that were performed in this thesis did account for Peltier-Thompson heating; however, it was not possible to examine the solution files to compare the Peltier-Thompson and joule heat powers due to the time constraints of this thesis.

B. DEVICE RELIABILITY AND LIFETIME

The results of this project suggest that it might be possible to predict the lifetime of GTO thyristor device by measuring the temperature of the hot spots that form during turn-off. Since many GTO thyristor failures are ultimately caused by thermally induced changes to the device structure, the mean time to failure can be estimated using the Arrhenius model for device failure. Before this approach could be used to compute an actual lifetime for the GTO thyristor, a physics of failure study would have to be performed to determine the activation energies of the possible failure mechanisms. However, the approach could be

used with estimated activation energies to examine how changes to the GTO thyristor structure or operating conditions might affect the lifetime of the device.

For example, the peak temperature in the multiple unit cell GTO thyristor during turn-off was 328K for the non-uniform device with a 10% difference in doping, 315K for the non-uniform device with a 5% difference in doping, and 310K for the uniform device. Using an activation energy of 1.0eV (estimated activation energy for temperature induced contact electromigration, [19]), it can be shown that the non-uniform GTO thyristors with a 10% difference in gate doping has an estimated lifetime that is seven times shorter than the expected lifetime of the uniform GTO thyristor. The non-uniform GTO thyristor with a 5% difference in gate doping has an estimated lifetime that is only two times shorter than the lifetime of the uniform GTO thyristor. Thus, the reduction in lifetime appears to be tied directly to the amount of non-uniformity in the device structure, which is expected given the fact that the peak temperature during turn-off is higher for the device with a higher degree of non-uniformity.

C. ENERGY TRACKING METHODOLOGY

The energy tracking methodology that was developed in this project was successfully used to track the flow of energy in the SPICE circuit and the GTO thyristor. The method was able to accurately measure the energy in the SPICE circuit components and track the amount of electrical energy input to the GTO thyristor during each current pulse. The energy tracking method was able to approximate the thermal energy stored within the structure of the GTO thyristor and track the flow of energy into and out off the device. The energy tracking method provided insights into the operation of the GTO thyristor; however, the method requires significant refinement before it can be used further.

Using the energy tracking method it was determined that most of the electrical energy input to the GTO thyristor was converted into thermal energy and stored within the structure of the device. Furthermore, the majority of the thermal energy in the device was stored in the aluminum electrodes. Given the

size of the anode and gate electrodes (and thus their total heat capacity) and the thermal resistance of the thermal contact, it would take a fairly long time for the GTO thyristor to reach thermal equilibrium under the operating conditions used in the multiple pulse simulations.

The results of this thesis suggest an explanation for the discrepancy between the rated current interruption capability of GTO thyristors and their actual current interruption capability in a pulsed power circuit (the later usually being 2-3 times higher). During each current pulse and especially at turn-off, the GTO thyristor receives electrical energy from the external circuit; this energy is converted into thermal energy and stored inside the device until it can be output through the thermal contact. The device requires significantly more time to output the thermal energy through the thermal contact than it does to absorb the electrical energy from the external circuit. Consequently, at high switching frequencies the turn-off current (usually the peak of the current pulse) has to be reduced to ensure that the device can dissipate all of the electrical energy from each current pulse through the thermal contact.

The results of this thesis also suggest that the specifications and rated capabilities of a semiconductor device are related to the device's ability to receive, store, and output energy. It might be possible to incorporate all of the device ratings—such as maximum interruptible current, maximum surge current, maximum repetitive on-state current, and maximum turn-off gate current—into a small set of energy-based specifications. These energy-based specifications would allow the performance of the device to be predicted for operating conditions that are different from those used by the manufacturer to determine the specifications and capabilities of the device.

VIII. FUTURE WORK

There is a significant amount of work that could be done to improve upon or extend the work done in this thesis. The following sections of this chapter discuss a few potential areas for follow on effort.

A. ENERGY TRACKING METHOD

The most obvious extension of this project would be to refine the energy tracking method to more accurately follow the energy in the GTO thyristor. The method developed for this project was able to show where thermal energy was stored within the structure of the GTO thyristor, but was not able to account for all of the energy in the device. It might be possible to improve the accuracy of the energy tracking method by modifying the number and position of the measurement locations to improve the accuracy of the thermal and electric energy calculations. Additionally, it might be necessary to modify the mesh grid in regions of high heat power density to more accurately simulate local heating.

The physical device model that was used in this project needs to be refined to improve the speed and numerical stability of the simulations. The single unit GTO thyristor was modeled using a device structure that had 8855 grid points and the multiple unit GTO thyristor was modeled using a device structure that had 18678 grid points. In order to meet the time constraints of this thesis, the simulations were conducted using a UNIX cluster of 8-core 3.0GHz Intel processors (each 8-core processor could run a single simulation). Using the cluster, it took 5-6 hours to complete a single pulse simulation with the single unit GTO thyristor structure and almost 48 hours to complete a single pulse simulation with the multiple unit GTO thyristor structure. Future projects should refine the GTO thyristor structures to achieve more reasonable simulation times.

One potential way to refine the physical device model would be to use SILVACO ATLAS^{TM} to regrid the device structure using some of the simulations performed for this thesis. The regrid process would increase the number of grid

points wherever things change quickly in the device (high electric fields, large temperature gradients, abrupt changes in doping concentration, etc.) and would reduce the number of grid points wherever things change slowly (in the center of a large semiconductor region). By refining the physical device structure, it might be possible to improve the speed and numerical stability of the simulations. Additionally, if refinements reduce the overall number of grid points in the single unit cell structure, then it might be possible to incorporate additional unit cells into the multiple unit cell device structure.

In addition to refining the energy tracking method to more accurately measure the thermal energy stored in the GTO thyristor, the method needs to be modified to track the generation of thermal energy in the device. This would allow the energy tracking methodology to proactively follow the thermal energy in the device (i.e., what is being generated) instead of reactively tracking the thermal energy in the device (i.e., what was generated). The modification would also allow the energy tracking method to be used in reliability studies because it would show the locations in the device that are responsible for energy generation and the locations that are responsible for energy storage.

The modified energy tracking method should be used to investigate the three thermal energy generation mechanisms—joule heating, recombination-generation heating, and Peliter Thompson heating—to determine how each affects the operation of the GTO thyristor. For this project, the energy tracking method only looked at recombination-generation heating and joule heating.

B. NUMERICAL STABILITY OF THE SIMULATIONS

Additional work is also required to improve the numerical stability of the simulations. One of the biggest obstacles to completing this project was numerical instabilities that would cause the simulations to either crash or take a very long time to compute (by requiring very small time steps for the simulations). SILVACO ATLAS^{TM} allows the user to specify the numerical methods and parameters (tolerance, maximum number of iterations, maximum change

between iteration, etc.) used in the simulation; these parameters affect the speed, stability, and accuracy of the device simulation. For future research projects, the numerical methods and parameters need to be adjusted in order to improve the speed and stability of the MixedMode simulations of the GTO thyristor.

C. MODEL VALIDATION

For this project, it was not possible to adjust the physical device model and the SPICE circuit model to perfectly match the experimental GTO thyristor waveforms. Additionally, it was not possible to determine the exact physical dimensions and doping concentration of the GTO thyristor used in [2]. The simulations could be improved by reverse engineering[2] an actual GTO thyristor device to determine the exact dimensions of the device. The simulations could also be improved by experimentally measuring the thermal characteristics of the GTO thyristor in order to rigorously validate the physical device model.

Another area of future effort would be to modify the SPICE circuit model to simulate a more realistic gate driver circuit. For this project, the gate driver only consisted of a simple voltage source, capacitor bank, and variable resistor; a realistic gate driver would incorporate multiple semiconductor switches (MOSFET, IGBT, BJTs, etc.), several capacitor banks, blocking diodes, and the circuitry to control the gate driver switches. Using a more realistic gate driver in the SPICE circuit would allow the operating characteristics of the GTO thyristor to be more accurately studied. The more realistic gate driver would also allow the SPICE circuit to be more accurately matched to an actual inductive pulsed power circuit.

---

[2] In the past decade, the semiconductor industry has developed procedures and techniques that can be used to determine the physical makeup of semiconductor devices. These techniques, originally developed to check for patent and intellectual property infringement, can be used to measure the physical dimensions, material composition, and doping concentrations of a semiconductor device.

In some of the high power electrical systems currently being developed by the different members of the IAPG, the systems fail due to problems with the gate driver switches instead of the primary switching devices; this might be due to the fact that the primary switching devices are often robust or significantly derated, while the switches in the gate driver are often operated much closer to their design limits. Since ATLAS™ allows more than one physical device model to be incorporated into a MixedMode simulation, it would be possible to incorporate physical device models of the gate switches into the SPICE circuit model of the inductive pulsed power source in order to investigate the effect of the GTO thyristor on the gate driver switches.

D. PHYSICS-BASED SIMULATION TOOL

A final area of additional work would be to modify the SILVACO simulation suite to simulate the physical degradation of the GTO thyristor. For this project, the simulations assume that the physical device structure does not change during the simulations regardless of the amount of energy that is transferred through the device. In real life, the thermal or electric energy passing through a device causes atoms in the device material(s) to move; the process can take a long time, i.e., electromigration or thermal migration, or occur very quickly, i.e., dielectric breakdown or thermal failure (aka. melting). Regardless of how fast the change takes place, the flow of energy through a device will change the structure of that device over time.

SILVACO incorporates a program called ATHENA™ to simulate the fabrication of semiconductor devices; ATHENA™ uses physics-based models of the various semiconductor fabrication processes to construct a physical device structure to use in ATLAS™. If the SILVACO simulation suite can be modified to use ATHENA™ to modify an existing structure based on the energy that is input to the device during an ATLAS™ simulation, then SILVACO will be able to simulate physical device degradation. This capability would be incredibly useful to studying device failure mechanisms and device reliability.

APPENDIX A: LESSONS LEARNED

This appendix outlines some of the important lessons that were learned regarding the use of SILVACO for device simulations. The appendix also discusses the procedure that was used to access and utilize the UNIX cluster (hamming) to run the simulations for this thesis. Hopefully, this section can reduce the learning curve for future users of SILVACO.

For MixedMode simulations, it is important to consolidate energy storage elements as much as possible to improve the numerical stability of the simulations. If multiple elements are connected together, especially if they are connected in parallel, small amplitude, high frequency oscillating current and voltage transients can occur. These transients seriously impinge on the maximum step size that can be used in the simulations; if the transients are significantly fast and underdamped, the simulation can either fail completely (not converge) or enter a terminal state where the step size is 6-8 orders of magnitude smaller than the thyristor turn-off process (i.e., a femtosecond step size for a microsecond turn-off process).

SILVACO has several built-in extract routines that can be used to pull data from a log file or a structure file. The syntax can be used to read in multiple waveforms, algebraically manipulate the data, and output the data to a log file. Unfortunately, the extract routines have some serious limitations: First, the total line length of any single extract statement is 256 characters, which limits the number of waveforms that can be manipulated by any single extract statement. Second, the extract routines cannot be used to perform element-by-element operations on multiple waveforms. Consequently, the extract routines were not used for this project; instead, a MATLAB script was written to pull the saved simulation data from the log file, manipulate the data, and generate the voltage, current, power, energy, and temperature waveforms.

Most of the simulation data used for this thesis was collected using the hamming UNIX cluster at the Naval Postgraduate School High Performance Computing center. The cluster was accessed using a Putty terminal via the school intranet or remotely through a VPN client. The simulation input and output files were transferred to and from the cluster using WinSCP.

The basic procedure used to run simulations on the hamming cluster consisted of the following steps: First, open WinSCP, log into the hamming cluster, and transfer the simulation input file to the working directory on the cluster. Second, open a Putty window, log into the hamming cluster, and access the working directory of the cluster. Third, type the command *atlas* <*filename*> *-logfile* <*name*> to start the simulation; the cluster would then hand the input file to ATLAS™, which would run the simulation and generate the simulation output files (structure files or log files). The simulation would also generate a text file called *name* that contained the ATLAS™ debugging outputs.

The hamming cluster has some peculiar characteristics that required special considerations when running a simulation in ATLAS™. The cluster would not run multiple jobs in sequence if the jobs were contained in the same input file (each job was enclosed between the *go atlas* and *quit* commands). Consequently, three different simulation input files had to be run in sequence to complete the simulations for this thesis; the first input file generated the GTO thyristor structure, the second input file applied the DC bias to the off-state device, and the third structure file simulated the transient current pulse(s).

Normally, input files are run using the Deckbuild™ program, which can acess the full range of SILVACO tools. (Deckbuild™ essentially reads the command line in the input file and passes the command to the appropriate simulation tool.) Unfortunately, the hamming cluster can not run Deckbuild™, TonyPlot™, or the other data manipulation tools in SILVACO. Consequently, the input files had to be passed directly to ATLAS™ (done using the command shown above) and could not contain any commands that called for TonyPlot™ or any of the other data display tools.

APPENDIX B: ATLAS™ INPUT FILE (SINGLE UNIT STRUCTURE)

```
go atlas

################  Define Mesh Grid for Device Model  ################
mesh

x.mesh loc=0.00   spac=15.0
x.mesh loc=65.0   spac=2.5
x.mesh loc=90.0   spac=0.25
x.mesh loc=140.0  spac=7.5
x.mesh loc=190.0  spac=0.25
x.mesh loc=215.0  spac=2.5
x.mesh loc=280.0  spac=15.0

y.mesh loc=0.0    spac=5.0
y.mesh loc=12.8   spac=0.2
y.mesh loc=13.0   spac=0.2
y.mesh loc=16.0   spac=5.0
y.mesh loc=44.0   spac=5.0
y.mesh loc=47.0   spac=1.0
y.mesh loc=50.0   spac=10.0
y.mesh loc=220.0  spac=25.0
y.mesh loc=376.0  spac=10.0
y.mesh loc=393.0  spac=0.5
y.mesh loc=410.0  spac=2.5
y.mesh loc=420.0  spac=2.5


#####################  Define Regions and Electrodes  ##################
region    num=1  silicon      x.min=90    x.max=190    y.min=0.0  y.max=13
region    num=2  silicon      x.min=0.0   x.max=280    y.min=13   y.max=410
region    num=3  insulator    x.min=65    x.max=90     y.min=0.0  y.max=13
region    num=4  insulator    x.min=190   x.max=215    y.min=0.0  y.max=13

electrode  num=1  x.min=90.  x.max=190  y.min=0.0  y.max=0.0   name=cathode
electrode  num=2  x.min=0.0  x.max=65   y.min=0.0  y.max=13    name=gate1
electrode  num=3  x.min=215 x.max=280  y.min=0.0  y.max=13    name=gate2
electrode  num=4  x.min=0.0  x.max=280  y.min=410 y.max=415  name=anode

contact   name=cathode  device=agto   aluminum
contact   name=gate1    device=agto   aluminum
contact   name=gate2    device=agto   aluminum
contact   name=anode    device=agto   aluminum
```

```
 ######################  Define Doping Profile  ######################
doping  reg=2  uniform  conc=1.e13  n.type

# Gate
doping  reg=2  gauss   conc=1.0e17  p.type  junc=47  x.l=0.0 x.r=280

# Cathode
doping  reg=1  gauss   conc=1e19  n.type  junc=16   x.l=97.5  x.r=182.5  rat=0.8

# Anode

doping  reg=2 gauss conc=1e20 p.type peak=410 junc=393 x.l=55 x.r=225 rat=.1
doping  reg=2 gauss  conc=1e17  n.type  peak=410  char=10    x.l=0.0  x.r=55
doping  reg=2 gauss  conc=1e17  n.type  peak=410  char=10    x.l=225 x.r=280
#####################################################################

solve init
save outf=GTOstruct.str
tonyplot GTOstruct.str -set GTOstruct.set

quit
```

APPENDIX C: ATLAS™ INPUT FILE (MULTI-UNIT STRUCTURE)

```
go atlas

 ################  Define Meshgrid for Device Model  ################
mesh

# Horizontal Mesh Specification
x.mesh loc=0.00   spac=10.0
x.mesh loc=40.0   spac=1.0
x.mesh loc=65.0   spac=1
x.mesh loc=115.0  spac=10
x.mesh loc=165.0  spac=1
x.mesh loc=190.0  spac=1.0
x.mesh loc=230.0  spac=10.0
x.mesh loc=270.0  spac=1.0
x.mesh loc=295.0  spac=1
x.mesh loc=345.0  spac=10
x.mesh loc=395.0  spac=1
x.mesh loc=420.0  spac=1.0
x.mesh loc=460.0  spac=10.0
x.mesh loc=500.0  spac=1.0
x.mesh loc=525.0  spac=1
x.mesh loc=575.0  spac=10
x.mesh loc=625.0  spac=1
x.mesh loc=650.0  spac=1.0
x.mesh loc=690.0  spac=10.0

# Vertical Mesh Specification
y.mesh loc=0.0    spac=5.0
y.mesh loc=12.5   spac=0.5
y.mesh loc=13.5   spac=0.5
y.mesh loc=16.0   spac=5.0
y.mesh loc=44.0   spac=5.0
y.mesh loc=47.0   spac=1.0
y.mesh loc=50.0   spac=5.0
y.mesh loc=220.0  spac=25.0
y.mesh loc=376.0  spac=5.0
y.mesh loc=390.0  spac=1.0
y.mesh loc=410.0  spac=5.0
y.mesh loc=420.0  spac=5.0
```

```
 ##################### Define Regions and Electrodes ###################
region  num=1  silicon     x.min=65   x.max=165   y.min=0.0  y.max=13
region  num=2  silicon     x.min=295  x.max=395   y.min=0.0  y.max=13
region  num=3  silicon     x.min=525  x.max=625   y.min=0.0  y.max=13
region  num=4  silicon     x.min=0.0  x.max=690   y.min=13   y.max=410
region  num=5  insulator   x.min=40   x.max=65    y.min=0.0  y.max=13
region  num=6  insulator   x.min=165  x.max=190   y.min=0.0  y.max=13
region  num=7  insulator   x.min=270  x.max=295   y.min=0.0  y.max=13
region  num=8  insulator   x.min=395  x.max=420   y.min=0.0  y.max=13
region  num=9  insulator   x.min=500  x.max=525   y.min=0.0  y.max=13
region  num=10 insulator   x.min=625  x.max=650   y.min=0.0  y.max=13

electrode  num=1  x.min=65.  x.max=165  y.min=0.0  y.max=0.0   name=cath1
electrode  num=2  x.min=295  x.max=395  y.min=0.0  y.max=0.0   name=cath2
electrode  num=3  x.min=525  x.max=625  y.min=0.0  y.max=0.0   name=cath3
electrode  num=4  x.min=0.0  x.max=40   y.min=0.0  y.max=13    name=gate1
electrode  num=5  x.min=190  x.max=270  y.min=0.0  y.max=13    name=gate2
electrode  num=6  x.min=420  x.max=500  y.min=0.0  y.max=13    name=gate3
electrode  num=7  x.min=650  x.max=690  y.min=0.0  y.max=13    name=gate4
electrode  num=8  x.min=0.0  x.max=690  y.min=410 y.max=420   name=anode

contact    name=cath1    device=agto   aluminum
contact    name=cath2    device=agto   aluminum
contact    name=cath3    device=agto   aluminum
contact    name=gate1    device=agto   aluminum
contact    name=gate2    device=agto   aluminum
contact    name=gate3    device=agto   aluminum
contact    name=gate4    device=agto   aluminum
contact    name=anode    device=agto   aluminum


 ###################### Define Doping Profile ######################
doping  reg=4  uniform  conc=1.e13  n.type

# Gate
doping  reg=4  gauss  conc=1.1e17  p.type  junc=47  x.l=0.0  x.r=230
doping  reg=4  gauss  conc=0.9e17  p.type  junc=47  x.l=230 x.r=460
doping  reg=4  gauss  conc=1.0e17  p.type  junc=47  x.l=460 x.r=690

# Cathode
doping  reg=1  gauss  conc=1.0e19  n.type  junc=16  x.l=72.5   x.r=157.5  rat=0.8
doping  reg=2  gauss  conc=1.0e19  n.type  junc=16  x.l=302.5 x.r=387.5  rat=0.8
doping  reg=3  gauss  conc=1.0e19  n.type  junc=16  x.l=532.5 x.r=617.5  rat=0.8
```

```
# Anode
dop  reg=4  gauss conc=1e20 p.type peak=410 junc=393 x.l=30 x.r=200   rat=0.1
dop  reg=4  gauss conc=1e20 p.type peak=410 junc=393 x.l=260 x.r=430 rat=0.1
dop  reg=4  gauss conc=1e20 p.type peak=410 junc=393 x.l=490 x.r=660 rat=0.1
dop  reg=4  gauss  conc=1.0e17  n.type  peak=410  char=10   x.l=0.0   x.r=30
dop  reg=4  gauss  conc=1.0e17  n.type  peak=410  char=10   x.l=200  x.r=260
dop  reg=4  gauss  conc=1.0e17  n.type  peak=410  char=10   x.l=430  x.r=490
dop  reg=4  gauss  conc=1.0e17  n.type  peak=410  char=10   x.l=660  x.r=690
#################################################################

solve init
save outf=MultiGTOHetero.str
```

THIS PAGE INTENTIONALLY LEFT BLANK

APPENDIX D: ATLAS™ INPUT FILE (THYRISTOR SIMULATION)

```
#########################################################################
 #          Single Pulse Simulation of a GTO with Protection Circuitry                #
  #     Models the Following Semiconductor Characteristics – Heat Storage      #
  #  Heat Transfer, Impact Ionization, Auger Recombination, Field Dependent  #
  #     Mobility, Concentration Dependent Mobility, Electron and Hole Temp     #
 #########################################################################
go atlas simflags="-P 8"

.begin
# Voltage Source #
Vs  2 0 100
Rs  3 2 10
Rgnd1 3 0 1e6
# Capacitor Bank #
C1 0 1 9.6mF
R1 1 3 54.7m
# Protection Diode #
Dgto   3 15 dd
LDgto 15  4 10nH
Rgnd2  4  0 1e6
# Gate Turn Off Thyristor #
agto 4=anode 7=cathode 13=gate1 14=gate2  width=1.0e4 infile=GTOstruct.str
Rint 13 14 10n
# Snubber Circuit
Dsnub 4 5 dd
Lsnub 5 6 5nH
Rsnub 4 6 100
Csnub 6 7 470nF
# Pulse Shaping Inductor #
Lpulse 7 8 4.62mH
Rpulse 8 0 1.03
Dpulse 0 7 dd
# H-Bridge Gate Driver #
Vg1   9 7 0.25  PULSE 0.25 5.0  2ms  100us 100us 100us  1
Vg2  10 9 -.25  PULSE -.25 -20  10ms 250ns   2ms  50us  1
Rsrc 10 11 25m
Cgate  7 11 10uF
Lgate 11 12 5nH
Rgate 12 13 5   PULSE 5 5m  10ms 100ns 100us 10us
Rgnd3  9 0 1e6
Rgnd4 10 0 1e6
```

```
# Options #
.numeric toldc=1.e-6 vchange=0.25 imaxdc=100
.model dd d is=1e-7
.options m2ln relpot print debug

# Anaylsis #
.tran 200us 100ms
.load infile=GTOoff100
.log outfile=SinglePulse
.end

################## Specify Models and Materials ###################
thermcon  device=agto num=1  x.min=0.0 x.max=280  y.min=420 y.max=420
ext.temp=300  alpha=1

material device=agto reg=1 taun0=2.4e-6 taup0=0.6e-6 hc.std tcon.polyn
tc.a=0.03 tc.b=0.00156 tc.c=1.65e-6
material device=agto reg=2 taun0=2.4e-6 taup0=0.6e-6 hc.std tcon.polyn
tc.a=0.03 tc.b=0.00156 tc.c=1.65e-6
material device=agto reg=3 permitti=1
material device=agto reg=4 permitti=1

impact device=agto selb reg=1
impact device=agto selb reg=2

models  device=agto reg=1  analytic fldmob conmob srh auger bgn lat.temp
heat.full hcte print
models  device=agto reg=2  analytic fldmob conmob srh auger bgn lat.temp
heat.full hcte print
#####################################################################

#################### Specify Output Parameters ####################
output flowlines  jx.e jy.e jx.h jy.h  e.temp h.temp  e.velocity h.velocity
method block newton
#####################################################################

############################## Probe ##################################
## TEMERATURE ##
probe device=agto name=K_t00 lat.temp x=100 y=3
probe device=agto name=K_t01 lat.temp x=100 y=6
probe device=agto name=K_t02 lat.temp x=100 y=9
probe device=agto name=K_t03 lat.temp x=100 y=12
probe device=agto name=K_t04 lat.temp x=110 y=5
probe device=agto name=K_t05 lat.temp x=110 y=10
probe device=agto name=K_t06 lat.temp x=120 y=3
```

probe device=agto name=K_t07 lat.temp x=120 y=6
probe device=agto name=K_t08 lat.temp x=120 y=9
probe device=agto name=K_t09 lat.temp x=120 y=12
probe device=agto name=K_t10 lat.temp x=130 y=5
probe device=agto name=K_t11 lat.temp x=130 y=10
probe device=agto name=K_t12 lat.temp x=140 y=3
probe device=agto name=K_t13 lat.temp x=140 y=6
probe device=agto name=K_t14 lat.temp x=140 y=9
probe device=agto name=K_t15 lat.temp x=140 y=12
probe device=agto name=K_t16 lat.temp x=150 y=5
probe device=agto name=K_t17 lat.temp x=150 y=10
probe device=agto name=K_t18 lat.temp x=160 y=3
probe device=agto name=K_t19 lat.temp x=160 y=6
probe device=agto name=K_t20 lat.temp x=160 y=9
probe device=agto name=K_t21 lat.temp x=160 y=12
probe device=agto name=K_t22 lat.temp x=170 y=5
probe device=agto name=K_t23 lat.temp x=170 y=10
probe device=agto name=K_t24 lat.temp x=180 y=3
probe device=agto name=K_t25 lat.temp x=180 y=6
probe device=agto name=K_t26 lat.temp x=180 y=9
probe device=agto name=K_t27 lat.temp x=180 y=12

probe device=agto name=G_t00 lat.temp x=50. y=15
probe device=agto name=G_t01 lat.temp x=50. y=30
probe device=agto name=G_t02 lat.temp x=50. y=45
probe device=agto name=G_t03 lat.temp x=60. y=20
probe device=agto name=G_t04 lat.temp x=60. y=40
probe device=agto name=G_t05 lat.temp x=70. y=15
probe device=agto name=G_t06 lat.temp x=70. y=30
probe device=agto name=G_t07 lat.temp x=70. y=45
probe device=agto name=G_t08 lat.temp x=80. y=20
probe device=agto name=G_t09 lat.temp x=80. y=40
probe device=agto name=G_t10 lat.temp x=90. y=20
probe device=agto name=G_t11 lat.temp x=90. y=40
probe device=agto name=G_t12 lat.temp x=100 y=15
probe device=agto name=G_t13 lat.temp x=100 y=30
probe device=agto name=G_t14 lat.temp x=100 y=45
probe device=agto name=G_t15 lat.temp x=110 y=20
probe device=agto name=G_t16 lat.temp x=110 y=40
probe device=agto name=G_t17 lat.temp x=120 y=15
probe device=agto name=G_t18 lat.temp x=120 y=30
probe device=agto name=G_t19 lat.temp x=120 y=45
probe device=agto name=G_t20 lat.temp x=130 y=15
probe device=agto name=G_t21 lat.temp x=130 y=30
probe device=agto name=G_t22 lat.temp x=130 y=45

probe device=agto name=G_t23 lat.temp x=140 y=15
probe device=agto name=G_t24 lat.temp x=140 y=25
probe device=agto name=G_t25 lat.temp x=140 y=35
probe device=agto name=G_t26 lat.temp x=140 y=45
probe device=agto name=G_t27 lat.temp x=150 y=15
probe device=agto name=G_t28 lat.temp x=150 y=30
probe device=agto name=G_t29 lat.temp x=150 y=45
probe device=agto name=G_t30 lat.temp x=160 y=15
probe device=agto name=G_t31 lat.temp x=160 y=30
probe device=agto name=G_t32 lat.temp x=160 y=45
probe device=agto name=G_t33 lat.temp x=170 y=20
probe device=agto name=G_t34 lat.temp x=170 y=40
probe device=agto name=G_t35 lat.temp x=180 y=15
probe device=agto name=G_t36 lat.temp x=180 y=30
probe device=agto name=G_t37 lat.temp x=180 y=45
probe device=agto name=G_t38 lat.temp x=190 y=20
probe device=agto name=G_t39 lat.temp x=190 y=40
probe device=agto name=G_t40 lat.temp x=200 y=20
probe device=agto name=G_t41 lat.temp x=200 y=40
probe device=agto name=G_t42 lat.temp x=210 y=15
probe device=agto name=G_t43 lat.temp x=210 y=30
probe device=agto name=G_t44 lat.temp x=210 y=45
probe device=agto name=G_t45 lat.temp x=220 y=20
probe device=agto name=G_t46 lat.temp x=220 y=40
probe device=agto name=G_t47 lat.temp x=230 y=15
probe device=agto name=G_t48 lat.temp x=230 y=30
probe device=agto name=G_t49 lat.temp x=230 y=45

probe device=agto name=N_t00 lat.temp x=30. y=90
probe device=agto name=N_t01 lat.temp x=30. y=185
probe device=agto name=N_t02 lat.temp x=60. y=90
probe device=agto name=N_t03 lat.temp x=60. y=185
probe device=agto name=N_t04 lat.temp x=80. y=75
probe device=agto name=N_t05 lat.temp x=80. y=137.5
probe device=agto name=N_t06 lat.temp x=80. y=200
probe device=agto name=N_t07 lat.temp x=100 y=75
probe device=agto name=N_t08 lat.temp x=100 y=137.5
probe device=agto name=N_t09 lat.temp x=100 y=200
probe device=agto name=N_t10 lat.temp x=30. y=250
probe device=agto name=N_t11 lat.temp x=30. y=350
probe device=agto name=N_t12 lat.temp x=60. y=250
probe device=agto name=N_t13 lat.temp x=60. y=350
probe device=agto name=N_t14 lat.temp x=80. y=225
probe device=agto name=N_t15 lat.temp x=80. y=300
probe device=agto name=N_t16 lat.temp x=80. y=375

probe device=agto name=N_t17 lat.temp x=100 y=225
probe device=agto name=N_t18 lat.temp x=100 y=300
probe device=agto name=N_t19 lat.temp x=100 y=375
probe device=agto name=N_t20 lat.temp x=120 y=75
probe device=agto name=N_t21 lat.temp x=120 y=137.5
probe device=agto name=N_t22 lat.temp x=120 y=200
probe device=agto name=N_t23 lat.temp x=135 y=50
probe device=agto name=N_t24 lat.temp x=140 y=125
probe device=agto name=N_t25 lat.temp x=140 y=200
probe device=agto name=N_t26 lat.temp x=145 y=50
probe device=agto name=N_t27 lat.temp x=160 y=75
probe device=agto name=N_t28 lat.temp x=160 y=137.5
probe device=agto name=N_t29 lat.temp x=160 y=200
probe device=agto name=N_t30 lat.temp x=120 y=225
probe device=agto name=N_t31 lat.temp x=120 y=300
probe device=agto name=N_t32 lat.temp x=120 y=375
probe device=agto name=N_t33 lat.temp x=130 y=375
probe device=agto name=N_t34 lat.temp x=140 y=225
probe device=agto name=N_t35 lat.temp x=140 y=300
probe device=agto name=N_t36 lat.temp x=150 y=375
probe device=agto name=N_t37 lat.temp x=160 y=225
probe device=agto name=N_t38 lat.temp x=160 y=300
probe device=agto name=N_t39 lat.temp x=160 y=375
probe device=agto name=N_t40 lat.temp x=180 y=75
probe device=agto name=N_t41 lat.temp x=180 y=137.5
probe device=agto name=N_t42 lat.temp x=180 y=200
probe device=agto name=N_t43 lat.temp x=200 y=75
probe device=agto name=N_t44 lat.temp x=200 y=137.5
probe device=agto name=N_t45 lat.temp x=200 y=200
probe device=agto name=N_t46 lat.temp x=220 y=90
probe device=agto name=N_t47 lat.temp x=220 y=185
probe device=agto name=N_t48 lat.temp x=250 y=90
probe device=agto name=N_t49 lat.temp x=250 y=185
probe device=agto name=N_t50 lat.temp x=180 y=225
probe device=agto name=N_t51 lat.temp x=180 y=300
probe device=agto name=N_t52 lat.temp x=180 y=375
probe device=agto name=N_t53 lat.temp x=200 y=225
probe device=agto name=N_t54 lat.temp x=200 y=300
probe device=agto name=N_t55 lat.temp x=200 y=375
probe device=agto name=N_t56 lat.temp x=220 y=250
probe device=agto name=N_t57 lat.temp x=220 y=350
probe device=agto name=N_t58 lat.temp x=250 y=250
probe device=agto name=N_t59 lat.temp x=250 y=350

```
probe device=agto name=a0 lat.temp x=10. y=410
probe device=agto name=a1 lat.temp x=40. y=410
probe device=agto name=a2 lat.temp x=70. y=410
probe device=agto name=a3 lat.temp x=100 y=410
probe device=agto name=a4 lat.temp x=130 y=410
probe device=agto name=a5 lat.temp x=150 y=410
probe device=agto name=a6 lat.temp x=180 y=410
probe device=agto name=a7 lat.temp x=210 y=410
probe device=agto name=a8 lat.temp x=240 y=410
probe device=agto name=a9 lat.temp x=270 y=410

## ELECTRON QUASI FERMI LEVEL ##
probe device=agto name=K_qfn00 qfn x=100 y=3
probe device=agto name=K_qfn01 qfn x=100 y=6
probe device=agto name=K_qfn02 qfn x=100 y=9
probe device=agto name=K_qfn03 qfn x=100 y=12
probe device=agto name=K_qfn04 qfn x=110 y=5
probe device=agto name=K_qfn05 qfn x=110 y=10
probe device=agto name=K_qfn06 qfn x=120 y=3
probe device=agto name=K_qfn07 qfn x=120 y=6
probe device=agto name=K_qfn08 qfn x=120 y=9
probe device=agto name=K_qfn09 qfn x=120 y=12
probe device=agto name=K_qfn10 qfn x=130 y=5
probe device=agto name=K_qfn11 qfn x=130 y=10
probe device=agto name=K_qfn12 qfn x=140 y=3
probe device=agto name=K_qfn13 qfn x=140 y=6
probe device=agto name=K_qfn14 qfn x=140 y=9
probe device=agto name=K_qfn15 qfn x=140 y=12
probe device=agto name=K_qfn16 qfn x=150 y=5
probe device=agto name=K_qfn17 qfn x=150 y=10
probe device=agto name=K_qfn18 qfn x=160 y=3
probe device=agto name=K_qfn19 qfn x=160 y=6
probe device=agto name=K_qfn20 qfn x=160 y=9
probe device=agto name=K_qfn21 qfn x=160 y=12
probe device=agto name=K_qfn22 qfn x=170 y=5
probe device=agto name=K_qfn23 qfn x=170 y=10
probe device=agto name=K_qfn24 qfn x=180 y=3
probe device=agto name=K_qfn25 qfn x=180 y=6
probe device=agto name=K_qfn26 qfn x=180 y=9
probe device=agto name=K_qfn27 qfn x=180 y=12

probe device=agto name=G_qfn00 qfn x=50. y=15
probe device=agto name=G_qfn01 qfn x=50. y=30
probe device=agto name=G_qfn02 qfn x=50. y=45
probe device=agto name=G_qfn03 qfn x=60. y=20
```

probe device=agto name=G_qfn04 qfn x=60. y=40
probe device=agto name=G_qfn05 qfn x=70. y=15
probe device=agto name=G_qfn06 qfn x=70. y=30
probe device=agto name=G_qfn07 qfn x=70. y=45
probe device=agto name=G_qfn08 qfn x=80. y=20
probe device=agto name=G_qfn09 qfn x=80. y=40
probe device=agto name=G_qfn10 qfn x=90. y=20
probe device=agto name=G_qfn11 qfn x=90. y=40
probe device=agto name=G_qfn12 qfn x=100 y=15
probe device=agto name=G_qfn13 qfn x=100 y=30
probe device=agto name=G_qfn14 qfn x=100 y=45
probe device=agto name=G_qfn15 qfn x=110 y=20
probe device=agto name=G_qfn16 qfn x=110 y=40
probe device=agto name=G_qfn17 qfn x=120 y=15
probe device=agto name=G_qfn18 qfn x=120 y=30
probe device=agto name=G_qfn19 qfn x=120 y=45
probe device=agto name=G_qfn20 qfn x=130 y=15
probe device=agto name=G_qfn21 qfn x=130 y=30
probe device=agto name=G_qfn22 qfn x=130 y=45
probe device=agto name=G_qfn23 qfn x=140 y=15
probe device=agto name=G_qfn24 qfn x=140 y=25
probe device=agto name=G_qfn25 qfn x=140 y=35
probe device=agto name=G_qfn26 qfn x=140 y=45
probe device=agto name=G_qfn27 qfn x=150 y=15
probe device=agto name=G_qfn28 qfn x=150 y=30
probe device=agto name=G_qfn29 qfn x=150 y=45
probe device=agto name=G_qfn30 qfn x=160 y=15
probe device=agto name=G_qfn31 qfn x=160 y=30
probe device=agto name=G_qfn32 qfn x=160 y=45
probe device=agto name=G_qfn33 qfn x=170 y=20
probe device=agto name=G_qfn34 qfn x=170 y=40
probe device=agto name=G_qfn35 qfn x=180 y=15
probe device=agto name=G_qfn36 qfn x=180 y=30
probe device=agto name=G_qfn37 qfn x=180 y=45
probe device=agto name=G_qfn38 qfn x=190 y=20
probe device=agto name=G_qfn39 qfn x=190 y=40
probe device=agto name=G_qfn40 qfn x=200 y=20
probe device=agto name=G_qfn41 qfn x=200 y=40
probe device=agto name=G_qfn42 qfn x=210 y=15
probe device=agto name=G_qfn43 qfn x=210 y=30
probe device=agto name=G_qfn44 qfn x=210 y=45
probe device=agto name=G_qfn45 qfn x=220 y=20
probe device=agto name=G_qfn46 qfn x=220 y=40
probe device=agto name=G_qfn47 qfn x=230 y=15
probe device=agto name=G_qfn48 qfn x=230 y=30

```
probe device=agto name=G_qfn49 qfn x=230 y=45

probe device=agto name=N_qfn00 qfn x=30. y=90
probe device=agto name=N_qfn01 qfn x=30. y=185
probe device=agto name=N_qfn02 qfn x=60. y=90
probe device=agto name=N_qfn03 qfn x=60. y=185
probe device=agto name=N_qfn04 qfn x=80. y=75
probe device=agto name=N_qfn05 qfn x=80. y=137.5
probe device=agto name=N_qfn06 qfn x=80. y=200
probe device=agto name=N_qfn07 qfn x=100 y=75
probe device=agto name=N_qfn08 qfn x=100 y=137.5
probe device=agto name=N_qfn09 qfn x=100 y=200
probe device=agto name=N_qfn10 qfn x=30. y=250
probe device=agto name=N_qfn11 qfn x=30. y=350
probe device=agto name=N_qfn12 qfn x=60. y=250
probe device=agto name=N_qfn13 qfn x=60. y=350
probe device=agto name=N_qfn14 qfn x=80. y=225
probe device=agto name=N_qfn15 qfn x=80. y=300
probe device=agto name=N_qfn16 qfn x=80. y=375
probe device=agto name=N_qfn17 qfn x=100 y=225
probe device=agto name=N_qfn18 qfn x=100 y=300
probe device=agto name=N_qfn19 qfn x=100 y=375
probe device=agto name=N_qfn20 qfn x=120 y=75
probe device=agto name=N_qfn21 qfn x=120 y=137.5
probe device=agto name=N_qfn22 qfn x=120 y=200
probe device=agto name=N_qfn23 qfn x=135 y=50
probe device=agto name=N_qfn24 qfn x=140 y=125
probe device=agto name=N_qfn25 qfn x=140 y=200
probe device=agto name=N_qfn26 qfn x=145 y=50
probe device=agto name=N_qfn27 qfn x=160 y=75
probe device=agto name=N_qfn28 qfn x=160 y=137.5
probe device=agto name=N_qfn29 qfn x=160 y=200
probe device=agto name=N_qfn30 qfn x=120 y=225
probe device=agto name=N_qfn31 qfn x=120 y=300
probe device=agto name=N_qfn32 qfn x=120 y=375
probe device=agto name=N_qfn33 qfn x=130 y=375
probe device=agto name=N_qfn34 qfn x=140 y=225
probe device=agto name=N_qfn35 qfn x=140 y=300
probe device=agto name=N_qfn36 qfn x=150 y=375
probe device=agto name=N_qfn37 qfn x=160 y=225
probe device=agto name=N_qfn38 qfn x=160 y=300
probe device=agto name=N_qfn39 qfn x=160 y=375
probe device=agto name=N_qfn40 qfn x=180 y=75
probe device=agto name=N_qfn41 qfn x=180 y=137.5
probe device=agto name=N_qfn42 qfn x=180 y=200
```

```
probe device=agto name=N_qfn43 qfn x=200 y=75
probe device=agto name=N_qfn44 qfn x=200 y=137.5
probe device=agto name=N_qfn45 qfn x=200 y=200
probe device=agto name=N_qfn46 qfn x=220 y=90
probe device=agto name=N_qfn47 qfn x=220 y=185
probe device=agto name=N_qfn48 qfn x=250 y=90
probe device=agto name=N_qfn49 qfn x=250 y=185
probe device=agto name=N_qfn50 qfn x=180 y=225
probe device=agto name=N_qfn51 qfn x=180 y=300
probe device=agto name=N_qfn52 qfn x=180 y=375
probe device=agto name=N_qfn53 qfn x=200 y=225
probe device=agto name=N_qfn54 qfn x=200 y=300
probe device=agto name=N_qfn55 qfn x=200 y=375
probe device=agto name=N_qfn56 qfn x=220 y=250
probe device=agto name=N_qfn57 qfn x=220 y=350
probe device=agto name=N_qfn58 qfn x=250 y=250
probe device=agto name=N_qfn59 qfn x=250 y=350

## HOLE QUASI FERMI LEVEL ##
probe device=agto name=K_qfp00 qfp x=100 y=3
probe device=agto name=K_qfp01 qfp x=100 y=6
probe device=agto name=K_qfp02 qfp x=100 y=9
probe device=agto name=K_qfp03 qfp x=100 y=12
probe device=agto name=K_qfp04 qfp x=110 y=5
probe device=agto name=K_qfp05 qfp x=110 y=10
probe device=agto name=K_qfp06 qfp x=120 y=3
probe device=agto name=K_qfp07 qfp x=120 y=6
probe device=agto name=K_qfp08 qfp x=120 y=9
probe device=agto name=K_qfp09 qfp x=120 y=12
probe device=agto name=K_qfp10 qfp x=130 y=5
probe device=agto name=K_qfp11 qfp x=130 y=10
probe device=agto name=K_qfp12 qfp x=140 y=3
probe device=agto name=K_qfp13 qfp x=140 y=6
probe device=agto name=K_qfp14 qfp x=140 y=9
probe device=agto name=K_qfp15 qfp x=140 y=12
probe device=agto name=K_qfp16 qfp x=150 y=5
probe device=agto name=K_qfp17 qfp x=150 y=10
probe device=agto name=K_qfp18 qfp x=160 y=3
probe device=agto name=K_qfp19 qfp x=160 y=6
probe device=agto name=K_qfp20 qfp x=160 y=9
probe device=agto name=K_qfp21 qfp x=160 y=12
probe device=agto name=K_qfp22 qfp x=170 y=5
probe device=agto name=K_qfp23 qfp x=170 y=10
probe device=agto name=K_qfp24 qfp x=180 y=3
probe device=agto name=K_qfp25 qfp x=180 y=6
```

```
probe device=agto name=K_qfp26 qfp x=180 y=9
probe device=agto name=K_qfp27 qfp x=180 y=12

probe device=agto name=G_qfp00 qfp x=50. y=15
probe device=agto name=G_qfp01 qfp x=50. y=30
probe device=agto name=G_qfp02 qfp x=50. y=45
probe device=agto name=G_qfp03 qfp x=60. y=20
probe device=agto name=G_qfp04 qfp x=60. y=40
probe device=agto name=G_qfp05 qfp x=70. y=15
probe device=agto name=G_qfp06 qfp x=70. y=30
probe device=agto name=G_qfp07 qfp x=70. y=45
probe device=agto name=G_qfp08 qfp x=80. y=20
probe device=agto name=G_qfp09 qfp x=80. y=40
probe device=agto name=G_qfp10 qfp x=90. y=20
probe device=agto name=G_qfp11 qfp x=90. y=40
probe device=agto name=G_qfp12 qfp x=100 y=15
probe device=agto name=G_qfp13 qfp x=100 y=30
probe device=agto name=G_qfp14 qfp x=100 y=45
probe device=agto name=G_qfp15 qfp x=110 y=20
probe device=agto name=G_qfp16 qfp x=110 y=40
probe device=agto name=G_qfp17 qfp x=120 y=15
probe device=agto name=G_qfp18 qfp x=120 y=30
probe device=agto name=G_qfp19 qfp x=120 y=45
probe device=agto name=G_qfp20 qfp x=130 y=15
probe device=agto name=G_qfp21 qfp x=130 y=30
probe device=agto name=G_qfp22 qfp x=130 y=45
probe device=agto name=G_qfp23 qfp x=140 y=15
probe device=agto name=G_qfp24 qfp x=140 y=25
probe device=agto name=G_qfp25 qfp x=140 y=35
probe device=agto name=G_qfp26 qfp x=140 y=45
probe device=agto name=G_qfp27 qfp x=150 y=15
probe device=agto name=G_qfp28 qfp x=150 y=30
probe device=agto name=G_qfp29 qfp x=150 y=45
probe device=agto name=G_qfp30 qfp x=160 y=15
probe device=agto name=G_qfp31 qfp x=160 y=30
probe device=agto name=G_qfp32 qfp x=160 y=45
probe device=agto name=G_qfp33 qfp x=170 y=20
probe device=agto name=G_qfp34 qfp x=170 y=40
probe device=agto name=G_qfp35 qfp x=180 y=15
probe device=agto name=G_qfp36 qfp x=180 y=30
probe device=agto name=G_qfp37 qfp x=180 y=45
probe device=agto name=G_qfp38 qfp x=190 y=20
probe device=agto name=G_qfp39 qfp x=190 y=40
probe device=agto name=G_qfp40 qfp x=200 y=20
probe device=agto name=G_qfp41 qfp x=200 y=40
```

probe device=agto name=G_qfp42 qfp x=210 y=15
probe device=agto name=G_qfp43 qfp x=210 y=30
probe device=agto name=G_qfp44 qfp x=210 y=45
probe device=agto name=G_qfp45 qfp x=220 y=20
probe device=agto name=G_qfp46 qfp x=220 y=40
probe device=agto name=G_qfp47 qfp x=230 y=15
probe device=agto name=G_qfp48 qfp x=230 y=30
probe device=agto name=G_qfp49 qfp x=230 y=45

probe device=agto name=N_qfp00 qfp x=30. y=90
probe device=agto name=N_qfp01 qfp x=30. y=185
probe device=agto name=N_qfp02 qfp x=60. y=90
probe device=agto name=N_qfp03 qfp x=60. y=185
probe device=agto name=N_qfp04 qfp x=80. y=75
probe device=agto name=N_qfp05 qfp x=80. y=137.5
probe device=agto name=N_qfp06 qfp x=80. y=200
probe device=agto name=N_qfp07 qfp x=100 y=75
probe device=agto name=N_qfp08 qfp x=100 y=137.5
probe device=agto name=N_qfp09 qfp x=100 y=200
probe device=agto name=N_qfp10 qfp x=30. y=250
probe device=agto name=N_qfp11 qfp x=30. y=350
probe device=agto name=N_qfp12 qfp x=60. y=250
probe device=agto name=N_qfp13 qfp x=60. y=350
probe device=agto name=N_qfp14 qfp x=80. y=225
probe device=agto name=N_qfp15 qfp x=80. y=300
probe device=agto name=N_qfp16 qfp x=80. y=375
probe device=agto name=N_qfp17 qfp x=100 y=225
probe device=agto name=N_qfp18 qfp x=100 y=300
probe device=agto name=N_qfp19 qfp x=100 y=375
probe device=agto name=N_qfp20 qfp x=120 y=75
probe device=agto name=N_qfp21 qfp x=120 y=137.5
probe device=agto name=N_qfp22 qfp x=120 y=200
probe device=agto name=N_qfp23 qfp x=135 y=50
probe device=agto name=N_qfp24 qfp x=140 y=125
probe device=agto name=N_qfp25 qfp x=140 y=200
probe device=agto name=N_qfp26 qfp x=145 y=50
probe device=agto name=N_qfp27 qfp x=160 y=75
probe device=agto name=N_qfp28 qfp x=160 y=137.5
probe device=agto name=N_qfp29 qfp x=160 y=200
probe device=agto name=N_qfp30 qfp x=120 y=225
probe device=agto name=N_qfp31 qfp x=120 y=300
probe device=agto name=N_qfp32 qfp x=120 y=375
probe device=agto name=N_qfp33 qfp x=130 y=375
probe device=agto name=N_qfp34 qfp x=140 y=225
probe device=agto name=N_qfp35 qfp x=140 y=300

probe device=agto name=N_qfp36 qfp x=150 y=375
probe device=agto name=N_qfp37 qfp x=160 y=225
probe device=agto name=N_qfp38 qfp x=160 y=300
probe device=agto name=N_qfp39 qfp x=160 y=375
probe device=agto name=N_qfp40 qfp x=180 y=75
probe device=agto name=N_qfp41 qfp x=180 y=137.5
probe device=agto name=N_qfp42 qfp x=180 y=200
probe device=agto name=N_qfp43 qfp x=200 y=75
probe device=agto name=N_qfp44 qfp x=200 y=137.5
probe device=agto name=N_qfp45 qfp x=200 y=200
probe device=agto name=N_qfp46 qfp x=220 y=90
probe device=agto name=N_qfp47 qfp x=220 y=185
probe device=agto name=N_qfp48 qfp x=250 y=90
probe device=agto name=N_qfp49 qfp x=250 y=185
probe device=agto name=N_qfp50 qfp x=180 y=225
probe device=agto name=N_qfp51 qfp x=180 y=300
probe device=agto name=N_qfp52 qfp x=180 y=375
probe device=agto name=N_qfp53 qfp x=200 y=225
probe device=agto name=N_qfp54 qfp x=200 y=300
probe device=agto name=N_qfp55 qfp x=200 y=375
probe device=agto name=N_qfp56 qfp x=220 y=250
probe device=agto name=N_qfp57 qfp x=220 y=350
probe device=agto name=N_qfp58 qfp x=250 y=250
probe device=agto name=N_qfp59 qfp x=250 y=350

HOLE TEMP
probe device=agto name=K_Th00 p.temp x=100 y=3
probe device=agto name=K_Th01 p.temp x=100 y=6
probe device=agto name=K_Th02 p.temp x=100 y=9
probe device=agto name=K_Th03 p.temp x=100 y=12
probe device=agto name=K_Th04 p.temp x=110 y=5
probe device=agto name=K_Th05 p.temp x=110 y=10
probe device=agto name=K_Th06 p.temp x=120 y=3
probe device=agto name=K_Th07 p.temp x=120 y=6
probe device=agto name=K_Th08 p.temp x=120 y=9
probe device=agto name=K_Th09 p.temp x=120 y=12
probe device=agto name=K_Th10 p.temp x=130 y=5
probe device=agto name=K_Th11 p.temp x=130 y=10
probe device=agto name=K_Th12 p.temp x=140 y=3
probe device=agto name=K_Th13 p.temp x=140 y=6
probe device=agto name=K_Th14 p.temp x=140 y=9
probe device=agto name=K_Th15 p.temp x=140 y=12
probe device=agto name=K_Th16 p.temp x=150 y=5
probe device=agto name=K_Th17 p.temp x=150 y=10
probe device=agto name=K_Th18 p.temp x=160 y=3

probe device=agto name=K_Th19 p.temp x=160 y=6
probe device=agto name=K_Th20 p.temp x=160 y=9
probe device=agto name=K_Th21 p.temp x=160 y=12
probe device=agto name=K_Th22 p.temp x=170 y=5
probe device=agto name=K_Th23 p.temp x=170 y=10
probe device=agto name=K_Th24 p.temp x=180 y=3
probe device=agto name=K_Th25 p.temp x=180 y=6
probe device=agto name=K_Th26 p.temp x=180 y=9
probe device=agto name=K_Th27 p.temp x=180 y=12

probe device=agto name=G_Th00 p.temp x=50. y=15
probe device=agto name=G_Th01 p.temp x=50. y=30
probe device=agto name=G_Th02 p.temp x=50. y=45
probe device=agto name=G_Th03 p.temp x=60. y=20
probe device=agto name=G_Th04 p.temp x=60. y=40
probe device=agto name=G_Th05 p.temp x=70. y=15
probe device=agto name=G_Th06 p.temp x=70. y=30
probe device=agto name=G_Th07 p.temp x=70. y=45
probe device=agto name=G_Th08 p.temp x=80. y=20
probe device=agto name=G_Th09 p.temp x=80. y=40
probe device=agto name=G_Th10 p.temp x=90. y=20
probe device=agto name=G_Th11 p.temp x=90. y=40
probe device=agto name=G_Th12 p.temp x=100 y=15
probe device=agto name=G_Th13 p.temp x=100 y=30
probe device=agto name=G_Th14 p.temp x=100 y=45
probe device=agto name=G_Th15 p.temp x=110 y=20
probe device=agto name=G_Th16 p.temp x=110 y=40
probe device=agto name=G_Th17 p.temp x=120 y=15
probe device=agto name=G_Th18 p.temp x=120 y=30
probe device=agto name=G_Th19 p.temp x=120 y=45
probe device=agto name=G_Th20 p.temp x=130 y=15
probe device=agto name=G_Th21 p.temp x=130 y=30
probe device=agto name=G_Th22 p.temp x=130 y=45
probe device=agto name=G_Th23 p.temp x=140 y=15
probe device=agto name=G_Th24 p.temp x=140 y=25
probe device=agto name=G_Th25 p.temp x=140 y=35
probe device=agto name=G_Th26 p.temp x=140 y=45
probe device=agto name=G_Th27 p.temp x=150 y=15
probe device=agto name=G_Th28 p.temp x=150 y=30
probe device=agto name=G_Th29 p.temp x=150 y=45
probe device=agto name=G_Th30 p.temp x=160 y=15
probe device=agto name=G_Th31 p.temp x=160 y=30
probe device=agto name=G_Th32 p.temp x=160 y=45
probe device=agto name=G_Th33 p.temp x=170 y=20
probe device=agto name=G_Th34 p.temp x=170 y=40

probe device=agto name=G_Th35 p.temp x=180 y=15
probe device=agto name=G_Th36 p.temp x=180 y=30
probe device=agto name=G_Th37 p.temp x=180 y=45
probe device=agto name=G_Th38 p.temp x=190 y=20
probe device=agto name=G_Th39 p.temp x=190 y=40
probe device=agto name=G_Th40 p.temp x=200 y=20
probe device=agto name=G_Th41 p.temp x=200 y=40
probe device=agto name=G_Th42 p.temp x=210 y=15
probe device=agto name=G_Th43 p.temp x=210 y=30
probe device=agto name=G_Th44 p.temp x=210 y=45
probe device=agto name=G_Th45 p.temp x=220 y=20
probe device=agto name=G_Th46 p.temp x=220 y=40
probe device=agto name=G_Th47 p.temp x=230 y=15
probe device=agto name=G_Th48 p.temp x=230 y=30
probe device=agto name=G_Th49 p.temp x=230 y=45

probe device=agto name=N_Th00 p.temp x=30. y=90
probe device=agto name=N_Th01 p.temp x=30. y=185
probe device=agto name=N_Th02 p.temp x=60. y=90
probe device=agto name=N_Th03 p.temp x=60. y=185
probe device=agto name=N_Th04 p.temp x=80. y=75
probe device=agto name=N_Th05 p.temp x=80. y=137.5
probe device=agto name=N_Th06 p.temp x=80. y=200
probe device=agto name=N_Th07 p.temp x=100 y=75
probe device=agto name=N_Th08 p.temp x=100 y=137.5
probe device=agto name=N_Th09 p.temp x=100 y=200
probe device=agto name=N_Th10 p.temp x=30. y=250
probe device=agto name=N_Th11 p.temp x=30. y=350
probe device=agto name=N_Th12 p.temp x=60. y=250
probe device=agto name=N_Th13 p.temp x=60. y=350
probe device=agto name=N_Th14 p.temp x=80. y=225
probe device=agto name=N_Th15 p.temp x=80. y=300
probe device=agto name=N_Th16 p.temp x=80. y=375
probe device=agto name=N_Th17 p.temp x=100 y=225
probe device=agto name=N_Th18 p.temp x=100 y=300
probe device=agto name=N_Th19 p.temp x=100 y=375
probe device=agto name=N_Th20 p.temp x=120 y=75
probe device=agto name=N_Th21 p.temp x=120 y=137.5
probe device=agto name=N_Th22 p.temp x=120 y=200
probe device=agto name=N_Th23 p.temp x=135 y=50
probe device=agto name=N_Th24 p.temp x=140 y=125
probe device=agto name=N_Th25 p.temp x=140 y=200
probe device=agto name=N_Th26 p.temp x=145 y=50
probe device=agto name=N_Th27 p.temp x=160 y=75
probe device=agto name=N_Th28 p.temp x=160 y=137.5

probe device=agto name=N_Th29 p.temp x=160 y=200
probe device=agto name=N_Th30 p.temp x=120 y=225
probe device=agto name=N_Th31 p.temp x=120 y=300
probe device=agto name=N_Th32 p.temp x=120 y=375
probe device=agto name=N_Th33 p.temp x=130 y=375
probe device=agto name=N_Th34 p.temp x=140 y=225
probe device=agto name=N_Th35 p.temp x=140 y=300
probe device=agto name=N_Th36 p.temp x=150 y=375
probe device=agto name=N_Th37 p.temp x=160 y=225
probe device=agto name=N_Th38 p.temp x=160 y=300
probe device=agto name=N_Th39 p.temp x=160 y=375
probe device=agto name=N_Th40 p.temp x=180 y=75
probe device=agto name=N_Th41 p.temp x=180 y=137.5
probe device=agto name=N_Th42 p.temp x=180 y=200
probe device=agto name=N_Th43 p.temp x=200 y=75
probe device=agto name=N_Th44 p.temp x=200 y=137.5
probe device=agto name=N_Th45 p.temp x=200 y=200
probe device=agto name=N_Th46 p.temp x=220 y=90
probe device=agto name=N_Th47 p.temp x=220 y=185
probe device=agto name=N_Th48 p.temp x=250 y=90
probe device=agto name=N_Th49 p.temp x=250 y=185
probe device=agto name=N_Th50 p.temp x=180 y=225
probe device=agto name=N_Th51 p.temp x=180 y=300
probe device=agto name=N_Th52 p.temp x=180 y=375
probe device=agto name=N_Th53 p.temp x=200 y=225
probe device=agto name=N_Th54 p.temp x=200 y=300
probe device=agto name=N_Th55 p.temp x=200 y=375
probe device=agto name=N_Th56 p.temp x=220 y=250
probe device=agto name=N_Th57 p.temp x=220 y=350
probe device=agto name=N_Th58 p.temp x=250 y=250
probe device=agto name=N_Th59 p.temp x=250 y=350

ELECTRON TEMP
probe device=agto name=K_Te00 n.temp x=100 y=3
probe device=agto name=K_Te01 n.temp x=100 y=6
probe device=agto name=K_Te02 n.temp x=100 y=9
probe device=agto name=K_Te03 n.temp x=100 y=12
probe device=agto name=K_Te04 n.temp x=110 y=5
probe device=agto name=K_Te05 n.temp x=110 y=10
probe device=agto name=K_Te06 n.temp x=120 y=3
probe device=agto name=K_Te07 n.temp x=120 y=6
probe device=agto name=K_Te08 n.temp x=120 y=9
probe device=agto name=K_Te09 n.temp x=120 y=12
probe device=agto name=K_Te10 n.temp x=130 y=5
probe device=agto name=K_Te11 n.temp x=130 y=10

probe device=agto name=K_Te12 n.temp x=140 y=3
probe device=agto name=K_Te13 n.temp x=140 y=6
probe device=agto name=K_Te14 n.temp x=140 y=9
probe device=agto name=K_Te15 n.temp x=140 y=12
probe device=agto name=K_Te16 n.temp x=150 y=5
probe device=agto name=K_Te17 n.temp x=150 y=10
probe device=agto name=K_Te18 n.temp x=160 y=3
probe device=agto name=K_Te19 n.temp x=160 y=6
probe device=agto name=K_Te20 n.temp x=160 y=9
probe device=agto name=K_Te21 n.temp x=160 y=12
probe device=agto name=K_Te22 n.temp x=170 y=5
probe device=agto name=K_Te23 n.temp x=170 y=10
probe device=agto name=K_Te24 n.temp x=180 y=3
probe device=agto name=K_Te25 n.temp x=180 y=6
probe device=agto name=K_Te26 n.temp x=180 y=9
probe device=agto name=K_Te27 n.temp x=180 y=12

probe device=agto name=G_Te00 n.temp x=50. y=15
probe device=agto name=G_Te01 n.temp x=50. y=30
probe device=agto name=G_Te02 n.temp x=50. y=45
probe device=agto name=G_Te03 n.temp x=60. y=20
probe device=agto name=G_Te04 n.temp x=60. y=40
probe device=agto name=G_Te05 n.temp x=70. y=15
probe device=agto name=G_Te06 n.temp x=70. y=30
probe device=agto name=G_Te07 n.temp x=70. y=45
probe device=agto name=G_Te08 n.temp x=80. y=20
probe device=agto name=G_Te09 n.temp x=80. y=40
probe device=agto name=G_Te10 n.temp x=90. y=20
probe device=agto name=G_Te11 n.temp x=90. y=40
probe device=agto name=G_Te12 n.temp x=100 y=15
probe device=agto name=G_Te13 n.temp x=100 y=30
probe device=agto name=G_Te14 n.temp x=100 y=45
probe device=agto name=G_Te15 n.temp x=110 y=20
probe device=agto name=G_Te16 n.temp x=110 y=40
probe device=agto name=G_Te17 n.temp x=120 y=15
probe device=agto name=G_Te18 n.temp x=120 y=30
probe device=agto name=G_Te19 n.temp x=120 y=45
probe device=agto name=G_Te20 n.temp x=130 y=15
probe device=agto name=G_Te21 n.temp x=130 y=30
probe device=agto name=G_Te22 n.temp x=130 y=45
probe device=agto name=G_Te23 n.temp x=140 y=15
probe device=agto name=G_Te24 n.temp x=140 y=25
probe device=agto name=G_Te25 n.temp x=140 y=35
probe device=agto name=G_Te26 n.temp x=140 y=45
probe device=agto name=G_Te27 n.temp x=150 y=15

probe device=agto name=G_Te28 n.temp x=150 y=30
probe device=agto name=G_Te29 n.temp x=150 y=45
probe device=agto name=G_Te30 n.temp x=160 y=15
probe device=agto name=G_Te31 n.temp x=160 y=30
probe device=agto name=G_Te32 n.temp x=160 y=45
probe device=agto name=G_Te33 n.temp x=170 y=20
probe device=agto name=G_Te34 n.temp x=170 y=40
probe device=agto name=G_Te35 n.temp x=180 y=15
probe device=agto name=G_Te36 n.temp x=180 y=30
probe device=agto name=G_Te37 n.temp x=180 y=45
probe device=agto name=G_Te38 n.temp x=190 y=20
probe device=agto name=G_Te39 n.temp x=190 y=40
probe device=agto name=G_Te40 n.temp x=200 y=20
probe device=agto name=G_Te41 n.temp x=200 y=40
probe device=agto name=G_Te42 n.temp x=210 y=15
probe device=agto name=G_Te43 n.temp x=210 y=30
probe device=agto name=G_Te44 n.temp x=210 y=45
probe device=agto name=G_Te45 n.temp x=220 y=20
probe device=agto name=G_Te46 n.temp x=220 y=40
probe device=agto name=G_Te47 n.temp x=230 y=15
probe device=agto name=G_Te48 n.temp x=230 y=30
probe device=agto name=G_Te49 n.temp x=230 y=45

probe device=agto name=N_Te00 n.temp x=30. y=90
probe device=agto name=N_Te01 n.temp x=30. y=185
probe device=agto name=N_Te02 n.temp x=60. y=90
probe device=agto name=N_Te03 n.temp x=60. y=185
probe device=agto name=N_Te04 n.temp x=80. y=75
probe device=agto name=N_Te05 n.temp x=80. y=137.5
probe device=agto name=N_Te06 n.temp x=80. y=200
probe device=agto name=N_Te07 n.temp x=100 y=75
probe device=agto name=N_Te08 n.temp x=100 y=137.5
probe device=agto name=N_Te09 n.temp x=100 y=200
probe device=agto name=N_Te10 n.temp x=30. y=250
probe device=agto name=N_Te11 n.temp x=30. y=350
probe device=agto name=N_Te12 n.temp x=60. y=250
probe device=agto name=N_Te13 n.temp x=60. y=350
probe device=agto name=N_Te14 n.temp x=80. y=225
probe device=agto name=N_Te15 n.temp x=80. y=300
probe device=agto name=N_Te16 n.temp x=80. y=375
probe device=agto name=N_Te17 n.temp x=100 y=225
probe device=agto name=N_Te18 n.temp x=100 y=300
probe device=agto name=N_Te19 n.temp x=100 y=375
probe device=agto name=N_Te20 n.temp x=120 y=75
probe device=agto name=N_Te21 n.temp x=120 y=137.5

```
probe device=agto name=N_Te22 n.temp x=120 y=200
probe device=agto name=N_Te23 n.temp x=135 y=50
probe device=agto name=N_Te24 n.temp x=140 y=125
probe device=agto name=N_Te25 n.temp x=140 y=200
probe device=agto name=N_Te26 n.temp x=145 y=50
probe device=agto name=N_Te27 n.temp x=160 y=75
probe device=agto name=N_Te28 n.temp x=160 y=137.5
probe device=agto name=N_Te29 n.temp x=160 y=200
probe device=agto name=N_Te30 n.temp x=120 y=225
probe device=agto name=N_Te31 n.temp x=120 y=300
probe device=agto name=N_Te32 n.temp x=120 y=375
probe device=agto name=N_Te33 n.temp x=130 y=375
probe device=agto name=N_Te34 n.temp x=140 y=225
probe device=agto name=N_Te35 n.temp x=140 y=300
probe device=agto name=N_Te36 n.temp x=150 y=375
probe device=agto name=N_Te37 n.temp x=160 y=225
probe device=agto name=N_Te38 n.temp x=160 y=300
probe device=agto name=N_Te39 n.temp x=160 y=375
probe device=agto name=N_Te40 n.temp x=180 y=75
probe device=agto name=N_Te41 n.temp x=180 y=137.5
probe device=agto name=N_Te42 n.temp x=180 y=200
probe device=agto name=N_Te43 n.temp x=200 y=75
probe device=agto name=N_Te44 n.temp x=200 y=137.5
probe device=agto name=N_Te45 n.temp x=200 y=200
probe device=agto name=N_Te46 n.temp x=220 y=90
probe device=agto name=N_Te47 n.temp x=220 y=185
probe device=agto name=N_Te48 n.temp x=250 y=90
probe device=agto name=N_Te49 n.temp x=250 y=185
probe device=agto name=N_Te50 n.temp x=180 y=225
probe device=agto name=N_Te51 n.temp x=180 y=300
probe device=agto name=N_Te52 n.temp x=180 y=375
probe device=agto name=N_Te53 n.temp x=200 y=225
probe device=agto name=N_Te54 n.temp x=200 y=300
probe device=agto name=N_Te55 n.temp x=200 y=375
probe device=agto name=N_Te56 n.temp x=220 y=250
probe device=agto name=N_Te57 n.temp x=220 y=350
probe device=agto name=N_Te58 n.temp x=250 y=250
probe device=agto name=N_Te59 n.temp x=250 y=350

## Electron Concentration ##
probe device=agto name=K_nconc00 n.conc x=100 y=3
probe device=agto name=K_nconc01 n.conc x=100 y=6
probe device=agto name=K_nconc02 n.conc x=100 y=9
probe device=agto name=K_nconc03 n.conc x=100 y=12
probe device=agto name=K_nconc04 n.conc x=110 y=5
```

probe device=agto name=K_nconc05 n.conc x=110 y=10
probe device=agto name=K_nconc06 n.conc x=120 y=3
probe device=agto name=K_nconc07 n.conc x=120 y=6
probe device=agto name=K_nconc08 n.conc x=120 y=9
probe device=agto name=K_nconc09 n.conc x=120 y=12
probe device=agto name=K_nconc10 n.conc x=130 y=5
probe device=agto name=K_nconc11 n.conc x=130 y=10
probe device=agto name=K_nconc12 n.conc x=140 y=3
probe device=agto name=K_nconc13 n.conc x=140 y=6
probe device=agto name=K_nconc14 n.conc x=140 y=9
probe device=agto name=K_nconc15 n.conc x=140 y=12
probe device=agto name=K_nconc16 n.conc x=150 y=5
probe device=agto name=K_nconc17 n.conc x=150 y=10
probe device=agto name=K_nconc18 n.conc x=160 y=3
probe device=agto name=K_nconc19 n.conc x=160 y=6
probe device=agto name=K_nconc20 n.conc x=160 y=9
probe device=agto name=K_nconc21 n.conc x=160 y=12
probe device=agto name=K_nconc22 n.conc x=170 y=5
probe device=agto name=K_nconc23 n.conc x=170 y=10
probe device=agto name=K_nconc24 n.conc x=180 y=3
probe device=agto name=K_nconc25 n.conc x=180 y=6
probe device=agto name=K_nconc26 n.conc x=180 y=9
probe device=agto name=K_nconc27 n.conc x=180 y=12

probe device=agto name=G_nconc00 n.conc x=50. y=15
probe device=agto name=G_nconc01 n.conc x=50. y=30
probe device=agto name=G_nconc02 n.conc x=50. y=45
probe device=agto name=G_nconc03 n.conc x=60. y=20
probe device=agto name=G_nconc04 n.conc x=60. y=40
probe device=agto name=G_nconc05 n.conc x=70. y=15
probe device=agto name=G_nconc06 n.conc x=70. y=30
probe device=agto name=G_nconc07 n.conc x=70. y=45
probe device=agto name=G_nconc08 n.conc x=80. y=20
probe device=agto name=G_nconc09 n.conc x=80. y=40
probe device=agto name=G_nconc10 n.conc x=90. y=20
probe device=agto name=G_nconc11 n.conc x=90. y=40
probe device=agto name=G_nconc12 n.conc x=100 y=15
probe device=agto name=G_nconc13 n.conc x=100 y=30
probe device=agto name=G_nconc14 n.conc x=100 y=45
probe device=agto name=G_nconc15 n.conc x=110 y=20
probe device=agto name=G_nconc16 n.conc x=110 y=40
probe device=agto name=G_nconc17 n.conc x=120 y=15
probe device=agto name=G_nconc18 n.conc x=120 y=30
probe device=agto name=G_nconc19 n.conc x=120 y=45
probe device=agto name=G_nconc20 n.conc x=130 y=15

probe device=agto name=G_nconc21 n.conc x=130 y=30
probe device=agto name=G_nconc22 n.conc x=130 y=45
probe device=agto name=G_nconc23 n.conc x=140 y=15
probe device=agto name=G_nconc24 n.conc x=140 y=25
probe device=agto name=G_nconc25 n.conc x=140 y=35
probe device=agto name=G_nconc26 n.conc x=140 y=45
probe device=agto name=G_nconc27 n.conc x=150 y=15
probe device=agto name=G_nconc28 n.conc x=150 y=30
probe device=agto name=G_nconc29 n.conc x=150 y=45
probe device=agto name=G_nconc30 n.conc x=160 y=15
probe device=agto name=G_nconc31 n.conc x=160 y=30
probe device=agto name=G_nconc32 n.conc x=160 y=45
probe device=agto name=G_nconc33 n.conc x=170 y=20
probe device=agto name=G_nconc34 n.conc x=170 y=40
probe device=agto name=G_nconc35 n.conc x=180 y=15
probe device=agto name=G_nconc36 n.conc x=180 y=30
probe device=agto name=G_nconc37 n.conc x=180 y=45
probe device=agto name=G_nconc38 n.conc x=190 y=20
probe device=agto name=G_nconc39 n.conc x=190 y=40
probe device=agto name=G_nconc40 n.conc x=200 y=20
probe device=agto name=G_nconc41 n.conc x=200 y=40
probe device=agto name=G_nconc42 n.conc x=210 y=15
probe device=agto name=G_nconc43 n.conc x=210 y=30
probe device=agto name=G_nconc44 n.conc x=210 y=45
probe device=agto name=G_nconc45 n.conc x=220 y=20
probe device=agto name=G_nconc46 n.conc x=220 y=40
probe device=agto name=G_nconc47 n.conc x=230 y=15
probe device=agto name=G_nconc48 n.conc x=230 y=30
probe device=agto name=G_nconc49 n.conc x=230 y=45

probe device=agto name=N_nconc00 n.conc x=30. y=90
probe device=agto name=N_nconc01 n.conc x=30. y=185
probe device=agto name=N_nconc02 n.conc x=60. y=90
probe device=agto name=N_nconc03 n.conc x=60. y=185
probe device=agto name=N_nconc04 n.conc x=80. y=75
probe device=agto name=N_nconc05 n.conc x=80. y=137.5
probe device=agto name=N_nconc06 n.conc x=80. y=200
probe device=agto name=N_nconc07 n.conc x=100 y=75
probe device=agto name=N_nconc08 n.conc x=100 y=137.5
probe device=agto name=N_nconc09 n.conc x=100 y=200
probe device=agto name=N_nconc10 n.conc x=30. y=250
probe device=agto name=N_nconc11 n.conc x=30. y=350
probe device=agto name=N_nconc12 n.conc x=60. y=250
probe device=agto name=N_nconc13 n.conc x=60. y=350
probe device=agto name=N_nconc14 n.conc x=80. y=225

probe device=agto name=N_nconc15 n.conc x=80. y=300
probe device=agto name=N_nconc16 n.conc x=80. y=375
probe device=agto name=N_nconc17 n.conc x=100 y=225
probe device=agto name=N_nconc18 n.conc x=100 y=300
probe device=agto name=N_nconc19 n.conc x=100 y=375
probe device=agto name=N_nconc20 n.conc x=120 y=75
probe device=agto name=N_nconc21 n.conc x=120 y=137.5
probe device=agto name=N_nconc22 n.conc x=120 y=200
probe device=agto name=N_nconc23 n.conc x=135 y=50
probe device=agto name=N_nconc24 n.conc x=140 y=125
probe device=agto name=N_nconc25 n.conc x=140 y=200
probe device=agto name=N_nconc26 n.conc x=145 y=50
probe device=agto name=N_nconc27 n.conc x=160 y=75
probe device=agto name=N_nconc28 n.conc x=160 y=137.5
probe device=agto name=N_nconc29 n.conc x=160 y=200
probe device=agto name=N_nconc30 n.conc x=120 y=225
probe device=agto name=N_nconc31 n.conc x=120 y=300
probe device=agto name=N_nconc32 n.conc x=120 y=375
probe device=agto name=N_nconc33 n.conc x=130 y=375
probe device=agto name=N_nconc34 n.conc x=140 y=225
probe device=agto name=N_nconc35 n.conc x=140 y=300
probe device=agto name=N_nconc36 n.conc x=150 y=375
probe device=agto name=N_nconc37 n.conc x=160 y=225
probe device=agto name=N_nconc38 n.conc x=160 y=300
probe device=agto name=N_nconc39 n.conc x=160 y=375
probe device=agto name=N_nconc40 n.conc x=180 y=75
probe device=agto name=N_nconc41 n.conc x=180 y=137.5
probe device=agto name=N_nconc42 n.conc x=180 y=200
probe device=agto name=N_nconc43 n.conc x=200 y=75
probe device=agto name=N_nconc44 n.conc x=200 y=137.5
probe device=agto name=N_nconc45 n.conc x=200 y=200
probe device=agto name=N_nconc46 n.conc x=220 y=90
probe device=agto name=N_nconc47 n.conc x=220 y=185
probe device=agto name=N_nconc48 n.conc x=250 y=90
probe device=agto name=N_nconc49 n.conc x=250 y=185
probe device=agto name=N_nconc50 n.conc x=180 y=225
probe device=agto name=N_nconc51 n.conc x=180 y=300
probe device=agto name=N_nconc52 n.conc x=180 y=375
probe device=agto name=N_nconc53 n.conc x=200 y=225
probe device=agto name=N_nconc54 n.conc x=200 y=300
probe device=agto name=N_nconc55 n.conc x=200 y=375
probe device=agto name=N_nconc56 n.conc x=220 y=250
probe device=agto name=N_nconc57 n.conc x=220 y=350
probe device=agto name=N_nconc58 n.conc x=250 y=250
probe device=agto name=N_nconc59 n.conc x=250 y=350

Hole Concentration
probe device=agto name=K_pconc00 p.conc x=100 y=3
probe device=agto name=K_pconc01 p.conc x=100 y=6
probe device=agto name=K_pconc02 p.conc x=100 y=9
probe device=agto name=K_pconc03 p.conc x=100 y=12
probe device=agto name=K_pconc04 p.conc x=110 y=5
probe device=agto name=K_pconc05 p.conc x=110 y=10
probe device=agto name=K_pconc06 p.conc x=120 y=3
probe device=agto name=K_pconc07 p.conc x=120 y=6
probe device=agto name=K_pconc08 p.conc x=120 y=9
probe device=agto name=K_pconc09 p.conc x=120 y=12
probe device=agto name=K_pconc10 p.conc x=130 y=5
probe device=agto name=K_pconc11 p.conc x=130 y=10
probe device=agto name=K_pconc12 p.conc x=140 y=3
probe device=agto name=K_pconc13 p.conc x=140 y=6
probe device=agto name=K_pconc14 p.conc x=140 y=9
probe device=agto name=K_pconc15 p.conc x=140 y=12
probe device=agto name=K_pconc16 p.conc x=150 y=5
probe device=agto name=K_pconc17 p.conc x=150 y=10
probe device=agto name=K_pconc18 p.conc x=160 y=3
probe device=agto name=K_pconc19 p.conc x=160 y=6
probe device=agto name=K_pconc20 p.conc x=160 y=9
probe device=agto name=K_pconc21 p.conc x=160 y=12
probe device=agto name=K_pconc22 p.conc x=170 y=5
probe device=agto name=K_pconc23 p.conc x=170 y=10
probe device=agto name=K_pconc24 p.conc x=180 y=3
probe device=agto name=K_pconc25 p.conc x=180 y=6
probe device=agto name=K_pconc26 p.conc x=180 y=9
probe device=agto name=K_pconc27 p.conc x=180 y=12

probe device=agto name=G_pconc00 p.conc x=50. y=15
probe device=agto name=G_pconc01 p.conc x=50. y=30
probe device=agto name=G_pconc02 p.conc x=50. y=45
probe device=agto name=G_pconc03 p.conc x=60. y=20
probe device=agto name=G_pconc04 p.conc x=60. y=40
probe device=agto name=G_pconc05 p.conc x=70. y=15
probe device=agto name=G_pconc06 p.conc x=70. y=30
probe device=agto name=G_pconc07 p.conc x=70. y=45
probe device=agto name=G_pconc08 p.conc x=80. y=20
probe device=agto name=G_pconc09 p.conc x=80. y=40
probe device=agto name=G_pconc10 p.conc x=90. y=20
probe device=agto name=G_pconc11 p.conc x=90. y=40
probe device=agto name=G_pconc12 p.conc x=100 y=15
probe device=agto name=G_pconc13 p.conc x=100 y=30

probe device=agto name=G_pconc14 p.conc x=100 y=45
probe device=agto name=G_pconc15 p.conc x=110 y=20
probe device=agto name=G_pconc16 p.conc x=110 y=40
probe device=agto name=G_pconc17 p.conc x=120 y=15
probe device=agto name=G_pconc18 p.conc x=120 y=30
probe device=agto name=G_pconc19 p.conc x=120 y=45
probe device=agto name=G_pconc20 p.conc x=130 y=15
probe device=agto name=G_pconc21 p.conc x=130 y=30
probe device=agto name=G_pconc22 p.conc x=130 y=45
probe device=agto name=G_pconc23 p.conc x=140 y=15
probe device=agto name=G_pconc24 p.conc x=140 y=25
probe device=agto name=G_pconc25 p.conc x=140 y=35
probe device=agto name=G_pconc26 p.conc x=140 y=45
probe device=agto name=G_pconc27 p.conc x=150 y=15
probe device=agto name=G_pconc28 p.conc x=150 y=30
probe device=agto name=G_pconc29 p.conc x=150 y=45
probe device=agto name=G_pconc30 p.conc x=160 y=15
probe device=agto name=G_pconc31 p.conc x=160 y=30
probe device=agto name=G_pconc32 p.conc x=160 y=45
probe device=agto name=G_pconc33 p.conc x=170 y=20
probe device=agto name=G_pconc34 p.conc x=170 y=40
probe device=agto name=G_pconc35 p.conc x=180 y=15
probe device=agto name=G_pconc36 p.conc x=180 y=30
probe device=agto name=G_pconc37 p.conc x=180 y=45
probe device=agto name=G_pconc38 p.conc x=190 y=20
probe device=agto name=G_pconc39 p.conc x=190 y=40
probe device=agto name=G_pconc40 p.conc x=200 y=20
probe device=agto name=G_pconc41 p.conc x=200 y=40
probe device=agto name=G_pconc42 p.conc x=210 y=15
probe device=agto name=G_pconc43 p.conc x=210 y=30
probe device=agto name=G_pconc44 p.conc x=210 y=45
probe device=agto name=G_pconc45 p.conc x=220 y=20
probe device=agto name=G_pconc46 p.conc x=220 y=40
probe device=agto name=G_pconc47 p.conc x=230 y=15
probe device=agto name=G_pconc48 p.conc x=230 y=30
probe device=agto name=G_pconc49 p.conc x=230 y=45

probe device=agto name=N_pconc00 p.conc x=30. y=90
probe device=agto name=N_pconc01 p.conc x=30. y=185
probe device=agto name=N_pconc02 p.conc x=60. y=90
probe device=agto name=N_pconc03 p.conc x=60. y=185
probe device=agto name=N_pconc04 p.conc x=80. y=75
probe device=agto name=N_pconc05 p.conc x=80. y=137.5
probe device=agto name=N_pconc06 p.conc x=80. y=200
probe device=agto name=N_pconc07 p.conc x=100 y=75

probe device=agto name=N_pconc08 p.conc x=100 y=137.5
probe device=agto name=N_pconc09 p.conc x=100 y=200
probe device=agto name=N_pconc10 p.conc x=30. y=250
probe device=agto name=N_pconc11 p.conc x=30. y=350
probe device=agto name=N_pconc12 p.conc x=60. y=250
probe device=agto name=N_pconc13 p.conc x=60. y=350
probe device=agto name=N_pconc14 p.conc x=80. y=225
probe device=agto name=N_pconc15 p.conc x=80. y=300
probe device=agto name=N_pconc16 p.conc x=80. y=375
probe device=agto name=N_pconc17 p.conc x=100 y=225
probe device=agto name=N_pconc18 p.conc x=100 y=300
probe device=agto name=N_pconc19 p.conc x=100 y=375
probe device=agto name=N_pconc20 p.conc x=120 y=75
probe device=agto name=N_pconc21 p.conc x=120 y=137.5
probe device=agto name=N_pconc22 p.conc x=120 y=200
probe device=agto name=N_pconc23 p.conc x=135 y=50
probe device=agto name=N_pconc24 p.conc x=140 y=125
probe device=agto name=N_pconc25 p.conc x=140 y=200
probe device=agto name=N_pconc26 p.conc x=145 y=50
probe device=agto name=N_pconc27 p.conc x=160 y=75
probe device=agto name=N_pconc28 p.conc x=160 y=137.5
probe device=agto name=N_pconc29 p.conc x=160 y=200
probe device=agto name=N_pconc30 p.conc x=120 y=225
probe device=agto name=N_pconc31 p.conc x=120 y=300
probe device=agto name=N_pconc32 p.conc x=120 y=375
probe device=agto name=N_pconc33 p.conc x=130 y=375
probe device=agto name=N_pconc34 p.conc x=140 y=225
probe device=agto name=N_pconc35 p.conc x=140 y=300
probe device=agto name=N_pconc36 p.conc x=150 y=375
probe device=agto name=N_pconc37 p.conc x=160 y=225
probe device=agto name=N_pconc38 p.conc x=160 y=300
probe device=agto name=N_pconc39 p.conc x=160 y=375
probe device=agto name=N_pconc40 p.conc x=180 y=75
probe device=agto name=N_pconc41 p.conc x=180 y=137.5
probe device=agto name=N_pconc42 p.conc x=180 y=200
probe device=agto name=N_pconc43 p.conc x=200 y=75
probe device=agto name=N_pconc44 p.conc x=200 y=137.5
probe device=agto name=N_pconc45 p.conc x=200 y=200
probe device=agto name=N_pconc46 p.conc x=220 y=90
probe device=agto name=N_pconc47 p.conc x=220 y=185
probe device=agto name=N_pconc48 p.conc x=250 y=90
probe device=agto name=N_pconc49 p.conc x=250 y=185
probe device=agto name=N_pconc50 p.conc x=180 y=225
probe device=agto name=N_pconc51 p.conc x=180 y=300
probe device=agto name=N_pconc52 p.conc x=180 y=375

```
probe device=agto name=N_pconc53 p.conc x=200 y=225
probe device=agto name=N_pconc54 p.conc x=200 y=300
probe device=agto name=N_pconc55 p.conc x=200 y=375
probe device=agto name=N_pconc56 p.conc x=220 y=250
probe device=agto name=N_pconc57 p.conc x=220 y=350
probe device=agto name=N_pconc58 p.conc x=250 y=250
probe device=agto name=N_pconc59 p.conc x=250 y=350
#####################################################################

Quit
```

THIS PAGE INTENTIONALLY LEFT BLANK

APPENDIX E: MATLAB® – ENERGY TRANSFER ANALYSIS

```
%% THESIS DATA ANALYSIS SCRIPT
%    Organization:  United States Navy
%    Location:  Naval Postgraduate School
%    Author: ENS Gerald E. Vineyard USN
%    Date:   18 May 2009

clc
clear
format compact

D   = importdata('Pulse_Full.xls');
S   = D.data.Sheet1;    % SPICE IV Data
T   = D.data.Sheet2;    % Lattice Temperature
QFN = D.data.Sheet3;    % Electron Quasi-fermi Level
QFP = D.data.Sheet4;    % Hole Quasi-fermi Level
TE  = D.data.Sheet5;    % Electron Temperature
TP  = D.data.Sheet6;    % Hole Temperature
CN  = D.data.Sheet7;    % Electron Concentration
CP  = D.data.Sheet8;    % Hole Concentration


%%%%%%%%%%%%%%%%%%%%%%%%%%%%%%%%%%%%%%%%%%%%%%%%%%%%%%
%                  I,V,time data for GTO Thyristor                 %
%%%%%%%%%%%%%%%%%%%%%%%%%%%%%%%%%%%%%%%%%%%%%%%%%%%%%%
  % Voltage and Current Waveform for GTO thyristor
    time = S(:,1);                          % Simulation Time
    Vak = S(:,6)-S(:,7);                    % Anode Voltage
    Vgk = 0.5*(S(:,8)+S(:,9))-S(:,7);       % Gate Voltage
    Ia  = S(:,25); Ik  = S(:,26);           % Anode-Cathode Current
    Ig1 = S(:,27); Ig2 = S(:,28);           % Gate Current

  % Plot Waveforms
    Time = time*1000; Ts = 0; Tf = floor(time(end)*1000)*1;
    h1 = figure(1);
    plot(Time,Ia,'r.-',Time,Vak,'b.-',Time,Ig1+Ig2,'gx-',Time,Vgk,'cx-');
    title('GTO Thyristor Turn Off');
    xlabel('Time - ms');
    ylabel('Current (A) and Voltage (V) ');
    legend('I_A_n_o_d_e (A)','V_A_n_o_d_e (V)','I_G_a_t_e','V_G_a_t_e');
    legend('location','North','Orientation','Horizontal');
    legend boxoff
    axis ([Ts,Tf,-40,110]);
```

```
%%%%%%%%%%%%%%%%%%%%%%%%%%%%%%%%%%%%%%%%%%%%%%%
%          Electrical Energy Input/Output in SPICE Circuit and Thyristor          %
%%%%%%%%%%%%%%%%%%%%%%%%%%%%%%%%%%%%%%%%%%%%%%%
  % Circuit Component Values
    Vs = 100;  Rs = 10;  C1 = 9.6e-3;  R1 = 54.7e-3;  Ranode = 2.82e-6/28;
    Rgate = 2.82e-6*(13/65);  Rsnub = 100;  Csnub = 940e-9;  Lsnub = 12.5e-9;
    Rsrc = 25e-3;  Cgate  = 5e-3;  Lgate = 2.5e-9;  Rpulse = 1.03  Rgnd = 1e6;
    Lpulse = 4.62e-3;  Ldgto  = 10e-9;

  % Supplied Electrical Power
    P_vs = S(:,2).*S(:,18);              % Supplied by Voltage Source
    P_vg1 = (S(:,13)-S(:,7)).*S(:,35);    % Supplied by Turn-On Source
    P_vg2 = (S(:,14)-S(:,13)).*S(:,36);   % Supplied by Turn-Off Source

  % Supplied Electrical Energy
    E_vs=0; E_vg1=0; E_vg2=0;
    c1=0.445; c2=1-c1;                   % Averaging Coefficients
    for i=2:length(time)
      dt = (time(i)-time(i-1));
      E_vs = [E_vs; (c1*P_vs(i)+c2*P_vs(i-1))*dt + E_vs(i-1)];
      E_vg1 = [E_vg1; (c1*P_vg1(i)+c2*P_vg1(i-1))*dt + E_vg1(i-1)];
      E_vg2 = [E_vg2; (c1*P_vg2(i)+c2*P_vg2(i-1))*dt + E_vg2(i-1)];
    end

  % Dissipated Electrical Power: External Circuit
    P_rs       = Rs*S(:,19).^2;                       % Src. Res.
    P_r1       = R1*S(:,22).^2;                       % Cap. ESR
    P_rsnub    = Rsnub*S(:,31).^2;                    % Snub. Ind.
    P_rpuls    = Rpulse*S(:,34).^2;                   % Pulse Res.
    P_rsrc     = Rsrc*S(:,37).^2;                     % Gate Rsrc.
    P_rgate    = (S(:,16)-S(:,8)).*S(:,40);           % Gate Res.
    P_rgnd1    = Rgnd*S(:,20).^2;                     % Gnd. Res.1
    P_rgnd2    = Rgnd*S(:,24).^2;                     % Gnd. Res.2
    P_rgnd3    = Rgnd*S(:,41).^2;                     % Gnd. Res.3
    P_rgnd4    = Rgnd*S(:,42).^2;                     % Gnd. Res.4
    P_d1       = (S(:,3)-S(:,5)).*S(:,23);            % GTO Diode
    P_d2       = (-S(:,7)).*(S(:,33)-S(:,25)-S(:,32));   % Pulse Diode

  % Dissipated Electrical Power:  Thyristor
    P_a     = Ranode*S(:,26).^2;                 % Anode Contact
    P_g1    = Rgate*S(:,27).^2;                  % Left Gate Contact
    P_g2    = Rgate*S(:,28).^2;                  % Right Gate Contact
    P_ak    = (S(:,6)-S(:,7)).*S(:,25);                              % Anode
    P_gk    = (S(:,8)-S(:,7)).*S(:,27)+(S(:,9)-S(:,7)).*S(:,28);          % Gate
```

```
% Dissipated Electrical Energy
   E_d1=0; E_d2=0;                                  % Diodes
   E_ak=0; E_gk=0; E_a=0; E_g1=0; E_g2=0;           % Thyristor Resistance
   E_rs=0; E_r1=0;                                  % Source Resistors
   E_rsrc=0; E_rgate=0;                             % Gate Resistors
   E_rsnub=0; E_rpuls=0;                            % Snubber and Load Resistors
   E_gnd1=0; E_gnd2=0;                              % DC Path to Gnd. Resistors
   E_gnd3=0; E_gnd4=0;
for i=2:length(time)
   dt = (time(i)-time(i-1));
   E_gnd1   = [E_gnd1;  (c1*P_rgnd1(i)+c2*P_rgnd1(i-1))*dt+E_gnd1(i-1)];
   E_gnd2   = [E_gnd2;  (c1*P_rgnd2(i)+c2*P_rgnd2(i-1))*dt+E_gnd2(i-1)];
   E_gnd3   = [E_gnd3;  (c1*P_rgnd3(i)+c2*P_rgnd3(i-1))*dt+E_gnd3(i-1)];
   E_gnd4   = [E_gnd4;  (c1*P_rgnd4(i)+c2*P_rgnd4(i-1))*dt+E_gnd4(i-1)];
   E_d1     = [E_d1;    (c1*P_d1(i)+c2*P_d1(i-1))*dt+E_d1(i-1)];
   E_d2     = [E_d2;    (c1*P_d2(i)+c2*P_d2(i-1))*dt+E_d2(i-1)];
   E_rs     = [E_rs;    (c1*P_rs(i)+c2*P_rs(i-1))*dt+E_rs(i-1)];
   E_r1     = [E_r1;    (c1*P_r1(i)+c2*P_r1(i-1))*dt+E_r1(i-1)];
   E_rsnub  = [E_rsnub; (c1*P_rsnub(i)+c2*P_rsnub(i-1))*dt+E_rsnub(i-1)];
   E_rpuls  = [E_rpuls; (c1*P_rpuls(i)+c2*P_rpuls(i-1))*dt+E_rpuls(i-1)];
   E_rsrc   = [E_rsrc;  (c1*P_rsrc(i)+c2*P_rsrc(i-1))*dt+E_rsrc(i-1)];
   E_rgate  = [E_rgate; (c1*P_rgate(i)+c2*P_rgate(i-1))*dt+E_rgate(i-1)];
   E_ak     = [E_ak;    (c1*P_ak(i)+c2*P_ak(i-1))*dt+E_ak(i-1)];
   E_gk     = [E_gk;    (c1*P_gk(i)+c2*P_gk(i-1))*dt+E_gk(i-1)];
   E_a      = [E_a;     (c1*P_a(i)+c2*P_a(i-1))*dt+E_a(i-1)];
   E_g1     = [E_g1;    (c1*P_g1(i)+c2*P_g1(i-1))*dt+E_g1(i-1)];
   E_g2     = [E_g2;    (c1*P_g2(i)+c2*P_g2(i-1))*dt+E_g2(i-1)];
end

% Stored Electrical Energy
   E_c1     = 0.5*C1*S(:,4).^2;                     % Capacitor Bank
   E_csnub  = 0.5*Csnub*(S(:,7)-S(:,11)).^2;        % Snubber Capacitor
   E_cgate  = 0.5*Cgate*(S(:,15)-S(:,7)).^2;        % Gate Capacitor
   E_ldgto  = 0.5*Ldgto*S(:,23).^2;                 % Stray Inductance
   E_lsnub  = 0.5*Lsnub*S(:,30).^2;                 % Snubber Inductor
   E_lpuls  = 0.5*Lpulse*S(:,33).^2;                % Pulse Inductor
   E_lgate  = 0.5*Lgate*S(:,39).^2;                 % Gate Inductance

% Total Change in Electrical Energy (should be zero).
   E_in     = E_vs + E_vg1 + E_vg2 + (E_c1-E_c1(1)) - (E_csnub-E_csnub(1));
   E_stor   = E_lsnub + E_lgate + E_cgate + E_lpuls + E_ldgto;
   E_diss   = E_rs + E_r1 + E_rgate + E_rsrc + E_rsnub + E_rpuls + E_a +
E_g1 + E_g2 + E_gnd1 + E_gnd2 + E_gnd3 + E_gnd4 + E_d1 + E_d2;
   E_gto    = E_ak + E_gk;
   E_tot    = E_in + E_stor + E_diss + E_gto;
```

```
% Plot Energy Data
  h2 = figure(2);
  plot(Time,E_stor,Time,E_diss,Time,E_gto,Time,E_tot,Time,-E_in,')
  title('Electrical Energy in SPICE Circuit');
  xlabel('Time - \mus'); ylabel('Electrical Energy (J)');
  legend('E_s_t_o_r_e','E_d_i_s_s_i_p_a_t_e','E_G_T_O','E_t_o_t_al','E_i_n');
  legend('location','North','Orientation','Horizontal'); legend boxoff;
  axis([Ts,Tf,-2,18]);

%%%%%%%%%%%%%%%%%%%%%%%%%%%%%%%%%%%%%%%%%%%
%          Thermal Energy Generation and Output in GTO Thyristor          %
%%%%%%%%%%%%%%%%%%%%%%%%%%%%%%%%%%%%%%%%%%%
 % Material Properties, Contact Dimensions, and Region Volumes
  % Electrode Dimensions
    wa     = 0.0280;                    % Anode Electrode Width (cm)
    ta     = 0.0010;                    % Anode Electrode Thickness (cm)
    wg     = 0.0065;                    % Gate Electrode Width (cm)
    tg     = 0.0013;                   % Gate Electrode Thickness (cm)
    l      = 1.0;                      % Device Length (cm)
    Post   = [0; 0.00025; 0.0010];     % Positions of Anode Probe Points
  % Region Volumes:  (thickness*width*length)
    Vc1 = 0.0013*0.0150*l;           % Cathode Region Volume (cm^3)
    Vg1 = 0.0034*0.0075*l;           % Left Gate Region Volume (cm^3)
    Vg2 = 0.0034*0.0130*l;           % Center Gate Region Volume (cm^3)
    Vg3 = 0.0034*0.0075*l;           % Right Gate Region Volume (cm^3)
    Vn1 = 0.0363*0.0070*l;           % Left n-Base Region Volume (cm^3)
    Vn2 = 0.0363*0.0140*l;           % Center n-Base Region Volume (cm^3)
    Vn3 = 0.0363*0.0070*l;           % Right n-Base Region Volume (cm^3)
  % Electrode Volumes:  (thickness*width*length)
    Vanode   = ta*wa*l;               % Anode Electrode Volume (cm^3)
    Vgate1   = tg*wg*l;               % Left Electrode Volume (cm^3)
    Vgate2   = tg*wg*1;               % Right Electrode Volume (cm^3)
  % Temperature Dependent Thermal Conductivity Coefficients
    k_al     = 2.37;        % Thermal Conductivity of Aluminium: W/(cm K)
    alpha    = 1;           % Thermal Resist. of Anode Contact: W/(cm^2 K)
  % Temperature Dependent Heat Capacity Coefficients
    siHCa = 1.97;           % Silicon, First Coefficient: J/(cm^3 K)
    siHCb = 0.00036;        % Silicon, Second Coefficient: J/(cm^3 K^2)
    siHCc = 0;              % Silicon, Third Coefficient: J/(cm^3 K^3)
    siHCd = -3.7*10^4;      % Silicon, Fourth Coefficient: (J K)/cm^3
    alHCa = 55.8;           % Aluminium, First Coefficient: J/(cm^3 K)
    alHCb = 33.5;           % Aluminium, Second Coefficient: J/(cm^3 K^2)
    alHCc = 0;              % Aluminium, Third Coefficient: J/(cm^3 K^3)
    alHCd = 0;              % Aluminium, Fourth Coefficient: (J K)/cm^3
```

```
% Retrieve Temperature Data
  Tbase = 300;          % Base Temperature (K)
  Tk = T(:,1:28);       % Cathode Region Temperatures (K)
  Tg = T(:,29:78);      % Gate Region Temperatures (K)
  Tn = T(:,79:138);     % n-base Region Temperature (K)
  Ta = T(:,139:175);    % Thermal Contact Temperature (K)
  Tl = T(:,176:178);    % Left Gate Contact Temperature (K)
  Tr = T(:,179:181);    % Rigth Gate Contact Temperature (K)

% Thermal Contact Temp. and Thermal Energy Output
  % Thermal Contact Temperatures
    Tatop = mean(Ta(:,1:14),2);       % Semiconductor/Contact Interface
    Tamid = mean(Ta(:,29:37),2);      % 2.5um under Semiconductor/Contact
    Tabot = mean(Ta(:,15:28),2);      % Contact/Ambient Interface
  % Thermal Power and Heat Transfer
    P_thermIn  = 0; P_thermMid = 0; P_thermOut = 0;
    Qin  = 0; Qmid = 0; Qout = 0;
    for i=2:length(time)
      dt = time(i)-time(i-1);
      [Tdist, gof] =
fit(Post,[Tatop(i);Tamid(i);Tabot(i)],'rat11','Startpoint',[Tbase,0.1,0.0005]);
      p1 = Tdist.p1; p2 = Tdist.p2; q1 = Tdist.q1;
      dT1t        = (p1*(0+q1)-(0*p1+p2))/(0+q1)^2;
      dT1m        = (p1*(0.00025+q1)-(0.00025*p1+p2))/(0.00025+q1)^2;
      dT2t        = (Tamid(i)-Tatop(i))/(0.00025);
      dT2m        = (Tabot(i)-Tamid(i))/(0.00075);
      dTdx_top    = 0.5*dT1t + 0.5*dT2t;
      dTdx_mid    = 0.5*dT1m + 0.5*dT2m;
      P_thermIn       = [P_thermIn; -k_al*wa*l*dTdx_top];
      P_thermMid      = [P_thermMid; -k_al*wa*l*dTdx_mid];
      P_thermOut      = [P_thermOut; alpha*wa*l*(Tabot(i)-Tbase)];
      Qin     = [Qin;  P_thermIn(i)*dt+Qin(i-1)];          % Q Into Cont. (J)
      Qmid  = [Qmid; P_thermMid(i)*dt+Qmid(i-1)];   % Q Across Cont. (J)
      Qout   = [Qout; P_thermOut(i)*dt+Qout(i-1)];     % Q Out of Cont. (J)
    end

% Region Temperatures and Thermal Energy Storage
  % Region Temperatures (K)
    Tc1 = mean(Tk(:,1:end),2);
    Tg1 = mean(Tg(:,1:8),2);
    Tg2 = mean(Tg(:,9:42),2);
    Tg3 = mean(Tg(:,43:50),2;
    Tn1 = mean([Tn(:,1:4) Tn(:,11:14) Ta(:,1:4)],2);
    Tn2 = mean([Tn(:,5:10) Tn(:,15:46) Tn(:,51:56) Ta(:,5:10)],2);
    Tn3 = mean([Tn(:,47:50) Tn(:,57:60) Ta(:,12:14)],2);
```

```
  % Electrode Temperatures (K)
    Tanode = mean(Ta,2);
    Tgate1  = sum(0.31666*Tl,2)+0.05*Tg(:,1);
    Tgate2  = sum(0.31666*Tr,2)+0.05*Tg(:,50);
  % Reg. Heat Capacities:  C = HCa+HCb*T+HCc*T^2+HCd/T^2  [J/(cm^3 K)]
    Cc1 = siHCa + siHCb*Tc1 + siHCd./Tc1.^2;     % Cathode Reg.
    Cg1 = siHCa + siHCb*Tg1 + siHCd./Tg1.^2;     % Left Gate Reg.
    Cg2 = siHCa + siHCb*Tg2 + siHCd./Tg2.^2;     % Center Gate Reg.
    Cg3 = siHCa + siHCb*Tg3 + siHCd./Tg3.^2;     % Right Gate Reg.
    Cn1 = siHCa + siHCb*Tg1 + siHCd./Tg1.^2;     % Left n-Base Reg.
    Cn2 = siHCa + siHCb*Tg2 + siHCd./Tg2.^2;     % Center n-Base Reg.
    Cn3 = siHCa + siHCb*Tg3 + siHCd./Tg3.^2;     % Rigth n-Base Reg.
  % Elect. Heat Capacities:  C = HCa+HCb*T+HCc*T^2+HCd/T^2 [J/(cm^3 K)]
    Canode = alHCa + alHCb*Tanode;               % Anode Elec.
    Cgate1 = alHCa + alHCb*Tgate1;               % Left Gate Elec.
    Cgate2 = alHCa + alHCb*Tgate2;               % Rigth Gate Elec.
  % Region Thermal Energy Storage
    Qc1  = Cc1*Vc1.*(Tc1-Tbase);                 % Cathode Region (J)
    Qg1  = Cg1*Vg1.*(Tg1-Tbase);                 % Left n-Base Region (J)
    Qg2  = Cg2*Vg2.*(Tg2-Tbase);                 % Center n-Base Region (J)
    Qg3  = Cg3*Vg3.*(Tg3-Tbase);                 % Right n-Base Region (J)
    Qn1  = Cn1*Vn1.*(Tn1-Tbase);                 % Left Gate Region (J)
    Qn2  = Cn2*Vn2.*(Tn2-Tbase);                 % Center Gate Region (J)
    Qn3  = Cn3*Vn3.*(Tn3-Tbase);                 % Right Gate Region (J)
  % Electrode Thermal Energy Storage
    Qanode    = Canode*Vanode.*(Tanode-Tbase);  % Anode Electrode (J)
    Qgate1    = Cgate1*Vgate1.*(Tgate1-Tbase);  % Left Gate Electrode (J)
    Qgate2    = Cgate2*Vgate2.*(Tgate2-Tbase);  % Rigth Gate Electrode (J)


% Energy Balance for GTO Thyristor
  E_in   = E_gto;                    % Electrical Energy
  E_out  = Qout;                     % Thermal Energy
  E_Si   = Qc1+Qg1+Qg2+Qg3+Qn1+Qn2+Qn3;    % Q_Si
  E_Al   = Qanode+Qgate1+Qgate2;           % Q_Al
  E_SiAl = E_Si+E_Al;                % Q_net
  E_net  = E_in-E_out-E_SiAl;            % Net Change in Internal E.
```

```
% Plot Thermal Data
  % Plot Temperature Thermal Power Through Thermal Contact
    h3 = figure(3);
    subplot(1,2,1),
    plot(Time,mean(Tatop,2),Time,mean(Tamid,2),Time,mean(Tabot,2))
    title('Temperature at Thermal Contact Junctions')
    xlabel('Time (ms)'), ylabel('Temperature (K)')
    legend('Bulk-Contact','Mid. Contact','Contact-Ambient')
    legend('location','North','Orientation','Horizontal');
    legend boxoff
    axis ([Ts,Tf,300,301.5]);
    subplot(1,2,2),
    plot(Time,P_thermIn,Time,P_thermMid,Time,P_thermOut)
    title('Thermal Power through Thermal Contact Junctions')
    xlabel('Time (ms)'), ylabel('Thermal Power (W)')
    legend('Bulk-Contact','Mid. Contact','Contact-Ambient')
    legend('location','North','Orientation','Horizontal');
    legend boxoff
    axis ([Ts,Tf,0,120]);

  % Plot Thermal and Electrical Energy into Thermal Contact
    H4 = figure(4);
    plot(Time,Qin+E_a,'b.-',Time,Qout,'g.-',Time,Qanode,'k.-')
    title('Heat Transfer and Storage: Thermal Contact')
    xlabel('Time (ms)'), ylabel('Thermal Energy (J)')
    legend('Q_i_n','Q_o_u_t','\DeltaQ_a_n_o_d_e')
    legend('location','North','Orientation','Horizontal')
    legend boxoff;  axis ([Ts,Tf,-0.1,0.4])

  % Plot Temperature of Semiconductor Regions and Electrodes
    H5 = figure(5);
    subplot(1,2,1)
    plot(Time,Tc1,'b.-',Time,Tg2,'g.-',Time,Tn2,'k.-')
    title('Temperature - Semiconductor Regions')
    xlabel('Time (ms)'), ylabel('Temperature (K)')
    legend('Cathode','Gate (Center)','n-Base (Center)')
    legend('location','North','Orientation','Horizontal');  legend boxoff;
    axis ([Ts,Tf,300,330])
    subplot(1,2,2)
    plot(Time,Tanode,'b.-',Time,Tgate1,'kx-',Time,Tgate2,'g.:')
    title('Temperature - Electrodes')
    legend('Anode','Left Gate','Right Gate'
    legend('location','North','Orientation','Horizontal');
    legend boxoff
    axis([Ts,Tf,300,304])
```

```
% Plot Thermal Energy Stored in Electrodes and Semiconductor Regions
  H6 = figure(6);
  subplot(2,1,1)
  plot(Time,Qanode,'b.-',Time,Qgate1+Qgate2,'g.-')
  title('Stored Thermal Energy - Electrodes')
  xlabel('Time (ms)'), ylabel('Thermal Energy (J)')
  legend('Anode','Gate','location','North','Orientation','Horizontal')
  legend boxoff;
  axis ([Ts,Tf,-0.1,0.5])
  subplot(2,1,2)
  plot(Time,Qg1+Qg2+Qg3,'g.-',Time,Qc1,'r.-',Time,Qn1+Qn2+Qn3,'b.-')
  title('Stored Thermal Energy - Bulk Semiconductor')
  xlabel('Time (ms)'), ylabel('Thermal Energy (J)')
  legend('Gate Region','Cathode Region','n-Base Region')
  legend('location','North','Orientation','Horizontal')
  legend boxoff;
  axis ([Ts,Tf,-.01,0.05])

% Plot Total Energy Storage in GTO Thyristor
  h7 = figure(7);
  plot(Time,E_SiAl,'b.-',Time,E_Si,'g.-',Time,E_Al,'k.-')
  title('Thermal Energy Storage: Electrodes and Semiconductor Bulk')
  xlabel('Time (ms)'), ylabel('Thermal Energy (J)')
  legend('\DeltaQ_s_t_o_r_e','\DeltaQ_S_i','\DeltaQ_E_l_e_c_t_r_o_d_e_s')
  legend('location','Northeast','Orientation','Horizontal')
  legend boxoff;
  %axis ([Ts,Tf,0,125])

% Plot Total Change in Energy (Thermal and Electric) for the GTO thyristor
  h8 = figure(8);
  plot(Time,E_in,'b.-',Time,E_out,'g.-',Time,E_SiAl,'k.-',Time,E_net,'r -')
  title('GTO Thyristor Energy - Thermal and Electric')
  xlabel('Time (ms)'), ylabel('Energy (J)')
  legend('E_i_n','Q_o_u_t','\DeltaQ_s_t_o_r_e),'\DeltaE_G_T_O')
  legend('location','Northeast','Orientation','Horizontal')
  legend boxoff;
  axis ([Ts,Tf,-0.1,0.8])
```

```
%%%%%%%%%%%%%%%%%%%%%%%%%%%%%%%%%%%%%%%%%%%
%                    Electric Energy Storage in the GTO thyristor                    %
%%%%%%%%%%%%%%%%%%%%%%%%%%%%%%%%%%%%%%%%%%%
  % Material and Electric Constants
    kb = 8.617343e-5;           % Boltzman Constant (eV/K)
    q  = 1.602176487e-19;       % Electron Charge (C)

  % Extract Temperature, Potential, and Concentration Values
    % Lattice Temperature for Each Thyristor Region
      Tk = T(:,1:28);               % Cathode Region Temperatures (K)
      Tg = T(:,29:78);              % Gate Region Temperatures (K)
      Tn = T(:,79:138);             % n-base Region Temperature (K)
    % Electron and Hole Quasi-Fermi Levels for Each Thyristor Region
      QFNk = QFN(:,1:28);       % Cathode Region QFN (V)
      QFNg = QFN(:,29:78);      % Gate Region QFN (V)
      QFNn = QFN(:,79:138);     % n-Base Region QFN (V)
      QFPk = QFP(:,1:28);       % Cathode Region QFP (V)
      QFPg = QFP(:,29:78);      % Gate Region QFP (V)
      QFPn = QFP(:,79:138);     % n-Base Region QFP (V)
    % Electron and Hole Temperature for Each Thyristor Region
      TEk = TE(:,1:28);             % Cathode Electron Temperature (K)
      TEg = TE(:,29:78);            % Gate Electron Temperature (K)
      TEn = TE(:,79:138);           % n-Base Electron Temperature (K)
      TPk = TP(:,1:28);             % Cathode Hole Temperature (K)
      TPg = TP(:,29:78);            % Gate Hole Temperature (K)
      TPn = TP(:,79:138);           % n-Base Hole Temperature (K)
    % Electron and Hole Concentration for Each Thyristor Region
      CNk = CN(:,1:28);             % Cathode Electron Concentration (e-/cm^3)
      CNg = CN(:,29:78);            % Gate Electron Concentration (e-/cm^3)
      CNn = CN(:,79:138);           % n-Base Electron Concentration (e-/cm^3)
      CPk = CP(:,1:28);             % Cathode Hole Concentration (e+/cm^3)
      CPg = CP(:,29:78);            % Gate Hole Concentration (e+/cm^3)
      CPn = CP(:,79:138);           % n-Base Hole Concentration (e+/cm^3)

  % Compute Kinetic Energy in Moving Charges
    % Kinetic Energy Density  (J/cm^3)
      KENc1 = 1.5*kb*q*(TEk-Tk);
      KENg1 = 1.5*kb*q*(TEg(:,1:8)-Tg(:,1:8));
      KENg2 = 1.5*kb*q*(TEg(:,9:42)-Tg(:,9:42));
      KENg3 = 1.5*kb*q*(TEg(:,43:50)-Tg(:,43:50));
      KENn1 = 1.5*kb*q*([TEn(:,1:4) TEn(:,11:14)]-[Tn(:,1:4) Tn(:,11:14)]);
      KENn2 = 1.5*kb*q*([TEn(:,5:10) TEn(:,15:46) TEn(:,51:56)]-[Tn(:,5:10)
Tn(:,15:46) Tn(:,51:56)]);
      KENn3 = 1.5*kb*q*([TEn(:,47:50) TEn(:,57:60)]-[Tn(:,47:50) Tn(:,57:60)]);
      KEPc1 = 1.5*kb*q*(TPk-Tk);
```

```
        KEPg1 = 1.5*kb*q*(TPg(:,1:8)-Tg(:,1:8));
        KEPg2 = 1.5*kb*q*(TPg(:,9:42)-Tg(:,9:42));
        KEPg3 = 1.5*kb*q*(TPg(:,43:50)-Tg(:,43:50));
        KEPn1 = 1.5*kb*q*([TPn(:,1:4) TPn(:,11:14)]-[Tn(:,1:4) Tn(:,11:14)]);
        KEPn2 = 1.5*kb*q*([TPn(:,5:10) TPn(:,15:46) TPn(:,51:56)]-[Tn(:,5:10)
Tn(:,15:46) Tn(:,51:56)]);
        KEPn3 = 1.5*kb*q*([TPn(:,47:50) TPn(:,57:60)]-[Tn(:,47:50) Tn(:,57:60)]);
    % Compute Kinetic Energy for Each Region:
        KEc1 = Vc1*(mean(CNk,2).*mean(KENc1,2) +
mean(CPk,2).*mean(KEPc1,2));
        KEg1 = Vg1*(mean(CNg(:,1:8),2).*mean(KENg1,2) +
mean(CPg(:,1:8),2).*mean(KEPg1,2));
        KEg2 = Vg2*(mean(CNg(:,9:42),2).*mean(KENg2,2) +
mean(CPg(:,9:42),2).*mean(KEPg2,2));
        KEg3 = Vg3*(mean(CNg(:,43:50),2).*mean(KENg3,2) +
mean(CPg(:,43:50),2).*mean(KEPg3,2));
        KEn1 = Vn1*(mean([CNn(:,1:4) CNn(:,11:14)],2).*mean(KENn1,2) +
mean([CPn(:,1:4) CPn(:,11:14)],2).*mean(KEPn1,2));
        KEn2 = Vn2*(mean([CNn(:,5:10) CNn(:,15:46)
CNn(:,51:56)],2).*mean(KENn2,2) + mean([CPn(:,5:10) CPn(:,15:46)
CNn(:,51:56)],2).*mean(KEPn2,2));
        KEn3 = Vn3*(mean([CNn(:,47:50) CNn(:,57:60)],2).*mean(KENn3,2) +
mean([CPn(:,47:50) CPn(:,57:60)],2).*mean(KEPn3,2));

    % Plot Kinetic Energy Values
        Time = time*1000; Ts = 0; Tf = floor(time(end)*100)*10;
        h10 = figure(10);
        subplot(2,1,1)
        plot(Time,KEg1,'g.-',Time,KEg2,'b.-',Time,KEg3,'k :',Time,KEc1,'r.-')
        title('Kinetic Energy - Bulk Semiconductor')
        xlabel('Time (ms)'), ylabel('Kinetic Energy (J)')
        legend('Gate (Left)','Gate (Center)','Gate (Rigth)','Cathode')
        legend('location','North','Orientation','Horizontal')
        legend boxoff;
        %axis ([Ts,Tf,-5*10^-4,25*10^-4])
        subplot(2,1,2)
        plot(Time,KEn1,'g.-',Time,KEn2,'b.-',Time,KEn3,'K :')
        title('Kinetic Energy - Bulk Semiconductor')
        xlabel('Time (ms)'), ylabel('Kinetic Energy (J)')
        legend('n-Base (Left)','n-Base (Center)','n-Base (Right)')
        legend('location','North','Orientation','Horizontal')
        legend boxoff;
        %axis ([Ts,Tf,-0.01,0.03])
```

```
  % Compute Potential Energy in Moving Charges
    % Difference in QuasiFermi Level
      DQFLc1 = QFNk-QFPk;
      DQFLg1 = QFNg(:,1:8)-QFPg(:,1:8);
      DQFLg2 = QFNg(:,9:42)-QFPg(:,9:42);
      DQFLg3 = QFNg(:,43:50)-QFPg(:,43:50);
      DQFLn1 = [QFNn(:,1:4) QFNn(:,11:14)]-[QFPn(:,1:4) QFPn(:,11:14)];
      DQFLn2 = [QFNn(:,5:10) QFNn(:,15:46) QFNn(:,51:56)]-[QFPn(:,5:10)
QFPn(:,15:46) QFPn(:,51:56)];
      DQFLn3 = [QFNn(:,47:50) QFNn(:,57:60)]-[QFPn(:,47:50) QFPn(:,57:60)];
    % Energy Associated with Difference in Fermi Levels
      EQFLc1 = q*Vc1*mean(CNk,2).*mean(DQFLc1,2);
      EQFLg1 = q*Vg1*mean(CNg(:,1:8),2).*mean(DQFLg1,2);
      EQFLg2 = q*Vg2*mean(CNg(:,9:42),2).*mean(DQFLg2,2);
      EQFLg3 = q*Vg3*mean(CNg(:,43:50),2).*mean(DQFLg3,2);
      EQFLn1 = q*Vn1*mean([CNn(:,1:4) CNn(:,11:14)],2).*mean(DQFLn1,2);
      EQFLn2 = q*Vn2*mean([CNn(:,5:10) CNn(:,15:46)
CNn(:,51:56)],2).*mean(DQFLn2,2);
      EQFLn3 = q*Vn3*mean([CNn(:,47:50) CNn(:,57:60)],2).*mean(DQFLn3,2);


    % Plot Potential Energy Values
      Time = time*1000; Ts = 0; Tf = floor(time(end)*100)*10;
      h11 = figure(11);
      subplot(2,1,1)
      plot(Time,EQFLg1,Time,EQFLg2,Time,EQFLg3,Time,EQFLc1)
      title('Potential Energy - Fermi Level Difference')
      xlabel('Time (ms)'), ylabel('Potential Energy (J)')
      legend('Gate (Left)','Gate (Center)','Gate (Rigth)','Cathode')
      legend('location','North','Orientation','Horizontal')
      legend boxoff;
      %axis ([Ts,Tf,-5*10^-4,25*10^-4])
      subplot(2,1,2)
      plot(Time,EQFLn1,'g.-',Time,EQFLn2,'b.-',Time,EQFLn3,'K :')
      title('Potential Energy - Fermi Level Difference')
      xlabel('Time (ms)'), ylabel('Potential Energy (J)')
      legend('n-Base (Left)','n-Base (Center)','n-Base (Right)')
      legend('location','North','Orientation','Horizontal')
      legend boxoff;
      %axis ([Ts,Tf,-0.01,0.03])
```

```
  % Potential Energy Due to Position of QuasiFermi Levels
    PNc1 = q*Vc1*mean(CNk,2).*mean(QFNk,2);
    PNg1 = q*Vg1*mean(CNg(:,1:8),2).*mean(QFNg(:,1:8),2);
    PNg2 = q*Vg2*mean(CNg(:,9:42),2).*mean(QFNg(:,9:42),2);
    PNg3 = q*Vg3*mean(CNg(:,43:50),2).*mean(QFNg(:,43:50),2);
    PNn1 = q*Vn1*mean([CNn(:,1:4) CNn(:,11:14)],2).*mean([QFNn(:,1:4)
QFNn(:,11:14)],2);
    PNn2 = q*Vn2*mean([CNn(:,5:10) CNn(:,15:46)
CNn(:,51:56)],2).*mean([QFNn(:,5:10) QFNn(:,15:46) QFNn(:,51:56)],2);
    PNn3 = q*Vn3*mean([CNn(:,47:50) CNn(:,57:60)],2).*mean([QFNn(:,47:50)
QFNn(:,57:60)],2);
    PPc1 = q*Vc1*mean(CPk,2).*mean(QFPk,2);
    PPg1 = q*Vg1*mean(CPg(:,1:8),2).*mean(QFPg(:,1:8),2);
    PPg2 = q*Vg2*mean(CPg(:,9:42),2).*mean(QFPg(:,9:42),2);
    PPg3 = q*Vg3*mean(CPg(:,43:50),2).*mean(QFPg(:,43:50),2);
    PPn1 = q*Vn1*mean([CPn(:,1:4) CPn(:,11:14)],2).*mean([QFPn(:,1:4)
QFPn(:,11:14)],2);
    PPn2 = q*Vn2*mean([CPn(:,5:10) CPn(:,15:46)
CPn(:,51:56)],2).*mean([QFPn(:,5:10) QFPn(:,15:46) QFPn(:,51:56)],2);
    PPn3 = q*Vn3*mean([CPn(:,47:50) CPn(:,57:60)],2).*mean([QFPn(:,47:50)
QFPn(:,57:60)],2);

    % Plot Kinetic Energy Values
      Time = time*1000; Ts = 0; Tf = floor(time(end)*100)*10;
      h12 = figure(12);
      subplot(2,1,1)
      plot(Time,PPg1,'g.-',Time,PPg2,'b.-',Time,PPg3,'k :',Time,PPc1,'r.-')
      title('Potential Energy - Fermi Level Difference')
      xlabel('Time (ms)'), ylabel('Potential Energy (J)')
      legend('Gate (Left)','Gate (Center)','Gate (Rigth)','Cathode')
      legend('location','North','Orientation','Horizontal')
      legend boxoff;
      %axis ([Ts,Tf,-5*10^-4,25*10^-4])
      subplot(2,1,2)
      plot(Time,PNn1+PPn1,'g.-',Time,PNn2+PPn2,'b.-',Time,PNn3+PPn3,'K :')
      title('Potential Energy - Fermi Level Difference')
      xlabel('Time (ms)'), ylabel('Potential Energy (J)')
      legend('n-Base (Left)','n-Base (Center)','n-Base (Right)')
      legend('location','North','Orientation','Horizontal')
      legend boxoff;
      %axis ([Ts,Tf,-0.01,0.03])
```

APPENDIX F: GTO THYRISTOR DATASHEET (MGTO-1000)

Gate Turn-Off Thyristors

MGTO1000
MGTO1200

The GTO is a family of asymmetric gate turn-off thyristors designed primarily for dc power switching applications such as motor drives, switching power supplies, inverters, or wherever a need exists for high surge current capabilities and fast switching speeds.

- Fast Turn-Off With Reverse Gate Pulse
- High Voltage — V_{DRXM} = 1000 and 1200 Volts
- Momentary Forward Pulse For Turn-On
- Minimizes Drive Losses
- Interdigitated Emitter Geometry Aids Turn-On Current Spreading and Improves Turn-On di/dt
- Clip and Current Spreading Ring for Reliable High Surge Capability — I_{TSM} = 200 A

GTOs
18 AMPERES RMS
1000 and 1200 VOLTS

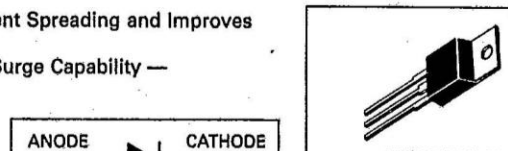

CASE 221A-04
(TO-220AB)
STYLE 3

MAXIMUM RATINGS

Rating	Symbol	Value	Unit
Repetitive Peak Off-State Voltage (T_J = −40 to +125°C, 1/2 Sine Wave 50 to 60 Hz) Note 1	V_{DRXM}	1000 1200	Volts
Repetitive Peak Reverse Voltage, Gate Open (T_J = −40 to +125°C), Note 2	V_{RRM}	15	Volts
Repetitive Peak Reverse Gate Voltage, Note 3	V_{GRM}	15	Volts
On-State Current at T_C = 65°C (1/2 Cycle Sine Wave, 50 to 60 Hz)	$I_{T(RMS)}$	18	Amps
Peak Nonrepetitive Surge Current (8.3 ms Conduction, Half Sine Wave T_C = 65°C)	I_{TSM}	200	Amps
Circuit Fusing (t = 8.3 ms)	I^2t	167	A^2s
Repetitive Controllable On-State Current, Note 4	I_{TCM}	50	Amps
Nonrepetitive Maximum Interruptable On-State Current, Note 5	I_{TCSM}	70	Amps
Peak Forward Gate Power	P_{GFM}	10	Watts
Average Forward Gate Power	$P_{GF(AV)}$	3	Watts
Peak Reverse Gate Power	P_{GRM}	400	Watts
Average Reverse Gate Power	$P_{GR(AV)}$	5	Watts
Operating Junction Temperature Range	T_J	−40 to +125	°C
Storage Temperature Range	T_{stg}	−40 to +150	°C

Notes: 1. V_{DRXM} for all types can be applied on a continuous basis without damage. Ratings apply for R = 39 Ω or shorted gate conditions or negative voltage on the gate. Devices should not be tested for blocking voltage such that the supply voltage exceeds the rating of the device.
2. This is an asymmetric anode shorted part with a blocking gate-cathode junction. The ability to support a reverse voltage depends on the gate-cathode terminal conditions. Gate-cathode reverse bias increases V_{RRM}.
3. Instantaneous voltage at turn-off may exceed rated V_{GRM} provided P_{GRM} is not exceeded.
4. V_D Maximum Peak = V_{DRXM} − 300 V, T_J < 125°C, L_G = 2 μH, V_{GR} = 12 V (See Figure 2)
   C_S = 0.1 μF for MGTO1000
   C_S = 0.05 μF for MGTO1200
5. V_D Maximum Peak = V_{DRXM} − 300 V, T_J < 125°C, L_G = 2 μH, V_{GR} = 12 V (See Figure 2)
   C_S = 0.2 μF for MGTO1000
   C_S = 0.1 μF for MGTO1200

THERMAL CHARACTERISTICS

Characteristic	Symbol	Value	Unit
Thermal Resistance, Junction to Case	$R_{\theta JC}$	1	°C/W
Thermal Resistance, Junction to Ambient	$R_{\theta JA}$	60	°C/W

ELECTRICAL CHARACTERISTICS (T_J = 25°C unless otherwise noted), Note 1

Characteristic	Symbol	Min	Typ	Max	Unit
Peak Forward Blocking Current (V_D = Rated V_{DRM}, R_{GK} = 39 Ω, T_J = 125°C)	I_{DRM}	—	—	5	mA
Peak On-State Voltage (I_{TM} = 50 A, Pulse Width ≤ 300 μs, Duty Cycle ≤ 2%, I_{GT} = 300 mAdc)	V_{TM}	—	2.7	3.1	Volts
Peak Gate Trigger Current (V_D = 12 Vdc, R_L = 1.4 Ω, Pulse Width ≥ 10 μs)	I_{GTM}	—	60	300	mA
Peak Gate Trigger Voltage (V_D = 12 Vdc, R_L = 1.4 Ω, Pulse Width ≥ 10 μs)	V_{GTM}	—	0.8	1.5	Volts
Reverse Gate Leakage Current (V_{GRM} = 15 V, T_J = 125°C)	I_{GRM}	—	—	5	mA
Latching Current (PW = 300 μs, f = 60 Hz, Gate Pulse = 1 A, 10 μs, V_D = 12 Vdc)	I_L	—	1	—	Adc
Holding Current (PW = 300 μs, f = 60 Hz, Gate Pulse = 1 A, 10 μs, Anode Pulse = 6 A, 100 μs, V_D = 12 Vdc)	I_H	—	700	—	mA

SWITCHING CHARACTERISTICS (T_J = 25°C unless otherwise noted)

RESISTIVE TURN-ON SWITCHING						
Gate Turn-On Time	V_D = 600 V, I_T = 50 A $I_{G(pk)}$ = 6 A, C_S = 0.1 μF dig/dt ≥ 7 A/μs See Figure 1 and Table 1(A)	t_{gt}	—	1.5	—	μs
Turn-On Delay Time		t_{dl}	—	0.6	—	
Rise Time		t_{ri}	—	0.9	—	
INDUCTIVE TURN-OFF SWITCHING						
Gate Tun-Off Time	$V_{D(pk)}$ = 700 V, I_T = 50 A, V_{GR} = 12 V $I_{G(pk)}$ = 6 A L_G = 2 μH, C_S = 0.1 μF See Figure 2 and Table 1(B)	t_{gq}	—	3	—	μs
Storage Time		T_{si}	—	2.6	—	
Fall Time		T_{fi}	—	0.4	—	
GATE TURN-OFF CHARGE						
Gate Charge	$V_{D(pk)}$ = 700 V, I_T = 50 A V_{GR} = 12 V L_G = 2 μH, C_S = 0.1 μF See Table 1(B)	Q_{GQ}	—	35	—	μC
Peak Reverse Gate Current		I_{GQ}	—	17	—	A
Peak Tail Current		I_{TLP}	—	5	—	
STATIC dv/dt						
Critical Exponent of Rise Time	$V_{(pk)} = V_{DRM}$ − 400 V R_{GK} = 39 Ω, T_J = 125°C Linear Waveform	dv/dt	—	10,000	—	V/μs

Note 1. This device is rated for use in applications subject to high surge conditions. Care must be taken to insure proper heat-sinking is used at sustained currents (see derating curves).

3

TABLE 1 — TERMS, SYMBOLS AND DEFINITIONS FOR SWITCHING WITH GTO'S

NOTE: The parameters are shown on two separate graphs for clarity.

Terms	Symbols	Definitions
RESISTIVE TURN-ON SWITCHING		
Turn-On Time	t_{gt}	
Delay Time	t_{di}	
Rise Time	t_{ri}	

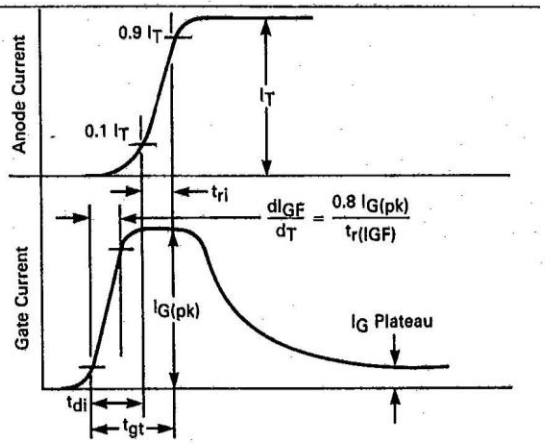

(A)

INDUCTIVE TURN-OFF SWITCHING

Gate Controlled Turn-Off Time	t_{gq}	
Current Storage Time	t_{si}	
Current Fall Time	t_{fi}	
Turn-Off Gate Charge	Q_{GQ}	
Peak Tail Current	I_{TLP}	

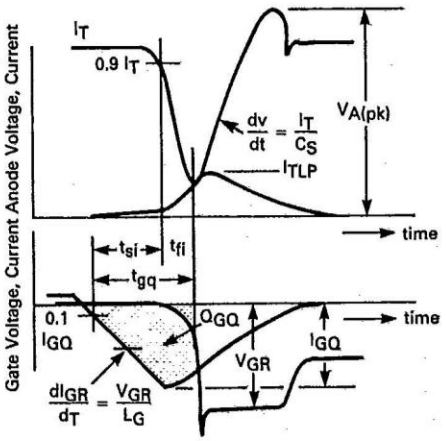

(B)

t_{si} — current storage time 10% I_{GR} to 90% I_T
t_{fi} — current fall time 90% I_T to I_{TLP} inflection point
t_{gq} — gate controlled turn-off time (t_{si} + t_{fi})
t_{di} — current delay time. 10% $I_{G(pk)}$ to 10% I_T
t_{ri} — current rise time. 10% I_T to 90% I_T
t_{gt} — turn-on time (t_{di} + t_{ri})

THIS PAGE INTENTIONALLY LEFT BLANK

LIST OF REFERENCES

[1] SILVACO International Technical Staff, “ATLAS User’s Manual: Device Simulation Software – Volume II,” SILVACO International, February 2000.

[2] G. Vineyard, J. Ciezki, and T. Salem, “Investigating the current interruption capability of a GTO thyristor in an inductive pulse forming network,” Trident Report, United States Naval Academy, Annapolis, MD, May 2008.

[3] Y. Shimizu, S. Kimura, H. Kozaka, N. Matsuura, T. Tanaka, and N. Monma, “A study on maximum turn-off current of a high-power GTO,” in *IEEE Transactions on Electron Devices*, vol. 46, no. 2, pp. 413-419, February 1999.

[4] S. Schroder, D. Detjen, and R. De Doncker, “Multicell circuit model for high power thyristor-type semiconductor devices,” in *IEEE Transactions on Industry Applications,* vol. 39, no. 6, November/December 2003

[5] Interagency Advanced Power Group, Conference Discussion – IAPG Conference 2009,” *Interagency Advance Power Group*, May 2009.

[6] Mitsubishi Electric Technical Staff, “Mitsubishi high power semiconductors: feature and application of gate turn off thyristors,” Mitsubishi Electric, 1998.

[7] N. Galster, S. Klaka, and A. Weber, “ABB Semiconductors AG: Product Design Guide Section 2,” ABB Semiconductors, 2007.

[8] E. Ho and P. Sen, “Effect of gate-drive circuits on GTO thyristor characteristics,” in *IEEE Transactions on Industrial Electronics,* vol. IE-33, issue 3, pp. 325-331, August 1986.

[9] Y. Liang and T. Kee, “Failure mechanism of GTO devices and optimization for minimum current crowding during turn-off,” *International Journal of Electronics*, vol. 77, no. 6, pp. 869-886, 1994

[10] A. Jaecklin, “Performance limitations of a GTO with near-perfect technology,” *IEEE Transactions on Electron Devices*, vol. 39, pp. 1507-1513, June 1992.

[11] X. He, B. Williams, and T. Green, “A composite gate turn-off thyristor model and its application,” in *Conference Record of the 1993 IEEE, Industry Applications Society Annual Meeting,* vol. 2, pp 1202-1207, October 1993.

[12] J. Schwartzenberg, C. Tsay, and R. Fischl, “A SPICE model for gate turn-off thyristors,” in *Proceedings of the Twenty-Second Annual North American Power Symposium,* pp. 145-154, October 1990.

[13] R. Dutta, C. Tsay, A. Rothwarf, and R. Fischl, “A physical and circuit level approach for modeling turn-off characteristics of GTO’s,” in *IEEE Transactions on Power Electronics*, vol. 9, no. 6, November 1994.

[14] F. Mezroua and R. Abid, “Two-dimensional simulation of the transient electrothermal effects during the gate turn-off thyristor turn-off,” in *Journal of Vacuum Science and Technology A*, vol. 18, no. 2, pp. 787-792, March/April 2000.

[15] SILVACO International Technical Staff, “ATLAS User’s Manual: Device Simulation Software – Volume I,” SILVACO International, February 2000.

[16] G. Wachutka, “Analytical model for the destruction mechanism of GTO-like devices by avalanche injection,” in *IEEE Transaction on Electron Devices*, vol. 38, no. 6, pp. 1516-1523, June 1991.

[17] M. Bakowski and U. Gustafsson, “The two basic failure modes in the GTO modeling and experiment,” in *Proceedings of the International Symposium on Power Semiconductor Device and ICs,* pp. 354-359, 1995.

[18] K. Tseng and P. Palmer, “Mathematical model of gate-turn-off thyristor for use in circuit simulations,” in *IEE Proceedings on Electric Power Applications,* vol. 141, no. 6, November 1994.

[19] F. Jensen, *Electronic Component Reliability: Fundamentals, Modeling, Evaluation, and Assurance*, New York: John Wiley & Sons, 1995, pp. 207.

INITIAL DISTRIBUTION LIST

1. Defense Technical Information Center
   Ft. Belvoir, Virginia

2. Dudley Knox Library
   Naval Postgraduate School
   Monterey, California

3. Dr. Todd Weatherford
   Naval Postgraduate School
   Monterey, California

4. Dr. John Ciezki
   United States Naval Academy
   Annapolis, Maryland

5. Dr. Thomas Salem
   United States Naval Academy
   Annapolis, Maryland

6. ENS Gerald E. Vineyard USN
   Naval Postgraduate School
   Monterey, California

7. Joe Borraccini
   Office of Naval Research
   Philadelphia, Pennsylvania

8. CAPT Lynn Petersen, USN
   NAVSEA
   Washington Navy Yard, Washington D.C.